THE BEHAVIOUR OF NITROGEN DURING THE AUTOGENOUS ARC WELDING OF STAINLESS STEEL

by

Madeleine du Toit

Submitted in partial fulfillment of the requirements for the degree

Philosophiae Doctor

in the Faculty of Engineering, the Built Environment and Information Technology,
University of Pretoria, Pretoria

April 2001

ACKNOWLEDGEMENTS

I would like to express my gratitude and appreciation to the following people and companies for their assistance during the course of this project:

- God the Father, Jesus Christ and the Holy Spirit, without whom none of this would have been possible.
- My husband Frans, and my parents, Johan and Miranda Coetzee, for their patience, love and support.
- Professor P.C. Pistorius for his supervision and invaluable advice.
- Johann Borman and Karin Frost for their assistance with the experimental work.
- Columbus Stainless for financial sponsorship of the project and for performing countless nitrogen analyses.
- The Physical Metallurgy Division at Mintek, for assistance with the literature survey and for producing the experimental alloys.
- The University of Pretoria for providing laboratory facilities and my colleagues in the Department of Materials Science and Metallurgical Engineering for their help and encouragement.

THE BEHAVIOUR OF NITROGEN DURING THE AUTOGENOUS ARC WELDING OF STAINLESS STEEL

Candidate: Madeleine du Toit
Supervisor: Prof P.C. Pistorius
Department: Department of Materials Science and Metallurgical Engineering, University of Pretoria
Degree: Philosophiae Doctor

ABSTRACT

Nitrogen-alloyed austenitic stainless steels are becoming increasingly popular, mainly due to their excellent combination of strength and toughness. Nitrogen desorption to the atmosphere during the autogenous welding of these steels is often a major problem, resulting in porosity and nitrogen losses from the weld. In order to counteract this problem, the addition of nitrogen to the shielding gas has been proposed.

This study deals with the absorption and desorption of nitrogen during the autogenous arc welding of a number of experimental stainless steels. These steels are similar in composition to type 310 stainless steel, but with varying levels of nitrogen and sulphur. The project investigated the influence of the base metal nitrogen content, the nitrogen partial pressure in the shielding gas and the weld surface active element concentration on the nitrogen content of autogenous welds.

The results confirm that Sievert's law is not obeyed during welding. The weld nitrogen content increases with an increase in the shielding gas nitrogen content at low nitrogen partial pressures, but at higher partial pressures a dynamic equilibrium is created where the amount of nitrogen absorbed by the weld metal is balanced by the amount of nitrogen evolved from the weld pool. In alloys with low sulphur contents, this steady-state nitrogen content is not influenced to any significant extent by the base metal nitrogen content, but in high sulphur alloys, an increase in the initial nitrogen concentration results in higher weld nitrogen contents over the entire range of nitrogen partial pressures evaluated.

A kinetic model can be used to describe nitrogen absorption and desorption during welding. The nitrogen desorption rate constant decreases with an increase in the sulphur concentration. This is consistent with a site blockage model, where surface active elements occupy a fraction of the available surface sites. The absorption rate constant is, however, not a strong function of the surface active element concentration.

Alloys with higher base metal nitrogen contents require increased levels of supersaturation prior to the onset of nitrogen evolution as bubbles. These increased levels of supersaturation for the higher-nitrogen alloys is probably related to the higher rate of nitrogen removal as N_2 at the onset of bubble formation. Given that nitrogen bubble formation and detachment require nucleation and growth, it is assumed that a higher nitrogen removal rate would require a higher degree of supersaturation.

Nitrogen losses from nitrogen-alloyed stainless steels can be expected during welding in pure argon shielding gas. Small amounts of nitrogen can be added to the shielding gas to counteract this effect, but this should be done with care to avoid bubble formation. Supersaturation before bubble formation does, however, extend the range of shielding gas compositions which can be used. Due to the lower desorption rates associated with higher surface active element concentrations, these elements have a beneficial influence during the welding of high nitrogen stainless steels. Although higher sulphur contents may not be viable in practice, small amounts of oxygen added to the shielding gas during welding will have a similar effect.

Keywords: welding, stainless steel, nitrogen, absorption, desorption, surface active elements, sulphur, kinetic model, bubbles, supersaturation

TABLE OF CONTENTS

CHAPTER 1

BACKGROUND

1.1 INTRODUCTION

The presence of small amounts of nitrogen in alloy steels has a beneficial or a deleterious influence on the properties of the material, depending on its concentration, the thermal processing of the alloy, and the presence of alloying elements. In mild steel, low alloy steel and ferritic stainless steel, nitrogen is generally considered an undesirable impurity, causing porosity and the formation of brittle nitrides[1]. In austenitic and duplex austenitic-ferritic stainless steels, however, nitrogen is often a valued alloying element. In part, this has stemmed from the desire to use nitrogen as a substitute for nickel, thereby reducing alloying element costs. In addition to the fact that the consumption of an expensive strategic metal is reduced, nitrogen is considered to be as much as thirty times as powerful as nickel as an austenite-former[2,3].

Nitrogen also imparts a number of other beneficial properties to austenitic and austenitic-ferritic duplex stainless steels. It is an excellent solid solution strengthening element in stainless steel, increasing the yield strength at room temperature and at sub-zero temperatures[4,5], with no significant decrease in toughness or ductility[5,6]. As a result, nitrogen-alloyed austenitic stainless steels offer a unique combination of strength and toughness. Nitrogen is also reported to improve the passivation characteristics of stainless steels. It increases resistance to localised corrosion[7,8], and reduces sensitisation effects during welding[9,10].

In order to realise the advantages associated with nitrogen alloying, the nitrogen has to be in solution in the metal matrix. Excess nitrogen tends to cause porosity or form brittle nitrides. Iron, mild steel and low alloy steel have low solubility limits for nitrogen (the equilibrium solubility of nitrogen in iron at its melting point is only approximately 0,044 per cent (by mass) at 1 atmosphere pressure[11]). It is therefore important to limit nitrogen absorption in these steels. This poses a particular problem during welding, where nitrogen from the surrounding atmosphere can be absorbed by the weld metal in spite of the precautions normally taken to shield the arc and the weld pool from the surroundings by slag and/or shielding gas. Without the benefits of effective shielding, nitrogen contents as high as 0,2 per cent have been reported in steel welds after arc welding[11]. These concentration levels are far greater than those in the base and filler metals and indicate the importance of the dissolution of nitrogen into the metal from the arc atmosphere during welding.

Austenitic stainless steels can accommodate significantly higher levels of nitrogen in solution. In nitrogen-alloyed austenitic stainless steels, the most important problem during welding is often not nitrogen absorption, but nitrogen desorption to the arc atmosphere, resulting in lower nitrogen levels in the weld metal. A decrease in nitrogen concentration in the region of the weld has a detrimental effect on the mechanical properties and corrosion resistance of the joint.

In order to control nitrogen absorption and evolution from the molten pool during welding, a fundamental knowledge of the absorption and desorption mechanisms is essential. Over the past years a number of studies has dealt with arc melting experiments under static conditions (stationary arc), others concerned experiments under more realistic welding conditions (travelling arc). The results of these studies show that nitrogen absorption and desorption are complex phenomena, influenced by a large number of factors. An important finding is that the amount of nitrogen absorbed in arc melts is generally significantly higher than the amount absorbed in non-arc melts under equilibrium conditions. Furthermore, it appears that the nitrogen level of the weld metal depends on the welding parameters and also on the presence of surface-active elements, notably oxygen and sulphur. Each of these factors are considered in more detail below.

1.2 NITROGEN DISSOLUTION IN LIQUID IRON UNDER EQUILIBRIUM CONDITIONS

The solubility of nitrogen in liquid iron under equilibrium conditions is primarily determined by the nitrogen partial pressure above the melt, the melt temperature and the presence of alloying elements. These three factors are considered in the following sections.

1.2.1 The influence of nitrogen partial pressure on the solubility of nitrogen in liquid iron under equilibrium conditions

Since nitrogen gas generally assumes the form of a diatomic molecule (N_2), the solution of nitrogen in liquid iron can be written as:

$$\tfrac{1}{2}\, N_2\,(g) \rightarrow \underline{N}\,(wt\%) \qquad \ldots(1.1)$$

where: $\underline{N}$ (wt%) refers to nitrogen in solution in the liquid metal (percentage by mass), and
N_2 (g) refers to diatomic nitrogen gas.

At constant temperature, the equilibrium solubility of nitrogen in liquid iron is governed by Sievert's law, which states that the nitrogen concentration in liquid iron is proportional to the square root of the partial pressure of diatomic nitrogen above the melt, as demonstrated by equation (1.2)[12]:

$$\underline{N}_{eq}\,(wt\%) = K_{eq}\sqrt{P_{N_2}} = \sqrt{P_{N_2}}.\exp\left(-\frac{\Delta G_1^0}{RT}\right) \qquad \ldots(1.2)$$

where: $\underline{N}_{eq}$ (wt%) is the nitrogen concentration in liquid iron at equilibrium with diatomic nitrogen,
K_{eq} is the equilibrium constant for reaction (1.1),
P_{N_2} is the partial pressure of N_2 in the atmosphere (atm),
ΔG_1^0 is the standard free energy for reaction (1.1),
R is the gas constant, and
T is the temperature of the liquid iron melt (K).

Sievert's law stipulates that a linear relationship exists between the solubility of nitrogen in liquid iron and the square root of the partial pressure of nitrogen in contact with the liquid metal, and implies that the nitrogen solubility limit in iron alloys can be raised by increasing the partial pressure of the diatomic gas

above the melt. This approach has been proposed for reducing nitrogen losses and for avoiding nitrogen-induced porosity during the welding of nitrogen-containing austenitic stainless steels. If Sievert's law applies under normal arc welding conditions, the addition of nitrogen to the shielding gas during welding should increase the nitrogen solubility in the weld pool and limit nitrogen losses. The validity of this approach is considered in §1.3.

1.2.2 The influence of temperature on the solubility of nitrogen in iron under equilibrium conditions

The influence of temperature on the nitrogen solubility limit in pure iron is illustrated in Figure 1.1, which indicates that the solubility of nitrogen in iron decreases slightly with decreasing temperature in the molten state, and decreases significantly on solidification. Mundra and DebRoy[13] calculated the equilibrium nitrogen concentration in austenite as a function of partial pressure and temperature, based on Sievert's law estimations. Their results, shown in Figure 1.2, indicate that at a given partial pressure of diatomic nitrogen, the equilibrium nitrogen concentration decreases slightly with increasing temperature. This is consistent with Figure 1.1 for temperatures corresponding to the austenite phase field and suggests that the solubility of diatomic nitrogen in iron is not a strong function of temperature. At a given temperature, the equilibrium concentration increases linearly with the square root of the partial pressure of diatomic nitrogen.

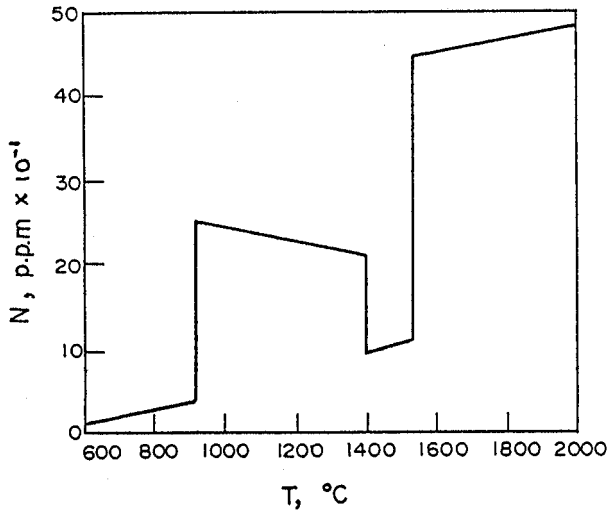

Figure 1.1 The solubility of nitrogen in pure iron[12].

1.2.3 The influence of alloy composition on the solubility of nitrogen in iron under equilibrium conditions

The presence of various alloying elements in iron has a significant influence on the solubility of nitrogen. As shown in Figure 1.3, the majority of the alloying elements commonly found in iron alloys increases the nitrogen solubility[14]. In this respect chromium and manganese play particularly important roles in increasing the nitrogen solubility limit in austenitic stainless steels. Nickel, another important alloying element commonly found in austenitic stainless steels, reduces the nitrogen solubility (as do tungsten,

copper, tin, silicon and cobalt). Alloying elements which increase the activity coefficient of nitrogen generally decrease the solubility. Solutes having greater affinity for nitrogen than iron will decrease the activity coefficient and increase the nitrogen solubility. The influence of various alloying elements on the nitrogen solubility in iron alloys was quantified by Wada and Pehlke[15] using the approach described below.

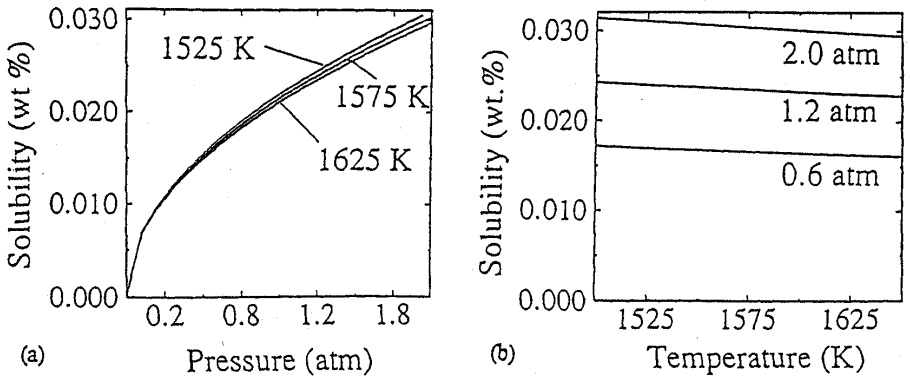

Figure 1.2 Computed equilibrium solubility of nitrogen in austenite exposed to diatomic nitrogen: (a) as a function of partial pressure of diatomic nitrogen at three temperatures, and (b) as a function of temperature at three partial pressures[13].

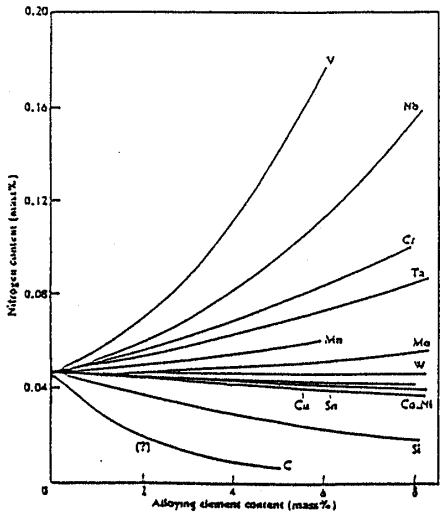

Figure 1.3 The solubility of nitrogen in binary iron alloys under equilibrium conditions at 1600°C and 1 atmosphere nitrogen pressure[14].

The equilibrium constant, K_{eq}, in equation (1.2) is described by the following relationship:

$$K_{eq} = a_N \sqrt{P_{N_2}} = f_N (\%\underline{N}_{eq}) \sqrt{P_{N_2}} \qquad \ldots(1.3)$$

where: a_N is the Henrian activity of nitrogen in the liquid alloy, and
f_N is the activity coefficient of nitrogen in the liquid alloy.

Based on equation (1.3) for the equilibrium constant, Wada and Pehlke[15] developed an equation that describes the equilibrium solubility of nitrogen in liquid Fe-Cr-Ni alloys containing manganese and molybdenum as a function of the activity coefficient of nitrogen, f_N, temperature, T, and the alloying element content. This relationship is shown in equation (1.4). The value of the activity coefficient of nitrogen, f_N, as a function of the alloying element content can be calculated using equation (1.5). In addition to chromium, nickel, molybdenum and manganese, the influence of a number of other elements (C, Si, P, S, Al, Ti, V, W and O) on the activity coefficient is also included in equation (1.5)[14].

$$\log(\underline{N}_{eq}) = -\frac{247}{T} - 1{,}22 - \left(\frac{4780}{T} - 1{,}51\right)\log f_{N,1873} - \left(\frac{1760}{T} - 0{,}91\right)(\log f_{N,1873})^2 \qquad \ldots(1.4)$$

$$\begin{aligned}\log f_N = \{&-164[\%Cr] + 8{,}33[\%Ni] - 33{,}2[\%Mo] - 134[\%Mn] + 1{,}68[\%Cr]^2 - 1{,}83[\%Ni]^2 \\ &- 2{,}78[\%Mo]^2 + 8{,}82[\%Mn]^2 + (1{,}6[\%Ni] + 1{,}2[\%Mo] + 2{,}16[\%Mn]).[\%Cr] + \\ &(-0{,}26[\%Mo] + 0{,}09[\%Mn]).[\%Ni]\}/T + \{0{,}0415[\%Cr] + 0{,}0019[\%Ni] + \\ &0{,}0064[\%Mo] + 0{,}035[\%Mn] - 0{,}0006[\%Cr]^2 + 0{,}001[\%Ni]^2 + 0{,}0013[\%Mo]^2 - \\ &0{,}0056[\%Mn]^2 + (-0{,}0009[\%Ni] - 0{,}0005[\%Mo] - 0{,}0005[\%Mn]).[\%Cr] + \\ &(0{,}0003[\%Mo] + 0{,}0007[\%Mn]).[\%Ni]\} + 0{,}13[\%C] + 0{,}06[\%Si] + 0{,}046[\%P] \\ &+ 0{,}007[\%S] + 0{,}01[\%Al] - 0{,}9[\%Ti] - 0{,}1[\%V] - 0{,}003[\%W] - 0{,}12[\%O]\end{aligned} \qquad \ldots(1.5)$$

where: $f_{N,1873}$ is the activity coefficient f_N at 1873 K, and
[%M] is the alloying element content in wt%.

Equations (1.4) and (1.5) can be used to calculate the equilibrium nitrogen solubility in molten iron-based alloys at any temperature. In order to determine whether Sievert's law and Wada and Pehlke's approach are appropriate for calculating the nitrogen content of welds, the next section describes some of the available literature on the influence of welding on the nitrogen solubility limit in iron alloys.

1.3 NITROGEN ABSORPTION AND DESORPTION DURING ARC MELTING AND WELDING

During the majority of fusion welding processes, including arc, laser and electron beam welding, a plasma phase resides above the weld pool. This plasma is composed of ionised gas consisting of electrons, ions, excited atoms and molecules, and can collectively be both electrically neutral and conductive[16]. It has become clear in recent years that the behaviour of a plasma-metal system is significantly different from that of the corresponding gas-metal system[17]. When a diatomic gas such as nitrogen is transformed into a plasma phase, it may dissociate, ionise, or become electrically or vibrationally excited. Each of these individual species has a different equilibrium with the liquid weld metal. As a result, Sievert's law cannot be applied to describe the dissolution of diatomic gas species into liquid metal in the presence of a plasma.

In a paper published in 1969, Lakomskii and Torkhov[18] described the results of arc melting experiments performed on iron samples in a number of argon-nitrogen shielding gas atmospheres. The authors reported that the nitrogen contents of iron samples exposed to low nitrogen partial pressures were

proportional to the square root of the nitrogen partial pressure in the plasma, as shown in Figure 1.4, however, the nitrogen concentrations measured were an order of magnitude higher than the concentrations predicted from equilibrium Sievert's law calculations. At higher nitrogen partial pressures (more than approximately 0,005 MPa), the nitrogen content of the weld metal reached a saturation level, and remained constant regardless of P_{N_2}. Kuwana and Kokawa[19] studied the addition of nitrogen to argon shielding gas during the gas tungsten arc welding of pure iron and, as shown in Figure 1.5, obtained results similar to those reported by Lakomskii and Torkhov. Kuwana and Kokawa reported that nitrogen absorption in iron weld metal does not obey Sievert's law and is dependent on the welding conditions. As shown in Figure 1.5, the weld metal nitrogen content increases with an increase in P_{N_2} at low partial pressures, exceeding the equilibrium concentrations predicted by Sievert's law.

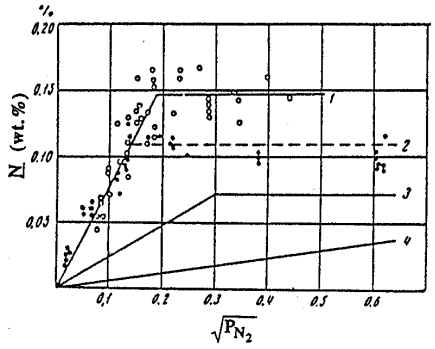

Figure 1.4 Isotherms of the reaction between nitrogen and liquid iron: (1) heating by an indirect-action plasmatron, (2) heating by a direct-action plasmatron, (3) heating by a free arc, and (4) induction heating[18].

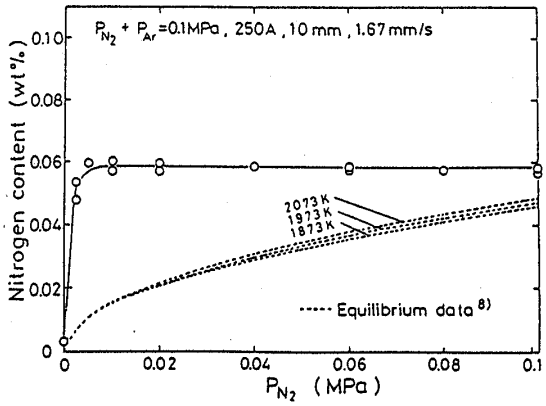

Figure 1.5 The relationship between the weld metal nitrogen content and the nitrogen partial pressure (P_{N_2}) in nitrogen-argon shielding gas mixtures during gas tungsten arc welding, compared to the equilibrium nitrogen solubilities at 1873 K, 1973 K and 2073 K[19].

Blake and Jordan[20] studied nitrogen absorption and desorption in iron during arc melting in argon and argon-nitrogen atmospheres as a function of time and welding variables. They reported that nitrogen is absorbed from argon-nitrogen shielding gas atmospheres, with the rate of absorption increasing with current and nitrogen partial pressure. After a certain time a saturation value is reached, characterised by

bubble formation in the molten metal. The final nitrogen concentrations in the iron samples were well above the values expected from the reaction of molecular nitrogen with molten iron. The molten iron appears to absorb nitrogen rapidly from the arc until it reaches saturation, followed by nucleation of molecular nitrogen bubbles in the melt. At this point a dynamic equilibrium is created whereby the rate of absorption at the melt surface is balanced by bubble formation in the melt. Blake and Jordan found that the steady-state nitrogen content is in excess of that required to provide an internal pressure of one atmosphere at the assumed temperature of the molten iron button, and concluded that some degree of supersaturation occurs.

Based on the linear relationship between the nitrogen solubility and the square root of the nitrogen partial pressure observed by Lakomskii and Torkhov[18] at low partial pressures (as shown in Figure 1.4), these authors concluded that the weld metal reacts with molecular nitrogen, and attributed the enhanced solubility of nitrogen at low partial pressures to the presence of excited nitrogen molecules, N_2^*, in the arc plasma. The proposed nitrogen absorption reactions are shown in equations (1.6) to (1.9). The excited nitrogen molecules possess high internal energy acquired through the interaction between electrons and neutral particles in the arc. The authors reasoned that the retention of sufficient vibrational energy in the nitrogen molecules plays a significant role in breaking the interatomic bond at the moment when nitrogen adsorbs onto the surface of the liquid iron before going into solution. The excitation energy lowers the energy required for dissociation of the nitrogen molecules on the metal surface before adsorption, thereby increasing the equilibrium constant, K^*, and the equilibrium concentration of nitrogen in solution. As shown in Figure 1.4, the nitrogen concentration in the weld metal becomes independent of the nitrogen partial pressure in the arc atmosphere at higher nitrogen partial pressures, reaching a constant steady-state concentration. In this region the metal is oversaturated with nitrogen, so the latter escapes from the metal in the form of gas bubbles.

$$N_2^* + \text{site} \rightarrow N_2^*\,(\text{ads}) \qquad \ldots(1.6)$$

$$N_2^*\,(\text{ads}) + \text{site} \rightarrow 2N\,(\text{ads}) \qquad \ldots(1.7)$$

$$2N\,(\text{ads}) \rightarrow \underline{2N}\,(\text{wt\%}) + 2\ \text{sites} \qquad \ldots(1.8)$$

$$N_2^*\,(g) \rightarrow \underline{2N}\,(\text{wt\%}) \qquad \ldots(1.9)$$

where: N_2^* represents nitrogen molecules with excess vibrational energy provided by the electric field, and
the postscript (ads) refers to an adsorbed species on the metal surface.

In response to Lakomskii and Torkhov's conclusions, Katz and King[21] argued that once an excited diatomic molecule is adsorbed onto a metal surface, its vibration is significantly dampened. Therefore, it cannot play a significant role in enhancing solubility. These authors postulated that the increased solubility in the presence of a plasma results from the existence of monatomic nitrogen, N, in the arc. The nitrogen atoms form as the gas is heated in the arc plasma and individual molecules acquire more energy. At low temperatures, this energy is mainly translational, i.e. the energy associated with the velocity of motion. At higher temperatures diatomic molecules such as nitrogen absorb energy firstly by rotation and secondly by vibration - an in-and-out movement of the two atoms relative to each other.

When the vibrational energy reaches a sufficiently high level, it may rupture the valence bonds holding the two atoms together, causing them to dissociate into the monatomic state[16].

Den Ouden and Griebling[22] studied the absorption of nitrogen in pure iron samples during arc melting in controlled gas atmospheres. They measured the amount of nitrogen in the samples as a function of various experimental conditions, including time, gas composition, arc current, and arc length. As shown in Figure 1.6, their experimental results confirm that the nitrogen concentrations in the metal samples are considerably higher than expected from equilibrium considerations. Figure 1.6 also shows that the weld metal becomes oversaturated at higher partial pressures, resulting in bubble formation and porosity. Like Katz and King[21], Den Ouden and Griebling attributed the enhanced solubility of nitrogen to monatomic nitrogen atoms formed in the arc by the dissociation of nitrogen molecules. The degree of dissociation depends on the arc temperature and the nitrogen content of the arc. The individual reactions describing the dissolution process are shown in equations (1.10) to (1.12). The authors proposed that monatomic nitrogen is absorbed by the weld pool directly under the arc and is then desorbed at the weld periphery. The amount of nitrogen leaving the liquid metal will increase with increasing nitrogen concentration, and a steady-state condition is reached when the amount of nitrogen entering the weld pool per unit time equals the amount of nitrogen leaving the weld pool per unit time.

$$N\,(g) + \text{site} \rightarrow N\,(\text{ads}) \qquad \ldots(1.10)$$

$$N\,(\text{ads}) \rightarrow \underline{N}\,(\text{wt\%}) + \text{site} \qquad \ldots(1.11)$$

$$N\,(g) \rightarrow \underline{N}\,(\text{wt\%}) \qquad \ldots(1.12)$$

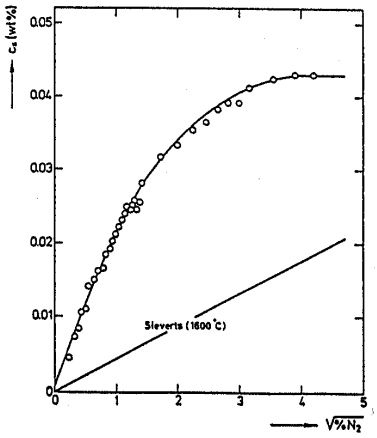

Figure 1.6 Nitrogen concentration in an iron sample as a function of the square root of the nitrogen partial pressure in the shielding gas[22].

Bandopadhyay *et al* [17] also attributed the enhanced nitrogen solubility in iron to the existence of neutral atoms (N) in the plasma, and confirmed this hypothesis by analysing isothermal helium-nitrogen plasmas using optical emission spectroscopy methods. They identified neutral atoms (N), excited atoms (N^*), excited molecules (N_2^*), and ions (N^-, N^+ and N_2^+) in the arc plasma. The authors reasoned that it is extremely improbable for nitrogen ions to contribute to the observed enhanced solubility since the flux of highly mobile electrons to the liquid surface in a plasma is far greater than the flux of heavier ion species.

As a result, an electrically insulating metal surface becomes negatively charged when exposed to a plasma and the adsorption of negatively charged species, such as N^-, is highly improbable. Furthermore, positively charged ions such as N^+ and N_2^+ are attracted towards the metal surface, where they absorb electrons near the surface and are converted to N and N_2. Excited molecules cannot contribute towards enhanced solubility because they lose their excess vibrational energy when adsorbed onto metal surfaces. Thus, the increased solubility most likely results from the presence of monatomic nitrogen in the plasma.

Gedeon and Eager[23] developed a model for the absorption of hydrogen (also a diatomic gas molecule) in iron weld metal and showed that Sievert's law cannot be applied since the assumption of a one-step absorption process which neglects the effects of dissociation, solute rejection upon solidification and diffusion of hydrogen away from the weld region, is too simplistic to provide realistic values. The authors attributed the enhanced hydrogen concentration in the weld metal to the presence of monatomic hydrogen in the plasma. They suggested a two-step absorption process in which hydrogen dissociates in the high temperature regions of the arc, followed by absorption of both diatomic and monatomic hydrogen into the weld pool at the temperature of the weld pool surface. Their results showed that appropriate hydrogen absorption values can be obtained if the dissociation temperature is approximately 10 to 20 per cent higher than the absorption temperature.

Although the enhanced dissolution process appears to be consistent with the presence of monatomic nitrogen in the arc plasma, a general model is needed to calculate the extent of enhancement for a given condition. In this respect determination of the nature of the plasma and the concentration of various species within the plasma phase is an important first step. Three issues are of special interest in welding: the extent of dissociation of a diatomic gas in the welding environment, the effect of temperature on the species concentration in the weld metal for different gases, and the concentration of dissolved species in the weld pool retained by the weld metal after cooling. The alloying element content of the weld metal, including the prior nitrogen content and the concentration of surface active elements, also plays a significant role. No unified theory for the quantitative understanding of the extent of enhanced dissolution in stainless steels has emerged up to this point.

An investigation into nitrogen dissolution in stainless steel weld metal has to start with an understanding of the solubility of nitrogen in pure iron welds. General rules of behaviour established for iron can then be extended to those for stainless steel weld metal, taking into account the influence of alloying elements as well as the nonequilibrium conditions that prevail during welding. In the following section two existing thermodynamic models for nitrogen dissolution in iron and stainless steel are discussed. The influence of the alloying element content of the weld metal on nitrogen absorption is also considered.

1.4 THERMODYNAMIC MODELS FOR NITROGEN DISSOLUTION IN WELD METAL

1.4.1 The two-temperature model

In 1987 Gedeon and Eager[23,24] developed a thermodynamic model describing the dissolution of hydrogen in steel welds. This model was subsequently modified by Mundra and DebRoy[13] and Palmer and

DebRoy[25] to describe the dissolution of nitrogen in weld metal. In accordance with available literature, the authors based their model on the assumption that monatomic nitrogen is responsible for the enhanced nitrogen solubility observed at low nitrogen partial pressures in molten iron exposed to plasma. The appropriate nitrogen dissolution reaction is represented by equation (1.12), and equation (1.13) displays the free energy relationship for this reaction.

$$\underline{N}(wt\%) = P_N \exp\left(-\frac{\Delta G_{12}^{0}}{RT}\right) \qquad \ldots(1.13)$$

where: P_N is the partial pressure of monatomic nitrogen in the arc plasma (atm), and
ΔG^0_{12} is the standard free energy for reaction (1.12).

Mundra and DebRoy[13] calculated the equilibrium solubility of monatomic nitrogen in iron using equation (1.13) and the applicable free energy data for reaction (1.12). Their results are shown in Figure 1.7 as a function of partial pressure and temperature. In contrast to the behaviour of the iron-diatomic nitrogen system shown in Figure 1.2, the equilibrium solubility of nitrogen in austenite exposed to monatomic nitrogen increases in a linear manner with increasing monatomic nitrogen partial pressure, and shows a significant decrease in a nonlinear manner with temperature. Since the monatomic nitrogen solubility increases sharply with decreasing temperature below approximately 1575 K, small changes in temperature can cause large changes in the ensuing equilibrium nitrogen concentration. Variation in temperature plays a much greater role than pressure in determining the extent of nitrogen dissolution in iron exposed to monatomic nitrogen.

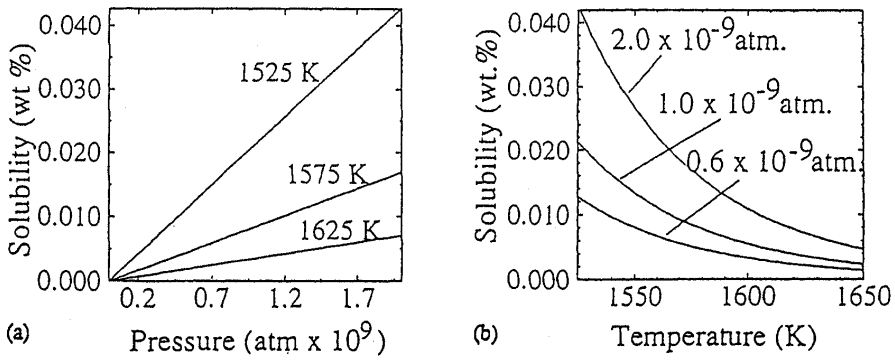

Figure 1.7 Computed equilibrium solubility of nitrogen in austenite exposed to monatomic nitrogen: (a) as a function of the partial pressure of monatomic nitrogen at three temperatures, and (b) as a function of temperature at three partial pressures[13].

The two-temperature model is based on the premise that the concentration of monatomic nitrogen formed in an arc plasma due to the dissociation of nitrogen molecules is higher than what would be obtained solely from consideration of thermal equilibrium between the two species at the system temperature and pressure. If the actual concentration of atomic nitrogen in the arc plasma is known, its concentration in iron can be estimated by considering equilibrium between the monatomic nitrogen and the metal. In a plasma, the extent of dissociation of diatomic nitrogen depends on factors such as the nature of the power

source, the energy dissipated, the overall system geometry, and the nature of the diatomic gas. The authors[13,23,24,25] defined a hypothetical dissociation temperature, T_d, at which the equilibrium thermal dissociation of diatomic nitrogen would produce the actual partial pressure of monatomic nitrogen present in the plasma. The monatomic nitrogen in the arc plasma then dissolves in the weld metal at the surface temperature of the molten pool, T_s. This model is schematically illustrated in Figure 1.8. It is fair to assume that, after dissociation of diatomic nitrogen at T_d, no significant change in the partial pressures of diatomic and monatomic nitrogen occurs during the transport of these species towards the metal surface. Unlike the dissociation of diatomic molecules, the recombination of the product atoms in the gas phase is difficult. First, because the extent of dissociation in the arc is small, the probability of collision between two nitrogen atoms is much smaller than that between N and N_2, or between N and inert gas atoms in the shielding gas. Second, because the recombination reaction is highly exothermic, exothermic heat has to be removed from the recombined molecule, as in a three-body collision. From a statistical consideration, the probability of a three-body collision is very small[25].

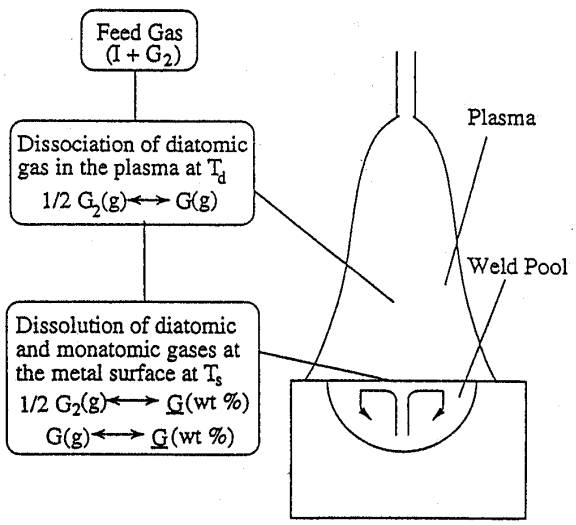

Figure 1.8 A schematic diagram showing the dissolution of a gas, G, from the plasma phase into a weld pool[13].

The nitrogen dissociation reaction in the arc is represented by equation (1.14) and the partial pressure of monatomic nitrogen in the plasma by equation (1.15):

$$\tfrac{1}{2}N_2\,(g) \rightarrow N\,(g) \qquad \ldots(1.14)$$

$$P_N = \sqrt{P_{N_2}}\exp\left(-\frac{\Delta G^0_{14,T_d}}{RT_d}\right) \qquad \ldots(1.15)$$

where: $\Delta G^0_{14,T_d}$ is the standard free energy for reaction (1.14) at T_d.

The extent of dissociation of diatomic nitrogen at T_d can be calculated from equation (1.15). Since the extent of dissociation of diatomic nitrogen is low under typical welding conditions, P_{N_2} can be assumed to be equal to the partial pressure of N_2 in the inlet gas, $P_{N_2}^{in}$. Combining equations (1.13) and (1.15), and

bearing in mind that the dissociation of N_2 is considered at T_d and the dissolution of N at T_s, the equilibrium nitrogen concentration in iron is given by equation (1.16):

$$\underline{N}(wt\%) = \sqrt{P_{N_2}^{in}} \exp\left(-\frac{1}{R}\left(\frac{\Delta G_{14}^0}{T_d} + \frac{\Delta G_{12}^0}{T_s}\right)\right) \qquad \ldots(1.16)$$

Equation (1.16) represents the solubility of nitrogen in iron exposed to a plasma environment with the metal at temperature T_s. The hypothetical dissociation temperature, T_d, is higher than the temperature of the sample, T_s, and is a measure of the partial pressure of the atomic nitrogen in the plasma.

In analysing the validity of the model, Mundra and DebRoy[13] used nitrogen solubility data from the available literature, substituting the data into equation (1.16), and calculating the effective dissociation temperatures which explain the enhanced solubility. The calculated dissociation temperatures fell within a range of 100 to 300 K above the sample temperature for all the systems analysed. Figure 1.9 illustrates the relationship between the percentage dissociation of diatomic nitrogen and T_d, based on the experimental work of Bandopadhyay *et al*[17], and shows that the dissociation of diatomic nitrogen increases with increasing temperature. Palmer and DebRoy[25] performed similar calculations and, as shown in Figure 1.10, reported effective dissociation temperatures approximately 100 to 215 K higher than the sample temperature. The authors concluded that, if experimental data are not available, a rough estimate of the nitrogen concentration can be obtained by assuming a hypothetical dissociation temperature about 100 to 200 K higher than the sample temperature.

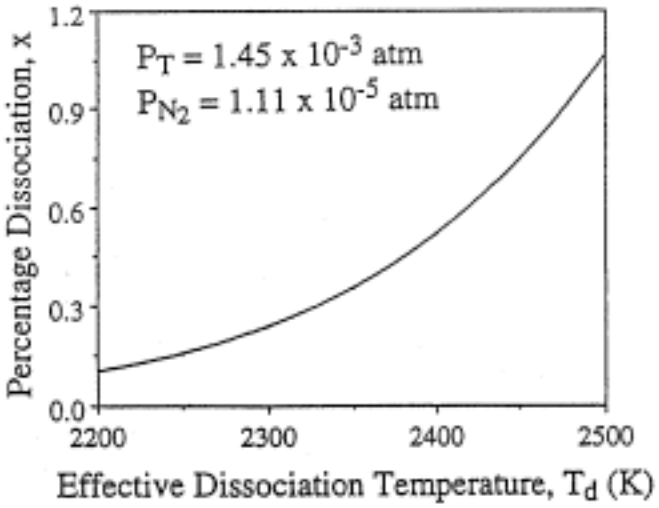

Figure 1.9 The percentage nitrogen dissociated as a function of the effective dissociation temperature[13].

Mundra and DebRoy[13] and Palmer and DebRoy[25] developed the two-temperature model based on the results of isothermal experiments performed in glow discharge plasmas. Unlike these experiments, the temperature of the weld pool surface during welding shows significant spatial variation. If the partial pressure of diatomic nitrogen was the main factor determining the nitrogen concentration in the weld metal, the consequences of the spatial variation in the weld pool surface temperature would be fairly

insignificant (as demonstrated in Figure 1.2). In contrast, for monatomic nitrogen species, a slight variation in temperature can lead to a significant variation in the equilibrium solubility of nitrogen (as shown in Figure 1.7). By making a few simplifying assumptions, Palmer and DebRoy[25] extended the application of the two-temperature model to actual welding experiments. The authors used published results obtained by Kuwana and Kokawa[19] during the gas tungsten arc welding of a low alloy steel in controlled nitrogen atmospheres.

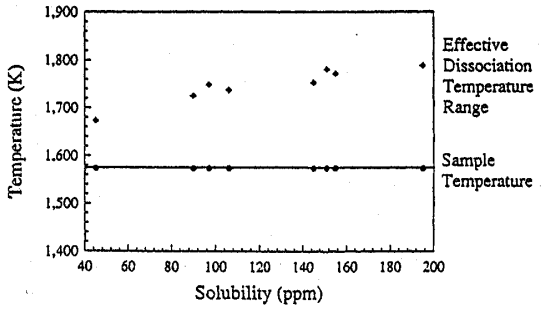

Figure 1.10 Comparison between the nitrogen solubility (wt%) and the effective dissociation temperature over the experimental pressure range[13].

Palmer and DebRoy's[25] first assumption concerned the extent of coverage of the weld pool by the arc plasma, as determined by the welding parameters. The significance of the extent of coverage of the pool surface is demonstrated in Figure 1.11. Complete coverage of the weld pool by the plasma can be assumed if welding is performed at reasonably low currents and the weld pool is fairly narrow. In order to compare the experimental data with the calculated values, the authors also needed the temperature distribution at the surface of the weld pool. Khan[26] demonstrated that the temperature distribution at the surface of the weld pool is represented by equation (1.17).

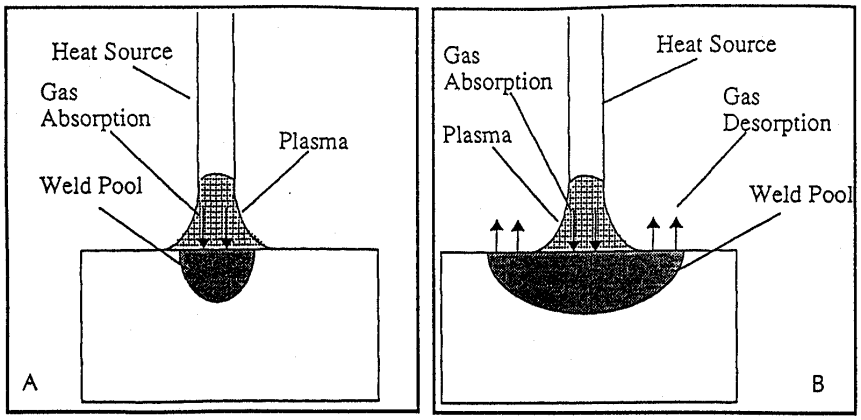

Figure 1.11 Schematic diagrams of a weld pool: (A) completely covered by plasma, and (B) incompletely covered by plasma[25].

$$T = T_{MAX} \exp\left(-ar^{*2}\right) \qquad \ldots(1.17)$$

where: T is the temperature at any location on the weld pool surface,
T_{MAX} is the weld pool surface temperature at the axis of the arc,
a is a constant,
r^* is a dimensionless distance from the axis of the arc given by the ratio r/r_0,
r is the radial distance from the centre of the molten pool or the arc axis, and
r_0 is the radius of the molten pool.

Since the temperature at the fusion line, i.e. at $r = r_0$, is known (the temperature at the solid/liquid interface is equal to the liquidus temperature of the base metal), the value of the variable a can be calculated if T_{MAX} is known. Palmer and DebRoy[25] assumed values for T_{MAX} and calculated the temperature distribution on the surface of the weld pool for these values. The calculated temperature profiles for two values of T_{MAX} are shown in Figure 1.12(a) as a function of the dimensionless distance, r^*.

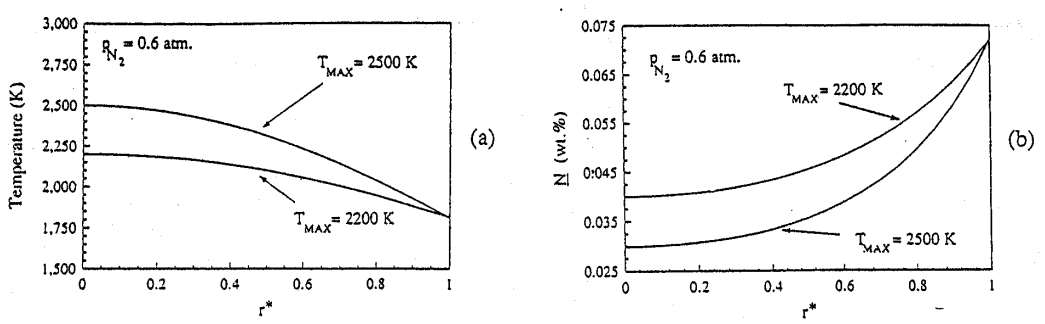

Figure 1.12 Computed values for: (a) temperature, and (b) nitrogen concentration, across the radius of the weld pool for T_{MAX} values of 2500 K and 2200 K and a diatomic nitrogen partial pressure of 0,6 atm[25].

In addition to the surface temperature distribution, the dissociation temperatures are necessary to calculate the nitrogen concentration distribution on the weld pool surface from equation (1.16). As shown earlier, Palmer and DebRoy[25] demonstrated that the value of the dissociation temperature, T_d, is approximately 100 to 200 K higher than the sample temperature. The exact difference between the surface temperature and the dissociation temperature depends on the concentration of monatomic gas in the plasma, which, in turn, depends on the properties of the plasma. The higher the partial pressure of monatomic nitrogen in the plasma, the higher the dissociation temperature. In view of the continuous movement of the arc with respect to the workpiece during welding, the plasma continually mixes with the surrounding gas, which tends to reduce the concentration of monatomic nitrogen in the plasma. As a result, a relatively small difference between the dissociation temperature and the surface temperature of the weld pool is appropriate. Palmer and DebRoy assumed a temperature difference of 125 K between the dissociation temperature and the surface temperature in the case of gas tungsten arc welding.

The equilibrium concentration of nitrogen at all locations on the surface of the weld pool can be computed from equation (1.17) once the dissociation temperature at each of these locations is known.

The computed nitrogen concentration values are shown as a function of the dimensionless distance in Figure 1.12(b). The nitrogen concentrations are higher at the outer edges of the weld pool since the monatomic nitrogen solubility increases sharply with decreasing temperature. In view of the fact that the weld metal undergoes vigorous recirculation, the nitrogen from the surface is readily transported to the interior of the weld pool.

Finally, Palmer and DebRoy[25] assumed that the overall nitrogen concentration in the weld metal, $\underline{N}_{AV}$ (wt%), if nitrogen is not lost from the pool in any appreciable amount, is determined by an average concentration of nitrogen on the weld pool surface integrated over the entire surface:

$$\underline{N}_{AV}(\text{wt\%}) = \frac{1}{\pi r_0^2}\int_0^{r_o} 2\pi r\,\underline{N}(wt\%)dr = \int_0^1 2r^*\,\underline{N}(wt\%)dr^* \qquad \ldots(1.18)$$

where: $\underline{N}$ (wt%) is the local value of the nitrogen concentration at any location on the weld pool surface, and

r^* is the dimensionless radial distance from the axis of the heat source on the weld pool surface.

The computed overall nitrogen concentration in the weld pool for two values of T_{MAX} is shown in Figure 1.13 as a function of P_{N_2} in H_2-N_2 shielding gas mixtures from the experimental data of Kuwana and Kokawa[19]. This figure shows that fair agreement exists between the computed results and the experimental data. Improved agreement between the experimental and predicted values can be obtained by selecting a temperature difference of approximately 100 K between the surface temperatures and the dissociation temperatures.

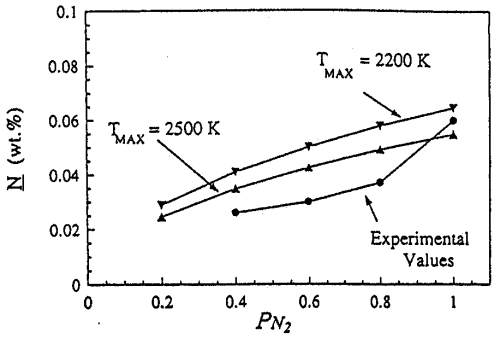

Figure 1.13 Comparison between the experimental solubility results of Kuwana and Kokawa[19] and the computed nitrogen solubility predictions based on the two-temperature model[25].

Although the two-temperature model developed by Gedeon and Eager[23,24], Mundra and DebRoy[13] and Palmer and DebRoy[25] appears to provide fair agreement between the calculated and experimentally determined nitrogen solubility values in iron, the model has significant limitations which restrict its extension to the current investigation. The first limitation is that the model does not take into account the alloy composition, which has been shown to have a significant effect on the solubility of nitrogen in iron (refer to §1.2.3). Kuwana *et al*[27] addressed this issue in the form of a thermodynamic model, discussed in

§1.4.2, developed to predict the nitrogen solubility in stainless steel weld metal. The second limitation is that the two-temperature model does not consider the influence of the surface active element concentration of the weld metal, the prior nitrogen content of the base metal or the welding parameters on nitrogen absorption and desorption during welding. These issues are considered in more detail in §1.5 and §1.6.

1.4.2 The thermodynamic model developed by Kuwana *et al*[27] for predicting the nitrogen solubility of stainless steel welds

Kuwana *et al*[27] studied the dissolution of nitrogen in iron and stainless steel welds during autogenous gas tungsten arc welding with nitrogen containing shielding gas mixtures. They attributed the enhanced nitrogen solubility observed during welding to the presence of monatomic nitrogen in the arc, but in contrast to the two-temperature model considered in §1.4.1, Kuwana *et al* also assumed that undissociated diatomic nitrogen in the plasma can contribute towards nitrogen absorption. They suggested that three reactions, represented by equations (1.19) to (1.21), occur simultaneously during welding.

$$N_2\,(g) = 2\underline{N}\,(wt\%) \quad \ldots(1.19)$$

$$N_2\,(g) = 2N\,(g) \quad \ldots(1.20)$$

$$N\,(g) = \underline{N}\,(wt\%) \quad \ldots(1.21)$$

Equation (1.19) describes the absorption of diatomic nitrogen from the arc atmosphere, and equation (1.21) the absorption of monatomic nitrogen produced by dissociation, equation (1.20), in the arc. As shown in Figure 1.14, Kuwana *et al* proposed that dissociation of diatomic nitrogen according to equation (1.20) produces a thin nitrogen-rich surface region exposed to the arc, but that the greater part of nitrogen absorption is controlled by reaction (1.19) at the temperature of the central region of the molten pool due to active convection. The authors stated that the nitrogen content approaches the equilibrium solubility of nitrogen at the temperature of the central region of the molten pool. When the nitrogen content of the central region is lower than the equilibrium solubility, nitrogen is transferred from the nitrogen-rich surface region to the central region. When the nitrogen content of the central region is higher than the equilibrium solubility, the excess nitrogen is released to the atmosphere through the weld pool surface not covered by the arc.

After exposure to the arc the weld pool cools down to room temperature. During the cooling cycle, the equilibrium solubility of nitrogen changes with temperature. As shown in Figure 1.1, the weld metal loses a small amount of nitrogen during cooling in the molten state, and a significant amount during solidification due to the large solubility gap between the liquid and solid states. Nitrogen losses after solidification are negligible due to the lower diffusivity of nitrogen in the solid state.

Accordingly, the nitrogen content of a steel gas tungsten arc weld at room temperature, $(\%\underline{N})_w$, can be described by equation (1.22):

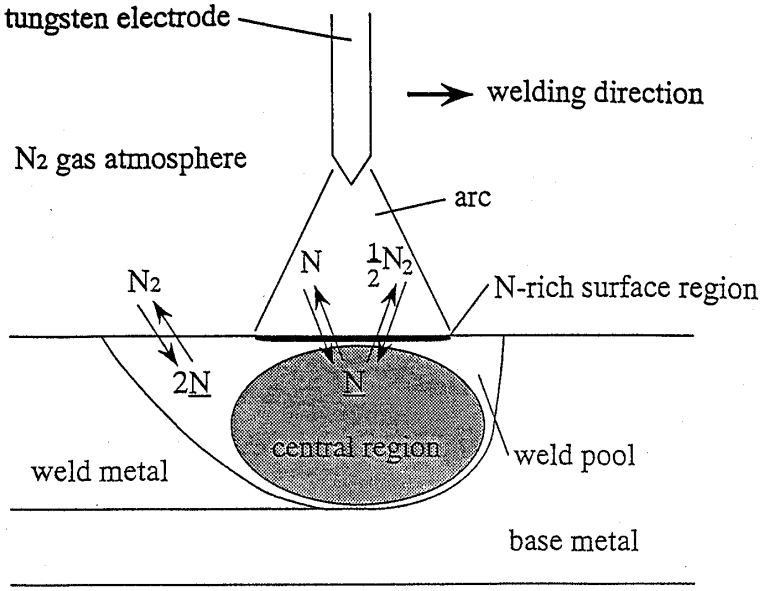

Figure 1.14 A schematic illustration of the behaviour of nitrogen during gas tungsten arc welding according to Kuwana *et al*[27].

$$(\%\underline{N})_w = (\%\underline{N})_{eq} + \Delta A + \Delta B + \Delta C \qquad \ldots(1.22)$$

where: $(\%\underline{N})_{eq}$ is the equilibrium solubility of nitrogen at the temperature of the central region of the molten weld pool,

$(\%\underline{N})_{eq} + \Delta A$ is the nitrogen content of the weld pool exposed to the arc,

ΔB is the change in the nitrogen content of the liquid weld pool during cooling to solidification, and

ΔC is the amount of nitrogen evolved on solidification.

Based on these assumptions, Kuwana *et al* investigated the influence of chromium and nickel on the nitrogen solubility of iron gas tungsten arc welds. The sum of the chromium and nickel contents of each alloy was limited to less than 30 weight per cent in all cases. The outline of the procedure followed by the authors in calculating $(\%\underline{N})_w$ is as follows: First, the temperature of the central region of the molten weld pool was determined as a function of the chemical composition of the alloy, and the equilibrium solubility of nitrogen, $(\%\underline{N})_{eq}$, was calculated at the weld pool temperature and 0,1 MPa nitrogen atmosphere. Next, $\Delta A+\Delta B+\Delta C$ was described as a function of alloy content using the difference between the experimental nitrogen content of the weld metal and $(\%\underline{N})_{eq}$. Following this, equations to predict the nitrogen content of gas tungsten arc welded iron alloys in 0,1 MPa nitrogen atmospheres were determined based on equation (1.22). The prediction was then extended to nitrogen partial pressures of 0 to 0,1 MPa in the arc atmosphere. Each of these steps are considered in more detail below.

- Weld pool temperature

The temperature of the central region of the molten weld pool is required in order to calculate the equilibrium solubility of nitrogen, $(\%\underline{N})_{eq}$, in the weld metal. Kuwana *et al*[27] measured the temperature of

the central region of the molten pool during gas tungsten arc welding using thermocouples, and derived an equation to describe the temperature of this region. Earlier work by the authors[28] established that the molten weld pool temperature during the gas tungsten arc welding of pure iron and type 304L austenitic stainless steel was approximately 100 K higher than the liquidus temperature of the weld metal, regardless of the welding current. Based on these results, the temperature of the weld pool during gas tungsten arc welding, T_{WP}, can be expressed in the form of equation (1.23) as a function of the liquidus temperature. The liquidus temperature of the weld metal can be calculated from the chemical composition of the melt[29,30].

$$T_{WP} = T_L + 100 \qquad \ldots(1.23)$$

where: T_L is the liquidus temperature of the weld metal.

- Equilibrium solubility of nitrogen

The equilibrium solubility of nitrogen, $(\%\underline{N})_{eq}$, at the temperature of the molten weld pool, T_{WP}, can be calculated using equations (1.4) and (1.5) considered earlier.

- Nitrogen absorption from nitrogen containing shielding gas atmospheres

If the experimental nitrogen content of gas tungsten arc welds, $(\%\underline{N})_w$, and the equilibrium solubility of nitrogen, $(\%\underline{N})_{eq}$, calculated using equations (1.4), (1.5) and (1.23) at 0,1 MPa nitrogen atmosphere, are represented as iso-nitrogen contour lines on an Fe-Cr-Ni ternary diagram (as shown in Figure 1.15), the difference between the calculated and experimental values is large in the high and low chromium regions. The nitrogen content appears to be strongly dependent on the chromium content and the iso-nitrogen contour lines are roughly parallel to the [%Cr]=0 line. Figure 1.16 shows the calculated and experimental nitrogen contents on Fe-Cr and Fe-Ni binary cross sections. In the Fe-Ni system, the calculated nitrogen concentrations are slightly lower than the experimental values, but the difference is very small. In the Fe-Cr system, the calculated values are slightly lower than the experimental values in the low chromium region, but higher in the high chromium region. Chromium appears to influence nitrogen absorption by increasing the equilibrium nitrogen solubility and the period of time required to reach this equilibrium value.

Figure 1.17 demonstrates the influence of the weld metal chromium content on the difference, $\Delta(\%\underline{N})$, between the experimental nitrogen content of Fe-Cr welds, $(\%\underline{N})_w$, and the equilibrium solubility of nitrogen, $(\%\underline{N})_{eq}$, where $\Delta(\%\underline{N})=(\%\underline{N})_w-(\%\underline{N})_{eq}$. This figure indicates that in alloys containing less than about 7% chromium, $\Delta(\%\underline{N})$ increases slightly with chromium content, but at higher chromium levels, $\Delta(\%\underline{N})$ decreases with an increase in chromium content. The authors explained these results in terms of the time required to reach the equilibrium nitrogen solubility limit in these alloys. Due to the low solubility of nitrogen in low chromium alloys, the melting time during welding may be sufficient for nitrogen absorption to increase the weld metal nitrogen content to a level approaching the equilibrium value. In high chromium alloys with high solubility limits, enough time may not be available during welding for nitrogen absorption from the arc atmosphere to increase the weld metal nitrogen content to a

level approaching the equilibrium value. This results in an increasing difference between the measured and equilibrium nitrogen content, Δ(%N), with increasing chromium content.

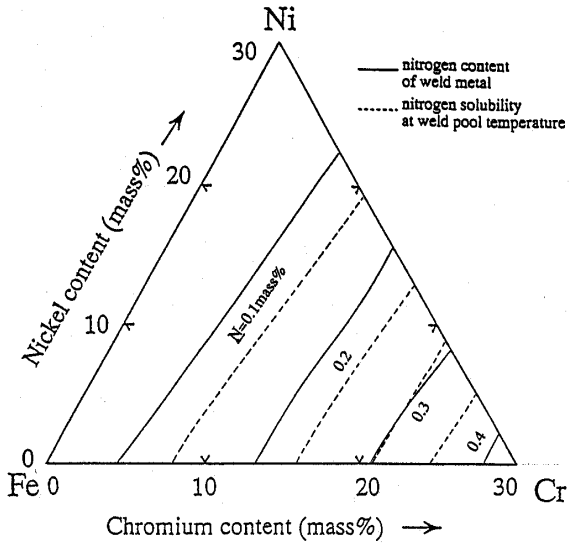

Figure 1.15 Iso-nitrogen contour lines on the Fe-Cr-Ni ternary phase diagram indicating the experimental nitrogen contents of gas tungsten arc welds and the equilibrium solubility values of nitrogen at the weld pool temperature[27].

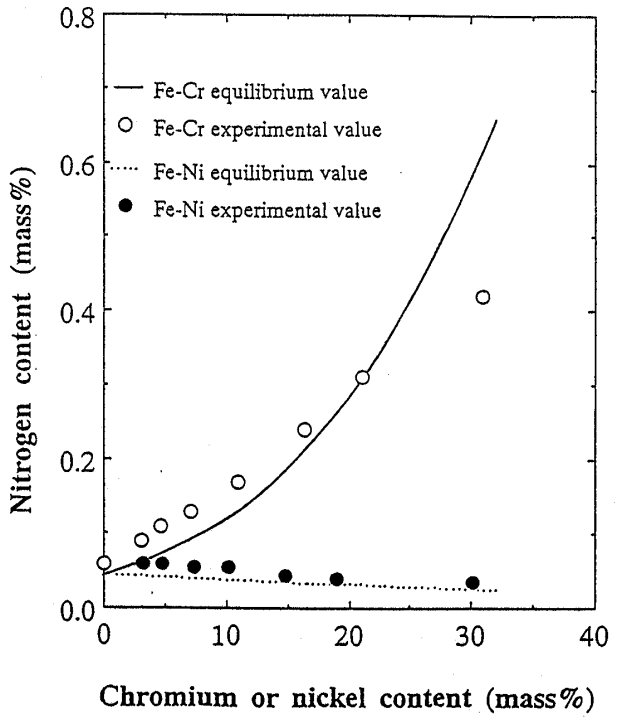

Figure 1.16 The influence of the chromium and nickel contents of binary Fe-Cr and Fe-Ni alloys on the nitrogen content of gas tungsten arc welds, compared to the equilibrium solubilities at the weld pool temperature[27].

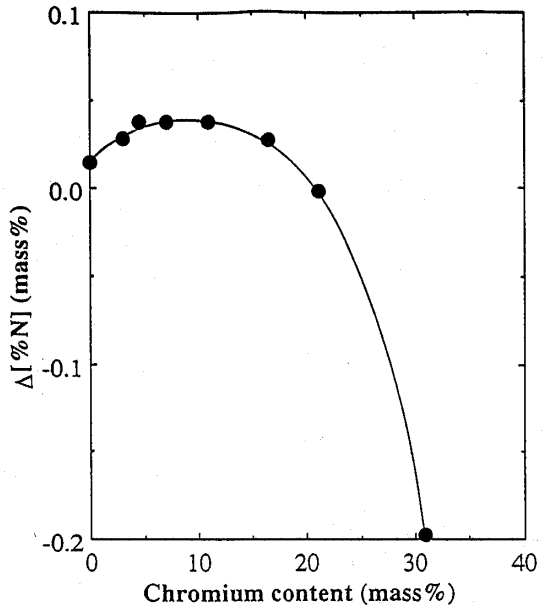

Figure 1.17 The influence of chromium on the difference between the weld metal nitrogen content, $(\%\underline{N})_w$, and the equilibrium nitrogen solubility, $(\%\underline{N})_{eq}$, in Fe-Cr welds[27].

Based on the results in Figure 1.17, Kuwana *et al* developed a relationship, shown in equation (1.24), for computing the calculated nitrogen content, $(\%\underline{N})_c$, of chromium containing weld metal as a function of the chromium content.

$$(\%\underline{N})_c = (\%\underline{N})_{eq} + (1{,}46x10^{-2}) + (7{,}12x10^{-3}).[\%Cr] - (7{,}25x10^{-4}).[\%Cr]^2 + (3{,}38x10^{-5}).[\%Cr]^3 - (8{,}08x10^{-7}).[\%Cr]^4 \quad \ldots(1.24)$$

As shown in Figure 1.18, good agreement was obtained between the calculated and experimental nitrogen contents of Fe-Cr welds. The nitrogen contents, $(\%\underline{N})_c$, of Fe-Cr-Ni welds were also calculated, using equations (1.4), (1.5), (1.23) and (1.24), and by assuming that the difference between the measured and equilibrium nitrogen contents is only a function of the chromium content, since the iso-nitrogen contour lines are roughly parallel to the [%Cr]=0 line in Figure 1.15. As shown in Figure 1.19, good agreement between the calculated and experimental nitrogen contents was also obtained for Fe-Cr-Ni welds.

In order to examine the application of this model to a typical stainless steel, the nitrogen content of a type 304L austenitic stainless steel, welded using the gas tungsten arc process with similar welding parameters, was calculated using equations (1.4), (1.5), (1.23) and (1.24). Kuwana *et al* predicted a $(\%\underline{N})_c$ value of 0,24 wt% for this alloy, which is slightly lower than the measured value, $(\%\underline{N})_w$, of 0,26 wt%. The authors attributed this small difference to an incorrect calculation of the liquidus temperature of the alloy. Overestimation of the molten weld pool temperature leads to an underestimation of the nitrogen content of high chromium weld metal.

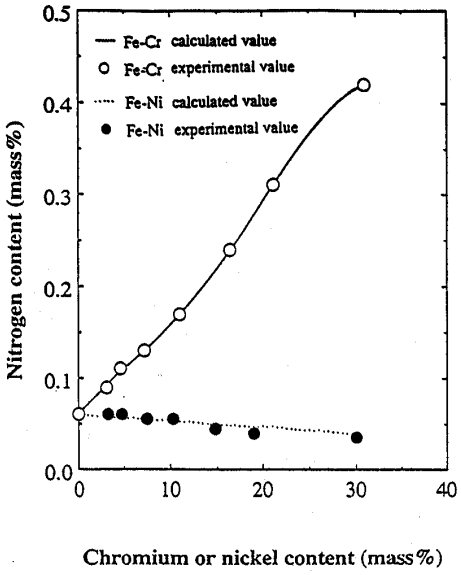

Figure 1.18 The influence of chromium or nickel on the experimental and calculated nitrogen contents of Fe-Cr and Fe-Ni welds[27].

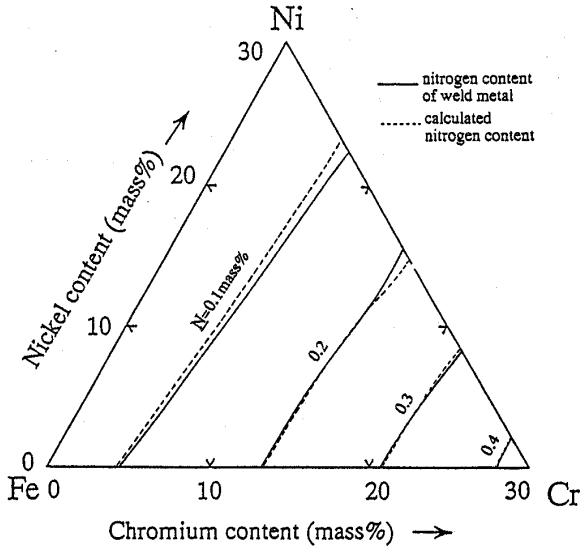

Figure 1.19 Iso-nitrogen contour lines showing the experimental and calculated nitrogen contents of Fe-Cr-Ni welds[27].

- Argon-nitrogen mixed shielding gas atmospheres

Kuwana *et al*[27] also extended the above calculations, which were performed for pure nitrogen shielding gas atmospheres (0,1 MPa nitrogen), to argon-nitrogen shielding gas mixtures with varying nitrogen partial pressures and a total pressure of 0,1 MPa.

Figure 1.20 illustrates the influence of the nitrogen partial pressure in Ar-N_2 shielding gas atmospheres on the nitrogen content of gas tungsten arc welded steel and stainless steel, compared to the equilibrium

solubility of nitrogen in these alloys at the molten pool temperature. The results confirm that the nitrogen content of welds tends to increase with nitrogen partial pressure up to a saturation level. At higher partial pressures the weld metal nitrogen content assumes a constant value, regardless of the nitrogen partial pressure in the shielding gas. Figure 1.20 also confirms that the nitrogen solubility in welds is enhanced over that predicted from equilibrium considerations at all nitrogen partial pressures, with the exception of alloys containing more than approximately 20 wt% chromium at nitrogen partial pressures approaching 0,1 MPa. It is also evident that stainless steel welds dissolve significantly more nitrogen than lower chromium alloys, presumably because chromium increases the nitrogen solubility limit in these alloys. Based on these results, Kuwana *et al* concluded that the dissociation of diatomic nitrogen in the arc plasma, equation (1.20), and the subsequent dissolution of monatomic nitrogen, equation (1.21), have a marked influence on nitrogen absorption. Accordingly, the authors developed a thermodynamic model, described below, to account for the observed nitrogen dissolution behaviour.

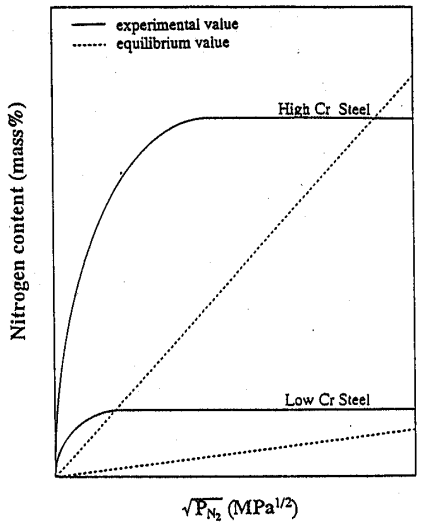

Figure 1.20 The influence of the nitrogen partial pressure in Ar-N_2 shielding gas mixtures on the nitrogen content of steel welds, and the equilibrium nitrogen solubility at the weld pool temperature[27].

Kuwana *et al*[27] assumed that the dissociation of molecular nitrogen gas into monatomic nitrogen in the arc plasma is represented by equation (1.20). The equilibrium constant, K, of this reaction is given by equation (1.25), and the relationship between K and the standard free energy for reaction (1.20), ΔG^0_{20}, is represented by equation (1.26).

$$K = \frac{(P_N)^2}{P_{N_2}} \qquad \ldots(1.25)$$

where: P_N is the partial pressure of monatomic nitrogen (N) in atm, and
P_{N_2} is the partial pressure of molecular nitrogen (N_2) in atm.

$$\ln K = -\frac{\Delta G^0_{20}}{RT} \qquad \ldots(1.26)$$

where: ΔG^0_{20} is the standard free energy for reaction (1.20), and
R is the universal gas constant.

Equation (1.27) can be derived by combining equations (1.25) and (1.26):

$$\ln\left[\frac{(P_N)^2}{P_{N_2}}\right] = -\frac{\Delta G^0_{20}}{RT} \qquad \ldots(1.27)$$

The standard Gibbs free energy change, ΔG^0_{20}, for the dissociation reaction is given by equation (1.28):

$$\Delta G^0_{20} = \Delta H^0_{20} - T\Delta S^0_{20} \qquad \ldots(1.28)$$

where: ΔH^0_{20} is the change in enthalpy for the dissociation of nitrogen (966,67 kJ/mol), and
ΔS^0_{20} is the change in entropy for the dissociation of nitrogen (136,44 J/K.mol).

Equations (1.27) and (1.28) provide a relationship between P_N (or P_{N_2}) and temperature at 0,1 MPa nitrogen pressure. Figure 1.21 shows the influence of the initial N_2 partial pressure in Ar-N_2 shielding gas mixtures on the degree of dissociation of diatomic gas at high temperatures, assuming that the total pressure remains at 0,1 MPa. This figure indicates that the degree of dissociation decreases with a decrease in temperature and an increase in the initial P_{N_2}. Even though a lower initial P_{N_2} in the shielding gas leads to a higher degree of dissociation, the partial pressure of monatomic nitrogen in the arc, P_N, does not increase because of the lower nitrogen concentration in the arc atmosphere. Figure 1.22 demonstrates the influence of the initial P_{N_2} in Ar-N_2 shielding gas mixtures on P_N at high temperatures, calculated using equations (1.27) and (1.28). It is evident that the partial pressure of monatomic nitrogen, P_N, decreases with a decrease in the initial P_{N_2} and rapidly approaches zero when the initial P_{N_2} approaches zero.

Based on these conclusions, Kuwana *et al* assumed that the weld metal nitrogen content increases with the nitrogen partial pressure up to a nitrogen partial pressure of P_{N_2}', and assumes a value of $(\%\underline{N})_{0,1}$ at nitrogen partial pressures higher than P_{N_2}', where $(\%\underline{N})_{0,1}$ is the nitrogen content of the weld metal calculated using equations (1.4), (1.5), (1.22), (1.23) and (1.24) at 0,1 MPa nitrogen partial pressure. The authors therefore assume that no supersaturation occurs in the weld metal. From the results of the Fe-Cr welds, and assuming that P_{N_2}' depends on the chromium content, the nitrogen content, $(\%\underline{N})_c$, of gas tungsten arc welded iron alloys in argon-nitrogen shielding gas mixtures can be calculated using equations (1.29) and (1.30):

when: $0 \le P_{N_2} < P_{N_2}'$, $\quad (\%\underline{N})_c = (0{,}0308.[\%Cr] + 0{,}271).(P_{N_2})^{1/4}$ $\quad \ldots(1.29)$

when: $P_{N_2}' \le P_{N_2} \le 0{,}1$ MPa, $\quad (\%\underline{N})_c = (\%\underline{N})_{0,1}$ $\quad \ldots(1.30)$

where: $$P_{N_2}' = \left\{\frac{(\%\underline{N})_{0,1}}{(0{,}0308.[\%Cr] + 0{,}271)}\right\}^4$$

As shown in Figure 1.23, the calculated and experimental nitrogen contents, $(\%\underline{N})_c$ and $(\%\underline{N})_w$, display good agreement for the range of steels investigated. However, the model developed by Kuwana *et al* is simplified and has several shortcomings which would limit wider application. It was developed for a specific set of welding parameters (gas tungsten arc welding with electrode negative polarity, an arc length of 10 mm and a travel speed of 3,33 mm/s). The model would probably need adjustment for other sets of welding parameters since the reaction time between the molten weld pool and nitrogen in the arc atmosphere is likely to change. The reaction time appears to play a significant role, particularly in the case of high chromium alloys. The model also does not take into account the influence of the base metal nitrogen content or the presence of surface active elements. These factors are considered in §1.5 and §1.6.

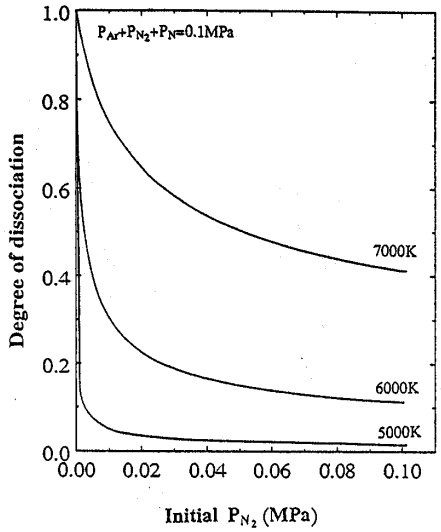

Figure 1.21 The influence of the initial N_2 partial pressure in mixed Ar-N_2 shielding gas atmospheres on the degree of dissociation at high temperatures[27].

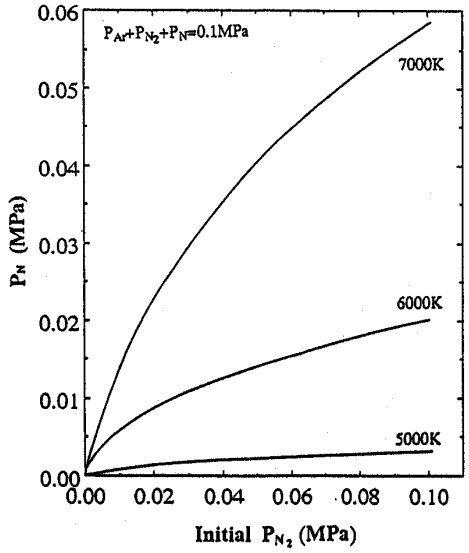

Figure 1.22 The influence of the initial N_2 partial pressure in Ar-N_2 shielding gas atmospheres on the partial pressure of monatomic nitrogen, P_N, at high temperatures[27].

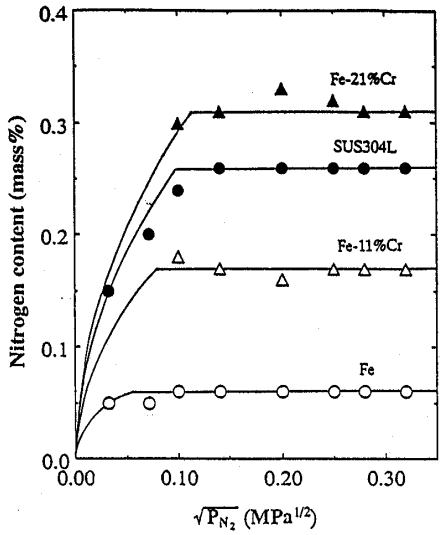

Figure 1.23 Experimental and calculated weld metal nitrogen contents as a function of the nitrogen partial pressure in Ar-N_2 shielding gas mixtures[27].

1.5 THE INFLUENCE OF ALLOYING ELEMENTS ON THE DISSOLUTION OF NITROGEN IN IRON DURING WELDING

The influence of alloying elements on the dissolution of nitrogen in iron alloys appears to be similar to the influence of the same elements on the equilibrium solubility, as considered in §1.2. However, the previous discussion did not take into consideration the influence of the base metal nitrogen content prior to welding, which is of particular significance in the case of high nitrogen stainless steels, nor the presence of surface active elements in the weld metal. The influence of each of these factors is discussed in the following section. The possible vaporisation of alloying elements from the weld pool due to the high temperatures associated with welding is an additional factor that may play a role in determining the solubility of nitrogen during welding. This factor is unlikely to influence the results obtained during this investigation to any significant extent, and will therefore not be considered further.

1.5.1 The influence of the base metal nitrogen content on the nitrogen content of welds

Limited information is currently available on the influence of the base metal nitrogen content on nitrogen dissolution in iron alloy welds. Okagawa *et al*[6] studied the influence of nitrogen additions to argon shielding gas during autogenous gas tungsten arc welding on the nitrogen content of type 304L stainless steel welds. The authors reported that the final weld metal nitrogen content was not influenced by the base metal nitrogen content (0,025% nitrogen in the type 304L stainless steel investigated), and concluded that the base metal nitrogen was in a form that did not take part in the nitrogen dissolution reaction during welding. They based this conclusion on the observation that the weld metal nitrogen content was the same as that of the original base metal when pure argon shielding gas was used. Suutala[31] studied autogenous gas tungsten arc welds in a number of austenitic stainless steels with base metal nitrogen levels varying between 0,008 and 0,076 wt%, and reported good correlation between the

nitrogen contents of the austenitic base metals and autogenous welds in the same materials with pure argon shielding gas, particularly in the presence of relatively high amounts of manganese. The results of Arata *et al*[32] indicated that the total weld metal nitrogen content is the sum of the residual nitrogen content of the base metal and the nitrogen picked up from the shielding gas-metal interaction.

The nitrogen levels of the steels investigated by these authors were relatively low, compared to the nitrogen contents of high nitrogen austenitic stainless steels, and were probably well below the nitrogen solubility limit of the weld metal. This is further evidenced by the influence of manganese, as reported by Suutala[31]. For this reason it is unlikely that the conclusions of the authors described above can be extended to the case of high nitrogen alloys, where the base metal nitrogen content is significantly higher and closer to the solubility limit.

1.5.2 The influence of surface active elements on the nitrogen content of welds

Ample evidence exists to show that the presence of surface active elements, in particular sulphur and oxygen, has a significant influence on nitrogen dissolution in iron alloy welds. A number of these studies is considered below.

Lancaster[1] reported that the amount of nitrogen absorbed during arc welding increases in the presence of oxygen, and Ogawa *et al*[33] demonstrated that nitrogen-induced porosity in austenitic stainless steel welds can be curbed by welding in an atmosphere containing a small amount of oxidising gas. According to Blake[11], the presence of oxygen in the arc plasma or weld metal leads to lower nitrogen desorption rates. Uda and Ohno[34] studied the effects of surface active elements, including sulphur, oxygen and selenium, on the nitrogen content of iron under arc melting conditions in a number of Ar-N_2 shielding gas mixtures. The presence of these surface active elements markedly increased the nitrogen content of the iron, as shown in Figure 1.24 for a number of iron-oxygen alloys. It is evident that the level of supersaturation of nitrogen in the welds increases with increasing concentrations of oxygen. Sinha and Gupta[35] studied the rate of nitrogen absorption during the arc melting of stainless steel and observed that the rate of absorption decreased in the presence of surface active elements.

Three hypotheses have been offered to explain the apparently conflicting results describing the influence of surface active elements on nitrogen dissolution:

1. Blake[11] attributed the observed increased rate of dissolution and the lower desorption rate in the presence of oxygen to the formation of nitric oxide, NO, in preference to monatomic nitrogen in the arc. This hypothesis is probably inaccurate, due to the experimental and theoretical evidence for the influence of monatomic nitrogen on enhanced solubility. Blake's hypothesis also does not account for the influence of sulphur, which is similar to that of oxygen.

2. The presence of surface active elements, such as sulphur and oxygen, in the weld pool promotes convergent surface tension driven flow (Marangoni flow). In a pure metal, Marangoni flow is outwards across the weld pool surface, but the presence of surface active elements may cause the gradient of surface tension as a function of temperature to reverse and become positive. The surface

flow is then inwards, towards the arc root, causing nitrogen-rich weld metal to flow downward[21]. In iron-oxygen alloys the gradient of surface tension with temperature becomes positive at oxygen contents in the range of 60 to 100 ppm[1]. This hypothesis is probably also unsound, since Marangoni flow generally plays only a minor role in determining mass flow patterns during welding, with the possible exception of low current gas tungsten arc welding. Divergent flow in a weld pool is usually a rare phenomenon.

3. Surface active elements tend to occupy a fraction of the available sites on the metal surface, making it more difficult for nitrogen to adsorb on or desorb from the metal surface[21]. This is currently the most likely explanation for the influence of surface active elements on nitrogen dissolution and evolution, and was used by Katz and King[21] to derive their kinetic model (to be considered in §1.7.1). In their study of nitrogen desorption kinetics, the authors found that in melts containing surface active elements, the rate of reaction was limited by the association of two absorbed nitrogen atoms to form an adsorbed nitrogen molecule. On the other hand, when the melts contained low amounts of sulphur and oxygen, mass transport in the melt was the rate-limiting step for the desorption reaction.

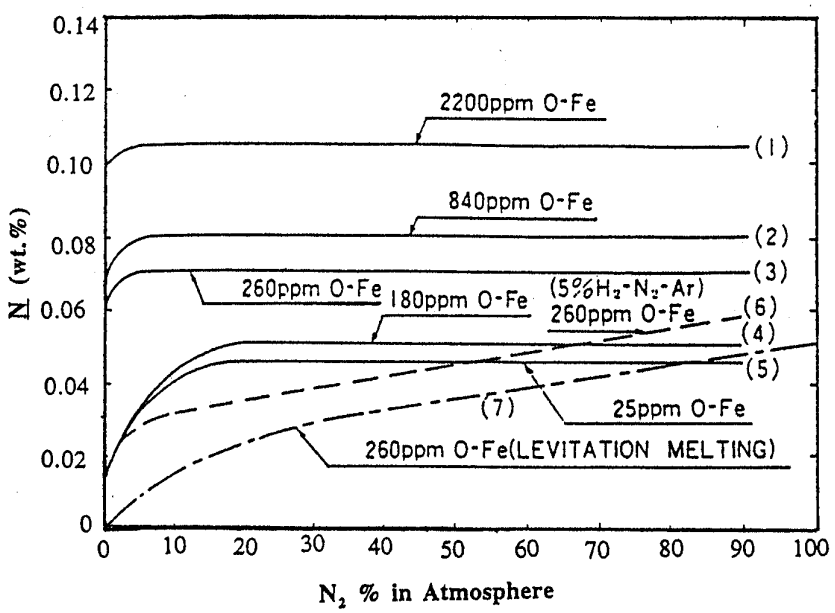

Figure 1.24 The nitrogen content of iron-oxygen alloys arc-melted at various nitrogen partial pressures[34].

The conflicting results discussed earlier were explained by Uda and Ohno[34], who proposed that the nitrogen content in iron is not an equilibrium value, but rather a steady-state concentration resulting from the absorption of nitrogen into the melt from the arc atmosphere and the evolution of nitrogen bubbles from the melt. Based on this steady-state assumption, the authors developed a model which is schematically illustrated in Figure 1.25. In this model, nitrogen is absorbed from the arc column, where the nitrogen exists in a number of activated states. Once absorbed into the melt, the nitrogen species are transported by fluid flow to the interior regions of the pool. The evolution of nitrogen bubbles from the melt occurs over the entire melt surface and is influenced by the characteristics of the surface in the

region not covered by the arc. If oxygen or sulphur covers part of the surface, nitrogen evolution is retarded. In the absence of surface active elements, nitrogen evolves much more readily. Sinha and Gupta[35] also stated that the final nitrogen content was the balance of nitrogen absorbed and desorbed over the range of exposure.

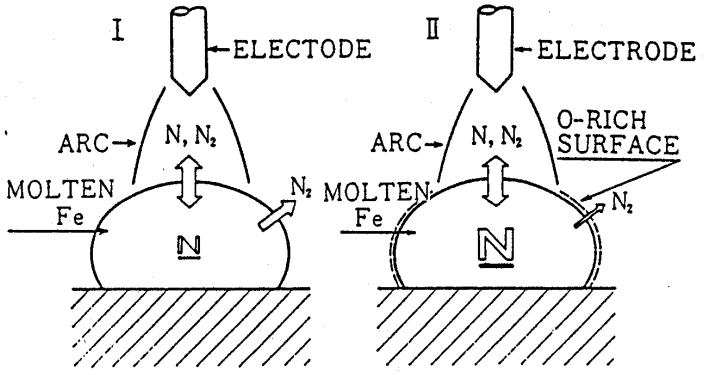

Figure 1.25 Schematic model of nitrogen dissolution and evolution from arc melted iron containing (I) low oxygen concentrations, and (II) high oxygen concentrations[34].

Uda and Ohno[36] also investigated the spattering of molten iron, containing 25 ppm and 260 ppm oxygen, under arc melting conditions in a nitrogen containing atmosphere. Spattering is a common phenomenon in the arc welding of steels and is driven by the high internal pressure and the high rate of bubble formation in liquid iron in the region of the arc spot. The authors explained the results of their spattering experiments using the model for the steady-state nitrogen concentration described above. At low oxygen concentrations (such as 25 ppm), the surface of the iron droplet outside of the arc column is not covered with an oxygen-rich film, thereby allowing the nitrogen, which is transported to this region by convection and diffusion, to be readily discharged from the surface. However, at high oxygen concentrations (such as 260 ppm), an oxygen-rich film forms on the surface of the droplet outside the jet impingement area, not allowing the nitrogen to evolve readily from the melt, and thereby increasing the nitrogen concentration within the drop.

1.6 THE INFLUENCE OF WELDING PARAMETERS ON THE NITROGEN CONTENT OF WELDS

Several researchers have reported that welding parameters, in particular the welding current, arc voltage, travel speed and electrode polarity, have a significant influence on nitrogen absorption and desorption reactions during welding. A number of these investigations are discussed below.

Kuwana and Kokawa[19] and Kuwana *et al*[28] studied nitrogen absorption in pure iron and stainless steel (AISI type 304L) samples during autogenous gas tungsten arc welding in pure nitrogen shielding gas (0,1 MPa nitrogen pressure). As shown in Figure 1.26(a), the authors observed that the weld metal nitrogen content decreases with increasing welding current. This reduction in nitrogen content with increasing

current is more significant in stainless steel than in iron, and the nitrogen contents of the stainless steel welds are also considerably higher than those of the iron welds. The authors attributed the enhanced nitrogen solubility in the stainless steel welds to the presence of chromium. They also observed that the weld cross-sectional area increases considerably with an increase in welding current. The relationship between the nitrogen content of iron and stainless steel welds and the arc length during welding is shown in Figure 1.26(b). The nitrogen content appears to be almost independent of the arc length for both the stainless steel and iron welds. Since the arc voltage increases linearly with an increase in arc length, the results suggest that the weld metal nitrogen content is almost independent of the arc voltage. The weld cross-sectional area initially increases with an increase in arc voltage, but becomes constant at higher arc lengths. Figure 1.26(c) shows the relationship between the nitrogen content of the weld metal and the torch travel speed. It is evident that the weld metal nitrogen content increases with an increase in travel speed. This increase in nitrogen content is more significant in stainless steel than in iron. The weld cross-sectional area decreases markedly with an increase in travel speed.

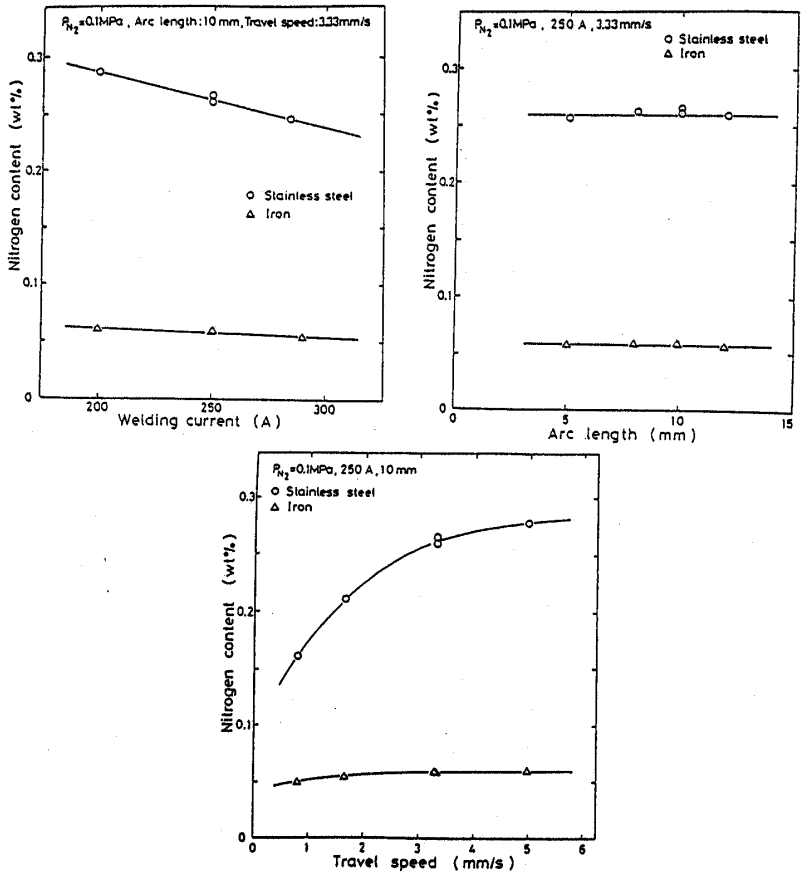

Figure 1.26 The relationship between the weld metal nitrogen content and the welding parameters during the autogenous gas tungsten arc welding of iron and stainless steel in 0,1 MPa nitrogen shielding gas: (a) the influence of welding current, (b) the influence of arc length, and (c) the influence of torch travel speed[28].

Kuwana *et al*[28] attributed these results to the influence of the welding parameters on the weld cross-sectional area. They observed that the weld metal nitrogen content generally decreases with increasing cross-sectional area and suggested that in the presence of pure nitrogen shielding gas, the nitrogen content

of the weld metal may be controlled mainly by nitrogen evolution during cooling. An increase in the weld cross-sectional area results in a decrease in the cooling rate after welding, thereby prolonging the period of time before solidification and resulting in an increase in the amount of evolved nitrogen. Figure 1.27 summarises the relationship between the nitrogen content of the weld metal and the weld metal cross-sectional area, and demonstrates that the nitrogen content of the weld metal decreases with an increase in weld cross-sectional area. The authors also observed that the nitrogen content of the weld metal decreases with an increase in the heat input during welding.

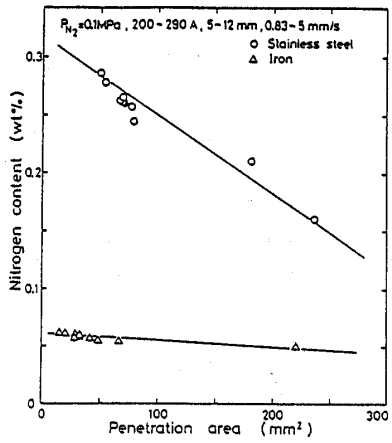

Figure 1.27 The relationship between the weld metal nitrogen content and the weld cross-sectional area during gas tungsten arc welding in pure nitrogen at a pressure of 0,1 MPa[28].

Kotecki[37] studied open-arc welding with self-shielded flux-cored stainless steel electrodes and reported that an increase in arc voltage causes the weld deposit nitrogen content to increase. This behaviour was attributed to the longer arc lengths associated with increasing arc voltage. At short arc lengths, the shielding gas atmosphere produced by shielding gas components in the flux has a low nitrogen content. As the arc length increases, more nitrogen from the surrounding atmosphere (air) is entrained in the arc plasma, thereby increasing the nitrogen content of the shielding gas atmosphere and resulting in high weld metal nitrogen contents. Kotecki also reported that increasing welding currents cause a decrease in the deposit nitrogen content. Increasing the current during flux-cored arc welding results in a higher wire electrode feed rate, which means that more metal per unit time passes through a given arc volume. Any nitrogen in the weld pool is diluted by the additional metal, resulting in a decreasing nitrogen content with increasing current.

Neuschutz *et al*[38] heated liquid steel in a tundish with argon-stabilised plasma arcs in order to study the influence of changes in the characteristics of the arc on the enhanced dissolution of nitrogen. The authors performed experiments with the plasma torch operating in three different configurations, namely DCEP (direct current electrode positive), AC (alternating current), and DCEN (direct current electrode negative). Nitrogen dissolution results for these different arc configurations showed that the lowest nitrogen levels were found when melting was performed under DCEP conditions, and the highest nitrogen contents under

DCEN conditions. The authors concluded that the rate of nitrogen pick-up during arc melting is determined by mass transport in the melt and by the rate of nitrogen desorption in the arc-free area of the molten pool, and suggested that the arc polarity affects nitrogen dissolution mainly by influencing stirring in the weld pool. The impact of the arc agitates the melt, thereby enhancing mass transport in the weld pool, and increasing the rate of nitrogen absorption. The melt is more strongly agitated with the torch serving as cathode (DCEP) than as anode (DCEN).

The results obtained by Kuwana and Kokawa[19] and Kuwana *et al*[28] for pure nitrogen shielding gas cannot be applied directly to gas tungsten arc welding in pure argon or argon-nitrogen shielding gas mixtures. Lower nitrogen levels in the arc atmosphere will probably change the relationship between the weld metal nitrogen content and the welding parameters. This is evidenced by the contradictory influence of the arc length on the weld metal nitrogen content as reported by Kuwana *et al*[28] and Kotecki[37].

1.7 KINETICS OF NITROGEN DESORPTION AND ABSORPTION DURING WELDING

The results published by Kuwana *et al*[27] described in §1.4.2 suggest that a kinetic approach may be more appropriate than a thermodynamic method for describing the dissolution of nitrogen in high alloy steels and stainless steels. This approach has not been investigated yet, with the majority of published kinetic studies focussing on the absorption and desorption of injected nitrogen gas in liquid iron melts in view of the practical importance of the control of the nitrogen content of steels. A notable exception is a study by Katz and King[21] who investigated the kinetics of nitrogen absorption and desorption from liquid iron during arc melting. Even though greater volumes of molten metal are involved and the melting times are longer, arc melting is thought to provide some insight into the behaviour of nitrogen during welding due to the presence of a plasma phase above the melt. The model developed by Katz and King[21] is considered below.

1.7.1 The Katz and King[21] model for nitrogen absorption and desorption during arc melting

Katz and King[21] studied the absorption and desorption kinetics of nitrogen during the arc melting of iron. The authors allowed samples to melt under a pure argon atmosphere and then changed to the appropriate mixed argon-nitrogen shielding gas atmosphere. Samples for chemical analysis were removed at one minute intervals, starting immediately after switching from pure argon to the mixed argon-nitrogen shielding gas. The nitrogen content of the liquid iron was found to increase with time until a steady-state value was reached, sometimes indicated by the escape of well-defined nitrogen bubbles from the surrounding melt. After reaching this plateau value, the nitrogen desorption reaction was investigated by changing back to pure argon shielding gas. A typical experimental plot of the nitrogen content of arc-melted iron as a function of melting time is shown in Figure 1.28. The curves characteristically exhibit three regions: absorption, the steady-state plateau and, finally, a region of desorption. Katz and King initiated their investigation into the kinetics of nitrogen absorption by studying nitrogen desorption kinetics as a prelude to understanding the absorption process. Their kinetic model is described in the following section.

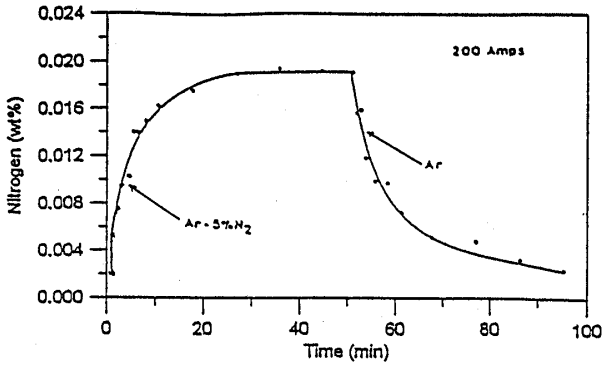

Figure 1.28 The nitrogen content of an arc-melted iron sample as a function of time for an Ar-5% nitrogen plasma.

a. Nitrogen desorption kinetics:

Katz and King studied the desorption of nitrogen from liquid iron into flowing argon during arc melting, based on the assumption that the following elementary steps, equations (1.31) to (1.35), apply to the desorption reaction, summarised by equation (1.36):

Elementary steps:

$$2N^{MB}\ (wt\%) = 2N^{MBL}\ (wt\%) \quad \ldots(1.31)$$

$$2N^{MBL}\ (wt\%) + 2\ sites = 2N\ (ads) \quad \ldots(1.32)$$

$$2N\ (ads) = N_2\ (ads) + site \quad \ldots(1.33)$$

$$N_2\ (ads) = N_2^{GMS}\ (g) + site \quad \ldots(1.34)$$

$$\underline{N_2^{GMS}\ (g) = N_2^{GB}\ (g)} \quad \ldots(1.35)$$

$$2N^{MB}\ (wt\%) = N_2^{GB}\ (g) \quad \ldots(1.36)$$

where: the superscript ^{MB} refers to the bulk metal,
the superscript ^{GB} refers to the bulk gas,
the superscript ^{MBL} refers to the metal-boundary layer, and
the superscript ^{GMS} refers to the gas-metal surface.

Katz and King observed both first- and second-order kinetics during their investigation, depending on the composition, and in particular the surface active element concentration, of the alloy. Alloys containing high levels of surface active elements displayed second-order desorption kinetics, whereas alloys with low concentrations of these elements displayed first-order kinetics.

- Second-order kinetics:

Katz and King observed that the association of two adsorbed nitrogen atoms to form a nitrogen molecule at the metal surface, reaction (1.33), is rate-limiting in alloys containing surface active elements. For a reaction which is second order with respect to dissolved nitrogen, the initial apparent rate of desorption is expressed as:

$$-\left(\frac{d\underline{N}(wt\%)}{dt}\right)_{t=0} = k^{app}[N_i(wt\%)]^2 - k^{app}P_{N_2}K' \quad \ldots(1.37)$$

where: k^{app} is the apparent rate constant for the desorption reaction, and

N_i is the initial nitrogen content of the melt (wt%).

Since desorption during the experiments occurred into pure argon, $P_{N_2} = 0$, and as the initial nitrogen content is the same as the steady-state value, the initial apparent rate equation reduces to:

$$-\left(\frac{d\underline{N}(wt\%)}{dt}\right)_{t=0} = k^{app}[N_{ss}(wt\%)]^2 \qquad \ldots(1.38)$$

where: N_{ss} is the steady-state nitrogen content of the melt (wt%).

The initial rate of desorption divided by the steady-state nitrogen content squared is equal to the initial apparent rate constant for desorption:

$$k^{app} = \frac{-\left(\frac{d\underline{N}(wt\%)}{dt}\right)_{t=0}}{[N_{ss}(wt\%)]^2} \qquad \ldots(1.39)$$

The initial rate of desorption can be obtained directly from plots such as Figure 1.28 by measuring the slope.

Katz and King's results indicate that the association of two adsorbed nitrogen atoms to form a nitrogen molecule at the surface (step (1.33)) is rate-limiting (as shown by the linear fit in Figure 1.29), with the apparent rate constant of the following form:

$$k^{app} = k^{bs}\,(1 - \theta_T)^2 \qquad \ldots(1.40)$$

where: k^{bs} is apparent rate constant on the bare melt surface, and

$1 - \theta_T$ is the total fraction of vacant surface sites (or the surface availability).

The total fraction of vacant sites (the surface availability) is given as:

$$(1-\theta_T) = \frac{1}{1 + K_O{}^{ads}(wt\%\,O) + K_S{}^{ads}(wt\%\,S)} \qquad \ldots(1.41)$$

where: $\log K_O^{ads} = \frac{12995}{T} - 4{,}96$, and

$K_S{}^{ads}$ is equal to 67 and 65 per wt% S at 1550°C and 1600°C, respectively.

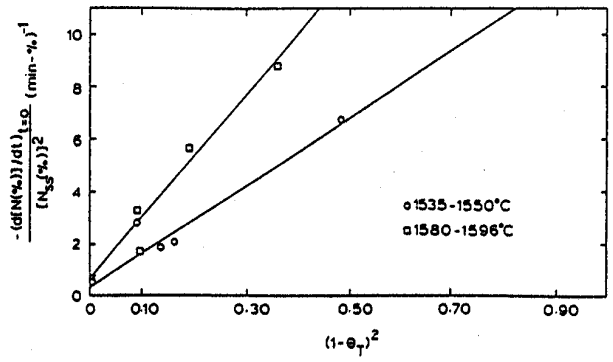

Figure 1.29 Initial apparent rate constants for desorption as a function of surface availability squared[21].

It is evident that the initial rate of desorption is second order with respect to nitrogen and proportional to $(1-\theta_T)^2$.

The specific and apparent rate constants are related as follows:

$$k^{spec} = k^{app}\frac{V}{A} \qquad \ldots(1.42)$$

where: V is the melt volume, and

A is the melt area.

The second-order integrated rate equation is obtained by integrating from $\underline{N}$(wt%) = $\underline{N}_{ss}$ (wt%), to $\underline{N}$(wt%) = $\underline{N}_t$(wt%) to obtain:

$$k^{app}t = \frac{1}{\underline{N}_t(wt\%)} - \frac{1}{\underline{N}_{ss}(wt\%)} \qquad \ldots(1.43)$$

where: $\underline{N}_t$(wt%) is the nitrogen content of the melt at time t.

- First-order kinetics:

For melts with low levels of surface-active elements, Katz and King reported that the second-order form of the integrated rate equation does not fit the data well. For these melts, a plot of the rate equation as a function of time is parabolic. These results are better represented by the first-order integrated rate equation which produces a more linear plot. The rate constants were found to correlate with superheat rather than surface coverage. Superheat was calculated by subtracting the liquidus temperature of the iron melt from the actual melt temperature. Since a plot against superheat produces the best correlation (refer to Figure 1.30), the first-order behaviour observed in this study seems to indicate that mass transport in the melt is the rate-limiting step.

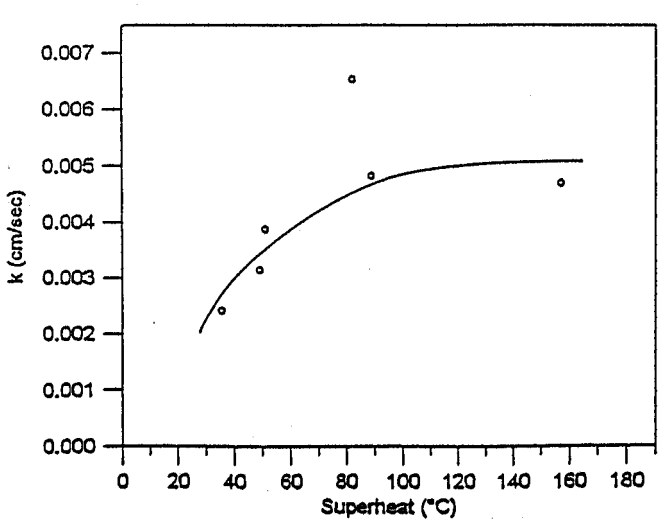

Figure 1.30 First-order rate constants for desorption vs. superheat.

b. Nitrogen absorption kinetics:

Katz and King studied nitrogen absorption kinetics during the arc melting of iron by assuming that the absorption process can be divided into the following sequence of steps:

1. the rate of supply of nitrogen,
2. mass transport through the gas-boundary layer,
3. chemical reaction control, and
4. mass transport through the melt-boundary layer.

Their investigation showed a first-order dependence with respect to nitrogen, which is consistent with mass transport through the melt-boundary layer. The surface-active element concentration was found to have a significant influence on the steady-state nitrogen content and the initial rate of absorption. Mass transfer in the melt appeared to be rate-limiting, and the rate constant was proportional to $(1-\theta_T)^{-1}$.

The initial rate of nitrogen absorption is dependent on the nitrogen content of the plasma. In general, the higher the nitrogen content, the higher the absorption rate. Based on the results shown in Figure 1.31, Katz and King concluded that the initial rate of nitrogen absorption is proportional to $(1-\theta_T)^{-1}[N_e(wt\%)]$. Examination of this figure, however, suggests that the initial rate of absorption is less dependent on $(1-\theta_T)$ than proposed by these authors.

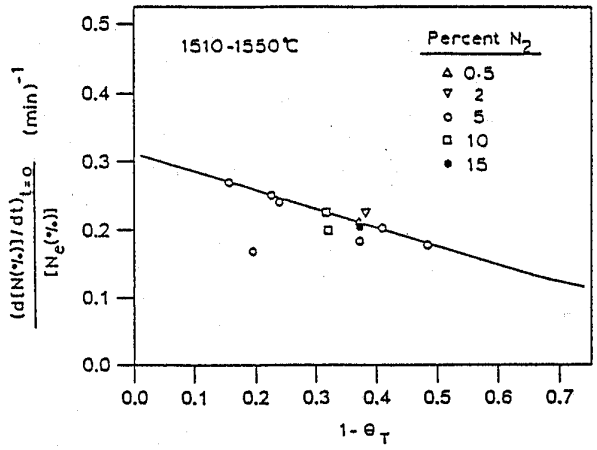

Figure 1.31 Initial rate of absorption divided by the equilibrium nitrogen content as a function of surface availability.

- The forward rate constant and nitrogen potential:

So far, the rate of absorption has been shown to be first order with respect to atomic nitrogen and limited by mass transfer in the melt. Two more parameters, however, are needed to characterise the absorption process fully: the forward rate constant and the atomic nitrogen potential of the arc. As shown earlier, the atomic nitrogen potential of the plasma arc exceeds the equilibrium value. The melt nitrogen content in equilibrium with the atomic nitrogen potential of the plasma arc will be denoted by $[N_f(wt\%)]$. The initial rate of absorption has been demonstrated experimentally to have the form shown in equation (1.44).

$$\left(\frac{d\underline{N}(wt\%)}{dt}\right)_{t=0} = k_F A\ [N_e(wt\%)] \qquad \ldots(1.44)$$

where: k_F is the forward rate constant,
N_e(wt%) is the equilibrium nitrogen content of the melt, and
A is a constant.

Since the steady-state nitrogen content exceeds [N_e(wt%)], the initial rate of absorption can be expressed as:

$$\left(\frac{d\underline{N}(wt\%)}{dt}\right)_{t=0} = k_F[N_f(wt\%)] \qquad \ldots(1.45)$$

where: [N_f (wt%)] is the nitrogen content of a melt in equilibrium with the atomic nitrogen potential of the plasma arc.

It then follows that [N_f(wt%)] = A[N_e(wt%)], i.e. the atomic nitrogen potential of the arc is proportional to the equilibrium nitrogen potential. Since there are two unknowns, [N_f(wt%)] and k_F, they can be solved for if there are two independent equations relating them. The first is simply the initial rate of absorption (equation (1.45)). The second is provided by the steady-state condition. At steady-state, absorption under the arc is balanced by desorption over the remainder of the melt surface. The condition is represented by the following equation:

$$k_F\{[N_f(\text{wt\%})] - [N_{ss}(\text{wt\%})]\} = k_B\{[N_e(\text{wt\%})^2 - [N_{ss}(\text{wt\%})]^2\} \qquad \ldots(1.46)$$

where: k_B is the backward rate constant.

Substituting to eliminate [N_f(wt%)]:

$$\left(\frac{dN(wt\%)}{dt}\right)_{t=0} - k_F[N_{ss}(wt\%)] = k_B\{[N_e(wt\%)]^2 - [N_{ss}(wt\%)]^2 \qquad \ldots(1.47)$$

This equation may be solved if k_F is the only unknown. Values for k_B, [N_{ss}(wt%)], {dN(wt%)/dt}$_{t=0}$, k_F and [N_f(wt%)^{ss}] can be obtained from Figure 1.29. The specific forward rate constant can now be calculated for a particular surface coverage and plasma impingement area. Since the rate of mass transfer in the melt is rate-limiting, the specific forward rate constant is the same as the mass transfer coefficient.

Melt mass transfer in a transferred plasma system is complex and can be influenced by at least four factors: electromagnetic stirring, natural convection, momentum transfer from impingement of the plasma jet and surface tension-driven flow. The only dependence of melt mass transfer observed in this study, as determined through measurement of the absorption rate at constant N_e(wt%), was with the concentration of surface-active elements. Katz and King concluded that surface tension-driven flow, i.e. Marangoni convection, is an important, if not dominant, contribution to melt mass transfer in the plasma furnace.

The Katz and King kinetic model appears to provide a promising approach to the modelling of nitrogen absorption and desorption during welding, even though the model has to be adjusted to incorporate the influence of alloying elements and welding parameters.

1.8 CONCLUSIONS

The nitrogen content of welds cannot be predicted using relationships, such as Sievert's law, derived under equilibrium conditions. Several researchers have reported nitrogen contents in weld metal far in excess of the values predicted under equilibrium conditions. This has been attributed to the presence of monatomic nitrogen in the arc plasma, formed as a result of the partial dissociation of diatomic nitrogen. A number of thermodynamic models have been developed to describe nitrogen dissolution in welds, but these models are generally highly simplified and do not consider several of the factors known to influence nitrogen absorption and desorption. These factors include the alloying element content of the weld metal, the prior nitrogen content and the surface active element concentration of the weld, and the weld parameters. Results published by Kuwana *et al* for nitrogen dissolution in stainless steel suggest that a kinetic approach may be more appropriate than a thermodynamic method for describing the dissolution of nitrogen in high alloy steels and stainless steels. Katz and King developed a kinetic model for nitrogen dissolution in iron under arc melting conditions, but such an approach has not yet been attempted for high alloy steels.

1.9 REFERENCES

1. J.F. Lancaster, "Metallurgy of welding". Abington Publishing, Cambridge. 1999.
2. R. Franks, W.O. Binder, and J. Thompson, "Austenitic chromium-manganese-nickel steels containing nitrogen". Transactions of the American Society for Metals, vol. 47. 1955. pp. 231-266.
3. A.L. Schaeffler, "Constitution diagram for stainless steel weld metal". Metal Progress, vol. 56, no. 11. 1949. pp. 680-680B.
4. R.P. Reed, "Nitrogen in austenitic stainless steels". JOM. March 1989. pp. 16-21.
5. V.F. Zackay, J.F. Carlson, and P.L. Jackson, "High nitrogen austenitic Cr-Mn steels". Transactions of the American Society for Metals, vol. 8. 1956. pp. 508-525.
6. R.K. Okagawa, R.D. Dixon, and D.L. Olson, "The influence of nitrogen from welding on stainless steel weld metal microstructures". Welding Journal, vol. 62, no. 8. August 1983. pp. 204s-209s.
7. M. Janik-Czachor, E. Lunarska, and Z. Szklarska-Smialowska, "Effect of nitrogen content in a 18Cr-5Ni-10 Mn stainless steel on the pitting susceptibility in chloride solutions". Corrosion, vol. 31, no. 11. 1975. pp. 394-398.
8. T. Ogawa, S. Aoki, T. Sakamoto, and T. Zaizen, "The weldability of nitrogen-containing austenitic stainless steel: Part I - Chloride pitting corrosion resistance". Welding Journal, vol. 6, no. 5. 1982. pp. 139-148.
9. T.A. Mozhi, W.A.T. Clark, K. Nishimoto, W.B. Johnson, and D.D. MacDonald, "The effect of nitrogen on the sensitisation of AISI 304 stainless steel". Corrosion, vol. 41, no. 10. 1985. p. 555-559.
10. R. Beneke, and R.F. Sandenbergh, "The influence of nitrogen and molybdenum on the sensitisation properties of low-carbon austenitic stainless steels". Corrosion Science, vol. 29, no. 5. 1989. pp 543-555.
11. P.D. Blake, "Nitrogen in steel weld metals". Metal Construction. April 1979. pp. 196-197.
12. L. Coudurier, D.W. Hopkins, and I. Wilkomirsky, "Fundamentals of Metallurgical Processes", 2nd Edition. Pergamon Press, Oxford. 1985.
13. K. Mundra, and T. DebRoy, "A general model for partitioning of gases between a metal and its plasma environment", Metallurgical and Materials Transactions B, vol. 26B. February 1995. pp. 149-157.

14. R.D. Pehlke, and J.F. Elliott, "Solubility of nitrogen in liquid iron alloys. 1. Thermodynamics", Transactions of the Metallurgical Society of AIME, vol. 218. December 1960. pp. 1088-1101.

15. H. Wada, and R.D. Pehlke, "Solubility of nitrogen in liquid Fe-Cr-Ni alloys containing manganese and molybdenum". Metallurgical Transactions B, vol. 8B. December 1977. pp. 675-682.

16. J.F. Lancaster (ed.), "The Physics of Welding". Pergamon Press, Oxford. 1984.

17. A. Bandopadhyay, A. Banerjee, and T. DebRoy, "Nitrogen activity determination in plasmas". Metallurgical Transactions B, vol. 23B. April 1992. pp. 207-214.

18. V.I. Lakomskii, and G.F. Torkhov, "Absorption of nitrogen from a plasma by liquid metal". Soviet Physics - Doklady, vol. 13, no. 11. May 1969. pp. 1159-1161.

19. T. Kuwana, and H. Kokawa, "The nitrogen absorption of iron weld metal during gas tungsten arc welding". Transactions of the Japan Welding Society, vol. 17, no. 1. April 1986. pp. 20-26.

20. P.D. Blake, and M.F. Jordan, "Nitrogen absorption during the arc melting of iron". Journal of the Iron and Steel Institute. March 1971. pp. 197-200.

21. J.D Katz, and T.B. King, "The kinetics of nitrogen absorption and desorption from a plasma arc by molten iron". Metallurgical Transactions B, vol. 20B. April 1989. pp. 175-185.

22. G. den Ouden, and O. Griebling, "Nitrogen absorption during arc welding". Proceedings of the 2nd International Conference on Trends in Welding Research, Gatlinburg, USA. 14-18 May 1989. ASM International. pp. 431-435.

23. S.A. Gedeon, and T.W. Eagar, "Thermochemical analysis of hydrogen absorption in welding", Welding Journal, vol. 69, no. 7. July 1991. pp. 264s-271s.

24. S.A. Gedeon, "Hydrogen assisted cracking of high strength steel welds". PhD Thesis, MIT. June 1987.

25. T.A. Palmer, and T. DebRoy, "Physical modeling of nitrogen partition between the weld metal and its plasma environment". Welding Journal, vol. 75, no. 7. July 1996. pp. 197s-207s.

26. P.A.A. Khan, "Mass transfer during laser welding of high manganese stainless steels". PhD Thesis, Pennsylvania State University. 1987. pp. 72-74.

27. T. Kuwana, H. Kokawa, and M. Saotome, "Quantitative prediction of nitrogen absorption by steel during gas tungsten arc welding". 3rd International Seminar on the Numerical Analysis of Weldability. Graz-Seggau, Austria. 25-27 September 1995.

28. T. Kuwana, H. Kokawa, and K. Naitoh, "The nitrogen absorption of stainless steel weld metal during gas tungsten arc welding". Transactions of the Japan Welding Society, vol. 17, no. 2. October 1986. pp. 117-123.

29. A.A. Howe, "Estimation of liquidus temperatures for steels". Iron and Steelmaking, vol. 15, no. 3. 1988. pp. 134-142.

30. E. Schürmann, M. Djurdjevic, and L. Nedeljkovic, "Calculation of liquidus temperature of low and high alloyed iron base melts from their chemical composition by means of the equivalence factors". Steel Research, vol. 68, no. 3. 1997. pp. 101-106.

31. N. Suutala, "Effect of manganese and nitrogen on the solidification mode in austenitic stainless steel welds". Metallurgical Transactions A, vol. 13A. December 1982. pp. 2121-2130.

32. Y. Arata, F. Matsuda, and S. Saruwatari, "Varestraint test for solidification crack susceptibility in weld metal of austenitic stainless steels". Transactions of the JWRI, vol. 3. 1974. pp. 79-88.

33. T. Ogawa, K. Suzuki, and T. Zaizen, "The weldability of nitrogen-containing austenitic stainless steel: Part II - Porosity, cracking and creep properties". Welding Journal, vol. 63, no. 7. July 1984. pp. 213s-223s.

34. M. Uda, and S. Ohno, "Effect of surface active elements on nitrogen content of iron under arc melting". Transactions of the National Research Institute of Metallurgy, vol. 15, no. 1. 1973. pp. 20-28.

35. O.P. Sinha, and R.C. Gupta, "Fe-Cr melt nitrogenation when exposed to nitrogen plasma". ISIJ International, vol. 33, no. 5. 1993. pp. 567-576.

36. M. Uda, and S. Ohno, "Spattering phenomenon for iron-nitrogen system during arc melting". Transactions of the National Research Institute of Metallurgy, vol. 20, no. 6. 1978. pp. 16-23.

37. D.J. Kotecki, "Welding parameter effects on open-arc stainless steel weld metal ferrite". Welding Journal, vol. 57, no. 4. 1978. pp. 109s-117s.

38. Neuschutz, Y. Zhai, and A. Hauck, "Nitrogen transfer into plasma heated steel melts as a function of arc polarity". Steel Research, vol. 65, no. 6. 1994. pp. 219-224.

CHAPTER 2

OBJECTIVES OF THE INVESTIGATION

The preceding literature survey illustrated that the absorption and desorption of nitrogen during welding are complex phenomena influenced by a number of different factors, such as the nature of the species present in the arc plasma, the weld metal alloying content and the welding parameters. Most of the theoretical models currently available in literature describe nitrogen absorption and desorption from autogenous iron or carbon steel welds and may not be appropriate for describing these processes in more highly alloyed stainless steel welds. This investigation aimed at examining the influence of a number of factors on the absorption and desorption of nitrogen during the autogenous welding of stainless steel. The variables examined during the course of the investigation were selected on the basis of the preceding literature survey to quantify the role of certain factors not addressed by currently available literature, to clarify inconsistencies in the existing literature, and to investigate the interaction between these variables in practice. The influence of the following factors on the behaviour of nitrogen during the welding of stainless steel was investigated:

- the shielding gas composition,
- the base metal nitrogen content prior to welding, and
- the surface active element concentration in the weld metal.

In order to examine the influence of each of these factors on the nitrogen content of stainless steel welds, the compositions of the parent metal and the shielding gas were adjusted to produce an experimental matrix quantifying the influence of each variable individually and in combination. The experimental procedure followed during the course of this investigation is described in Chapter 3. In order to avoid the introduction of too many variables, the same welding parameters (welding current, arc length, travel speed and shielding gas flow rate) were used during all the experiments, except where otherwise indicated. Following the experimental work, a kinetic model was derived to explain the results obtained. This model is described in Chapter 5.

CHAPTER 3

EXPERIMENTAL PROCEDURE

This chapter describes the experimental procedure followed during the course of the investigation and aims to examine the influence of the shielding gas composition, the base metal nitrogen content prior to welding and the surface active element concentration in the weld metal on the absorption and desorption of nitrogen during the autogenous arc welding of stainless steel.

3.1 STAINLESS STEEL ALLOYS STUDIED

During the course of this investigation, the influence of autogenous welding on the nitrogen content of eight stainless steel alloys was evaluated. The chemical compositions of these alloys are shown in Table 3.1. The first six alloys in the table are experimental alloys designed to have compositions similar to that of AISI type 310 stainless steel. Type 310 is a highly alloyed austenitic stainless steel that is normally produced without any deliberate nitrogen addition. It was selected as the base alloy for this investigation because it solidifies as austenite and remains fully austenitic down to room temperature. This prevents any bulk solid-state phase transformations, which can lead to changes in the solid-state nitrogen solubility in the alloy, from taking place after solidification. The last two alloys listed in Table 3.1 are commercially available stainless steels included in this investigation as reference samples. Cromanite is a nitrogen-alloyed austenitic stainless steel produced by Columbus Stainless, and AISI 304 is a general-purpose austenitic grade with no deliberate nitrogen addition.

Table 3.1 Chemical compositions of the stainless steel alloys investigated (percentage by mass, balance iron).

Alloy	Comments	Cr	Ni	Mn	Si	C	S	N
VFA 657	Low N, low S	24,4	20,1	1,91	1,60	0,075	**0,023**	**0,005**
VFA 658	Medium N, low S	24,6	19,9	1,89	1,63	0,080	**0,023**	**0,105**
VFA 659	High N, low S	24,3	19,9	1,93	1,63	0,085	**0,022**	**0,240**
VFA 752	Low N, high S	24,6	19,5	1,99	1,51	0,087	**0,052**	**0,006**
VFA 753	Medium N, high S	24,5	19,3	1,89	1,61	0,082	**0,061**	**0,097**
VFA 755	High N, high S	24,5	19,3	1,90	1,55	0,079	**0,049**	**0,280**
Cromanite	-	18,1	0,59	9,74	0,29	0,036	0,004	0,511
AISI 304	-	18,2	8,10	1,75	0,48	0,029	0,009	0,078

In order to study the influence of the base metal nitrogen content on nitrogen absorption and desorption during welding, the experimental type 310 alloys listed in Table 3.1 were produced with three different nitrogen concentrations:

- a *low* nitrogen level (residual nitrogen content of approximately 0,005%),
- a *medium* nitrogen level (approximately 0,1%), and

- a *high* nitrogen level (approximately 0,25%). This nitrogen level corresponds to the equilibrium nitrogen solubility limit in this steel calculated at a temperature of 1600ºC and a nitrogen pressure of 1 atmosphere using Wada and Pehlke's activity coefficients and interaction parameters[1].

The influence of the surface active element concentration in the steel on nitrogen absorption and desorption during welding was evaluated by producing each of the low, medium and high nitrogen type 310 experimental alloys described above at two different sulphur concentrations:

- a *low* sulphur content (approximately 0,02%), and
- a *high* sulphur content (approximately 0,05%).

This provides for a matrix of six experimental alloys with varying nitrogen and sulphur contents, as shown in Table 3.1. As an alternative to varying the sulphur content of the base metal, small amounts of oxygen can be added to the shielding gas during welding, thereby varying the absorbed oxygen content of the weld metal. Varying the sulphur content of the base metal was preferred during this investigation because it provides more accurate control of the surface active element concentration of the weld metal.

3.2 WELDING PROCEDURE

All the stainless steel samples were rolled to a thickness of 6 mm, thoroughly ground to remove any scale or surface oxides and degreased using acetone. Welding was performed using an automatic autogenous (i.e. no filler metal was added to the weld pool during welding) gas tungsten arc welding (GTAW) process in an enclosed glove box. Direct current electrode negative polarity and a 2% thoriated tungsten electrode, ground to an included angle of 90°, were used. The experimental arrangement is shown in Figure 3.1. The glove box was flushed with pure argon for at least fifteen minutes prior to welding, and a low argon flow rate was maintained through the box during welding to ensure a slight positive pressure inside the glove box. This was deemed necessary to avoid contamination from the surrounding atmosphere due to air entrapment in the arc during welding. Shielding was supplied by shielding gas flowing through the welding torch at a pressure of 1 atmosphere and a flow rate of 20 ℓ/minute. Welding was performed using a welding current of 150 A and an arc length of 2 mm (corresponding to an arc voltage of approximately 17 to 20 V, depending on the shielding gas composition). The welding speed was maintained at a level of 2,7 mm/s using an automatic tractor that moved the plate to be welded at a constant speed relative to the stationary welding torch.

3.3 MEASURING THE WELD POOL TEMPERATURE DURING WELDING

In order to compare the actual nitrogen content of each weld with the calculated equilibrium nitrogen solubility limit, the weld pool temperature is required for substitution into Wada and Pehlke's equations[1] described in §1.2.3 of the literature survey. An indication of the temperature of the molten weld metal during welding was obtained by measuring the temperature of the centre of the weld pool, based on the assumption that rapid convection in the weld pool ensures a fairly homogeneous temperature distribution in the molten metal during welding. The temperature measurement was performed by inserting a

thermocouple into the weld pool behind the arc during welding. The thermocouple was shielded from exposure to the arc by a ceramic sheath that left only the fused end of the wires uncovered. Accurate placement of the thermocouple in the center of the pool was facilitated by an adjustable steel guide tube attached to the main body of the welding torch and the thermoelectric signal from the thermocouple was recorded using a calibrated XY-recorder. The experimental arrangement is shown in Figure 3.2.

Figure 3.1 Experimental arrangement for autogenous welding.

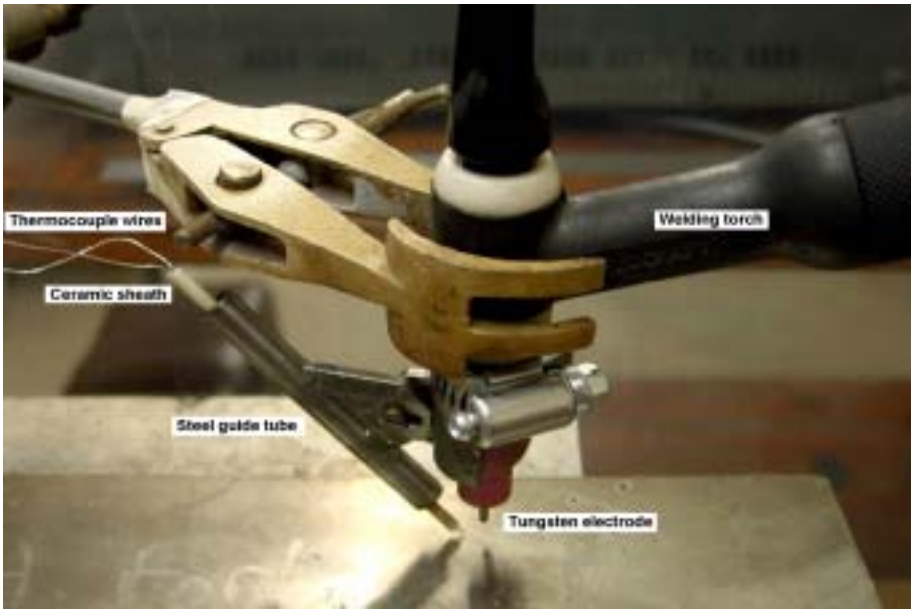

Figure 3.2 Experimental arrangement for measuring the weld pool temperature.

Initial experiments using this arrangement and the welding parameters described in §3.2 above were unsuccessful since the weld pool proved to be too shallow to allow full insertion of the thermocouple without fusing the wires to the bottom of the pool. Kuwana *et al*[2] performed similar experiments and concluded that the weld pool temperature during autogenous arc welding is not influenced to any significant extent by the welding current, but is determined principally by the liquidus temperature of the

alloy (as illustrated by equation (1.23) in Chapter 1). Based on the conclusions of these authors, the welding current was raised in an attempt to increase the size and depth of the weld pool, while maintaining the arc length and travel speed at the values described above. In order to confirm Kuwana *et al*'s[2] conclusions, the weld pool temperature was measured and compared at two different welding currents, 300 A and 350 A. Two measurements were performed at each current setting. The results proved to be very repeatable and no significant differences were detected between the temperatures measured at the different welding currents. The conclusion can therefore be drawn that the weld pool temperature during autogenous gas tungsten arc welding is not a strong function of the welding current, and that the temperatures measured at high current values will be equally valid at a current of 150 A.

3.4 THE INFLUENCE OF THE SHIELDING GAS NITROGEN CONTENT ON THE NITROGEN SOLUBILITY OF STAINLESS STEEL WELDS

Pure argon and four premixed shielding gases, listed below, were used during the course of the project to evaluate the influence of nitrogen additions to argon shielding gas on the absorption and desorption of nitrogen by stainless steel alloys:

- pure argon,
- argon – 1,09% N_2 shielding gas mixture,
- argon – 5,3% N_2 shielding gas mixture,
- argon – 9,8% N_2 shielding gas mixture, and
- argon – 24,5% N_2 shielding gas mixture.

All the stainless steel alloys listed in Table 3.1 were welded using these shielding gases and the welding procedure described in §3.2. After welding the beads were examined visually and the weld metal nitrogen content of each sample was analysed using an inert gas fusion analysis technique, taking care to remove the metal drillings required for analysis only from the weld. At least two analyses were performed on each sample to ensure adequate repeatability.

3.5 THE MINIMUM SHIELDING GAS NITROGEN CONTENT THAT LEADS TO THE EVOLUTION OF NITROGEN BUBBLES FROM THE WELD POOL DURING WELDING

As illustrated in §1.3, nitrogen dissolution during arc welding does not obey Sievert's law. The weld metal nitrogen content increases rapidly with an increase in the shielding gas nitrogen content at low nitrogen partial pressures, followed by steady-state behaviour where the weld reaches saturation and nitrogen absorption from the arc is balanced by nitrogen evolution from the weld pool[3]. This steady-state region is generally associated with violent degassing and bubble formation. In order to avoid severe nitrogen losses from nitrogen-alloyed stainless steels and to prevent the formation of nitrogen-induced porosity in welds, the shielding gas nitrogen content has to be limited to avoid initiating steady-state behaviour. The minimum shielding gas nitrogen content associated with the onset of steady-state behaviour was determined during the autogenous welding of each of the alloys listed in Table 3.1 by using a range of argon-nitrogen shielding gases, mixed using a system of flow meters. The flow meters

were calibrated to supply shielding gas with the desired argon-nitrogen ratio at a total flow rate of 20 ℓ/min to the welding torch. The shielding gas nitrogen content was increased from 0,5% to 5% in 0,5% increments, and the arc, weld pool and completed weld examined visually during and after welding to determine the minimum shielding gas nitrogen level associated with the onset of significant desorption during welding. This point was generally characterised by severe degassing, spattering and violent metal expulsion from the molten weld metal. The nitrogen contents of the welds corresponding to the onset of steady-state behaviour in each alloy were determined using inert gas fusion analysis techniques.

The series of experiments described above therefore aims at determining the influence of the shielding gas composition (argon-nitrogen ratio) and the weld metal chemical composition (base metal nitrogen and surface active element concentration) on nitrogen absorption and desorption during the welding of stainless steel. The results obtained during the investigation are described in Chapter 4.

3.6 REFERENCES

1. H. Wada, and R.D. Pehlke, "Solubility of nitrogen in liquid Fe-Cr-Ni alloys containing manganese and molybdenum". Metallurgical Transactions B, vol. 8B. December 1977. pp. 675-682.
2. T. Kuwana, H. Kokawa, and K. Naitoh, "The nitrogen absorption of stainless steel weld metal during gas tungsten arc welding". Transactions of the Japan Welding Society, vol. 17, no. 2. October 1986. pp. 117-123.
3. P.D. Blake, and M.F. Jordan, "Nitrogen absorption during the arc melting of iron". Journal of the Iron and Steel Institute. March 1971. pp. 197-200.

CHAPTER 4

RESULTS AND DISCUSSION

This chapter presents the results of the experiments described in the preceding chapter and demonstrates that nitrogen dissolution in the molten weld pool during autogenous arc welding is influenced to a significant extent by the nitrogen content of the shielding gas and the chemical composition of the weld metal, in particular the base metal nitrogen content prior to welding and the surface active element concentration.

4.1 THE WELD POOL TEMPERATURE DURING WELDING

A typical experimentally measured temperature profile, represented by the recorded thermoelectric voltage signal from a thermocouple immersed in the molten weld pool, is shown in Figure 4.1. The temperature measured by the thermocouple increases rapidly on insertion in the weld pool, and then stabilises at a plateau value that was assumed to be equal to the temperature of the central region of the weld pool. On removal of the thermocouple from the molten metal, the measured temperature rapidly decreases to ambient temperature, as shown in Figure 4.1.

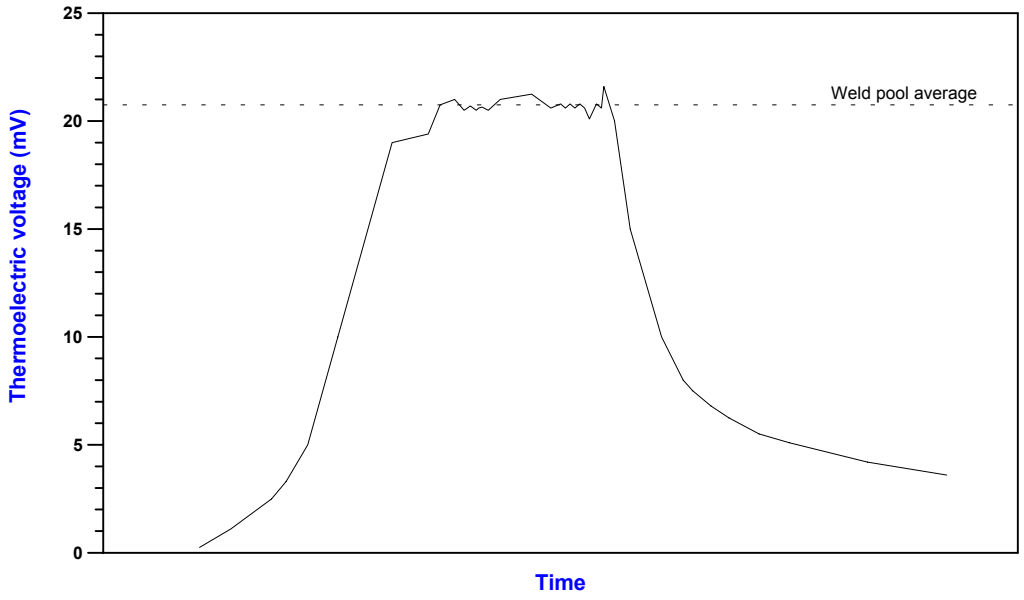

Figure 4.1 Typical thermoelectric voltage signal measured by a thermocouple inserted in the weld pool.

As described in §3.3, four weld pool temperature measurements were performed – two at a welding current of 300 A and two more at a welding current of 350 A. The four measurements yielded an average weld pool temperature of 1722°C ± 14°C. The results were very repeatable and no significant differences were detected between the temperatures measured at the two different welding currents. The difference

between the measured temperature and the liquidus temperature (the liquidus temperature of the experimental type 310 alloys is approximately 1500°C[1]) is greater than the 100°C difference proposed by Kuwana *et al*[2] in equation (1.23), but this can probably be attributed to a difference in the welding parameters (arc voltage and travel speed) employed by these authors, as compared to the current investigation. The experimentally measured weld pool temperature can now be substituted into equations (1.4) and (1.5) in the literature survey to calculate the equilibrium nitrogen solubility limit at the relevant nitrogen partial pressures in each of the experimental alloys.

4.2 THE INFLUENCE OF THE SHIELDING GAS NITROGEN CONTENT ON THE NITROGEN SOLUBILITY OF STAINLESS STEEL WELDS

4.2.1 Visual observations

Except for Cromanite and VFA 755 (the high nitrogen, high sulphur experimental alloy), no evidence of porosity or degassing was found in any of the samples welded in pure argon or argon-1,09% N_2 mixtures. The welds generally exhibited smooth profiles with very little ripple formation on the surface. An example of such a weld is shown in Figure 4.2. The Cromanite welds, however, showed severe porosity after welding in pure argon and Ar-1,09% N_2 shielding gas mixtures, often containing blow holes with diameters in excess of 1 mm (as shown in Figure 4.3). Autogenous welding of Cromanite in the presence of these shielding gases was also associated with unstable weld pools, severe spattering, flashes of light, a hissing sound and the violent expulsion of liquid metal droplets from the weld pool. Extreme cases of such instability resulted in the formation of a deposit on the surface of the tungsten electrode. Bennett and Mills[3] studied the weldability of a number of nitrogen-containing austenitic stainless steels and found this electrode deposit to be rich in tungsten, containing iron, chromium, manganese and some silicon. They attributed this behaviour to the evolution of nitrogen from the liquid metal that expels molten droplets from the weld pool during welding. The conclusion can be drawn that the nitrogen solubility limit in Cromanite was exceeded during welding, resulting in the nucleation of nitrogen bubbles in the weld pool. Some of these bubbles escaped, causing spatter and metal expulsion, while some were trapped by the advancing solidification front, resulting in the formation of blow holes in the solidified weld metal. The Cromanite weld metal appeared to be very viscous during welding, exhibiting coarse ripples and irregular bead surfaces after solidification. VFA 755 displayed smooth weld pool profiles and porosity-free welds after welding in pure argon, but spattering and bubble formation became evident with the addition of 1,09% nitrogen to the shielding gas.

At higher nitrogen levels in the shielding gas (i.e. 5,3% N_2, 9,8% N_2 and 24,5% N_2) all the alloys evaluated, including Cromanite and type 304 stainless steel, exhibited unstable weld pools and spattering during welding, resulting in uneven weld surfaces and visible porosity after welding. An increase in the base metal nitrogen concentration of the experimental alloys appeared to increase the amount of degassing and spattering during welding, whereas an increase in the shielding gas nitrogen content raised the amount of porosity in the welds. An example of such a weld is shown in Figure 4.4. The Cromanite

welds, however, exhibited less visible porosity, although welding was associated with violent gas evolution, spattering, flashes and very uneven weld profiles (as shown in Figure 4.5). This indicates that nitrogen was evolved from the weld pool during welding, even though less porosity was visible in the weld metal after welding. Although the presence of blowholes in the weld metal confirms that nitrogen desorption occurred during welding, it must be emphasised that the absence of porosity after solidification does not rule out the possibility that nitrogen evolution took place. Degassing and bubble formation were often observed during the welding of samples that displayed no visible porosity after cooling. It is postulated that any nitrogen bubbles formed in these welds escaped to the atmosphere prior to solidification, causing the observed spattering and flashing phenomena. As a result, the presence or absence of porosity in the weld metal after welding cannot be used to gauge whether nitrogen desorption took place during welding. Visual observation of the molten weld pool proved to be a more accurate way of determining whether nitrogen bubble evolution occurred.

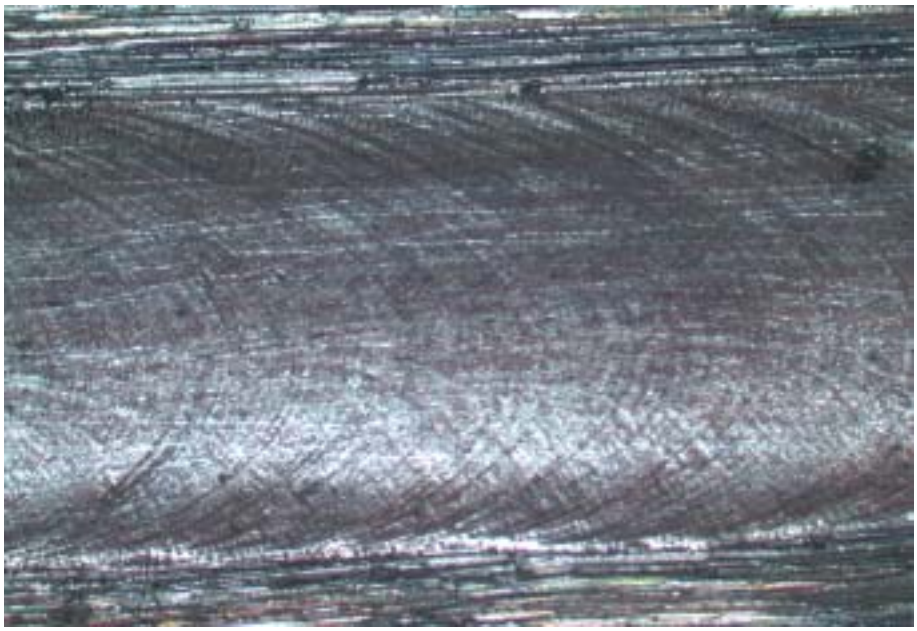

Figure 4.2 Surface appearance of VFA 752 (low N, high S) welded in pure argon. Magnification: 8x.

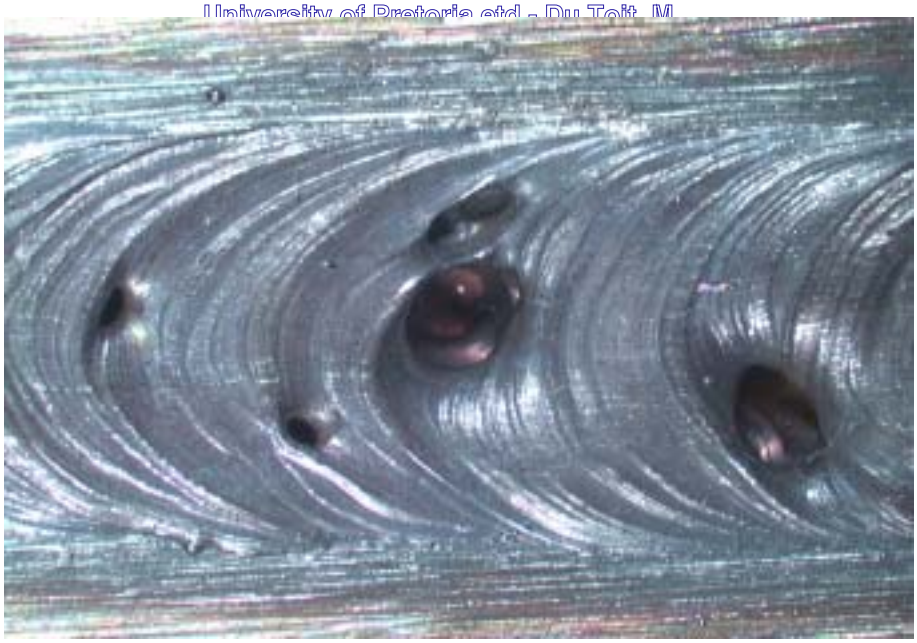

Figure 4.3 Surface appearance of Cromanite welded in pure argon. Magnification: 8x.

Figure 4.4 Surface appearance of VFA 752 (low N, high S) welded in an Ar-24,5%N_2 shielding gas atmosphere. Magnification: 8x.

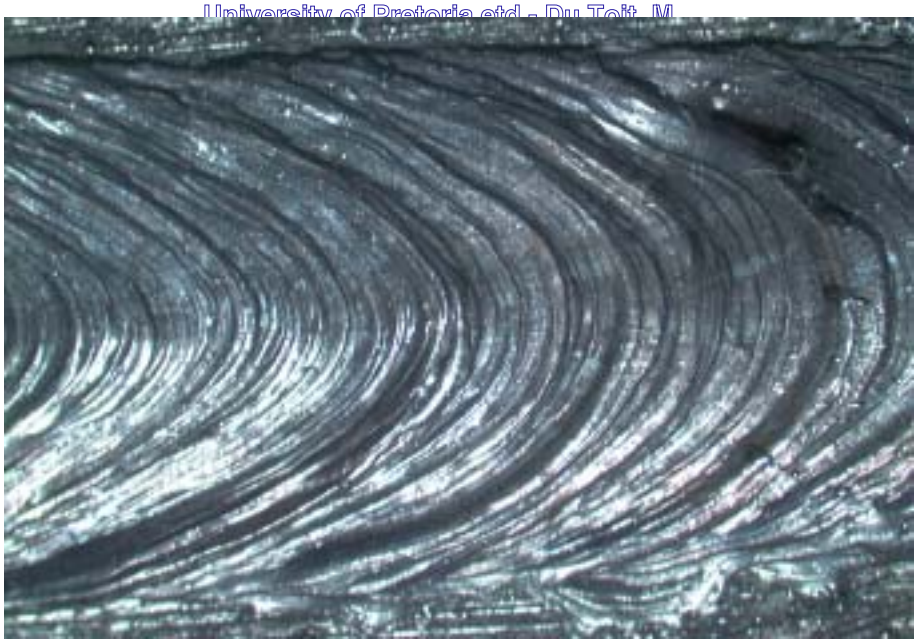

Figure 4.5 Surface appearance of Cromanite welded in an Ar-24,5%N_2 shielding gas atmosphere. Magnification: 8x.

4.2.2 Weld metal nitrogen contents

The average weld metal nitrogen contents measured in the different samples are given in Table 4.1, and represented graphically in Figures 4.6, 4.7 and 4.8 for the low sulphur, high sulphur and commercial alloys (Cromanite and AISI 304), respectively. The equilibrium nitrogen solubility limit, also shown in Figures 4.6, 4.7 and 4.8, was calculated at the measured weld pool temperature (1722°C) for each nitrogen partial pressure using Wada and Pehlke's coefficients and interaction parameters[4].

Table 4.1 Average weld metal nitrogen contents of the different welded samples (percentage by mass).

Alloy	Comments	Base metal N content	Weld metal N content for various shielding gas compositions				
			Pure Ar	Ar-1,09%N_2	Ar-5,3%N_2	Ar-9,8%N_2	Ar-24,5%N_2
VFA 657	Low N, low S	0,005%	0,017%	0,082%	0,196%	0,242%	0,257%
VFA 658	Medium N, low S	0,105%	0,105%	0,166%	0,230%	0,245%	0,270%
VFA 659	High N, low S	0,240%	0,216%	0,240%	0,267%	0,265%	0,277%
VFA 752	Low N, high S	0,006%	0,016%	0,082%	0,180%	0,184%	0,194%
VFA 753	Medium N, high S	0,097%	0,118%	0,150%	0,220%	0,230%	0,226%
VFA 755	High N, high S	0,280%	0,271%	0,280%	0,331%	0,325%	0,330%
Cromanite	-	0,511%	0,433%	0,450%	0,528%	0,550%	0,686%
AISI 304	-	0,078%	0,094%	0,172%	0,240%	0,303%	0,336%

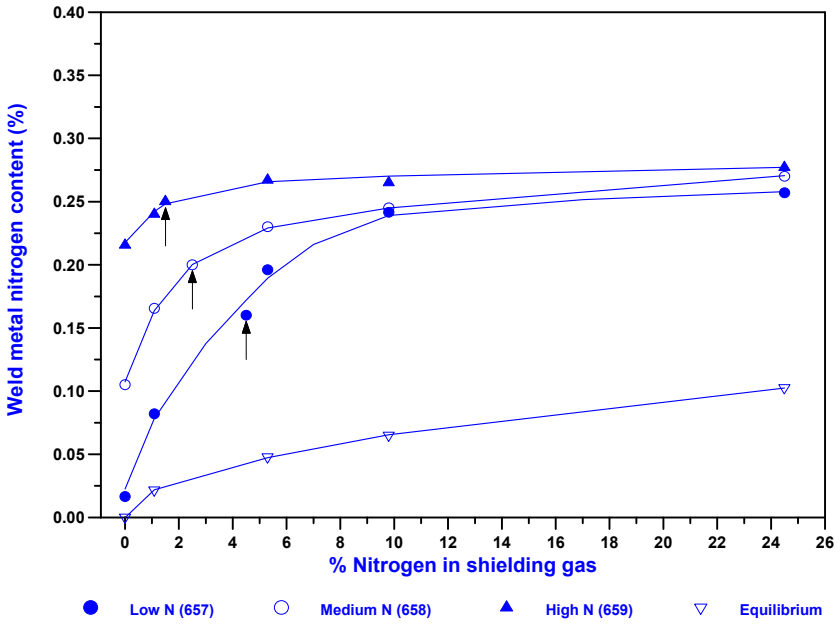

Figure 4.6 Weld metal nitrogen concentration as a function of the shielding gas nitrogen content for the experimental low sulphur alloys. The arrows indicate the onset of bubble formation during welding.

The influence of nitrogen additions to argon shielding gas on the nitrogen content of the autogenous welds appears to be consistent with that described in literature for carbon steels and stainless steels (refer to Figures 1.5, 1.6 and 1.20). The weld metal nitrogen content initially increases as the shielding gas nitrogen content increases, and then reaches a constant steady-state value that is independent of the actual nitrogen partial pressure. This steady-state level is associated with a dynamic equilibrium where the rate of absorption of nitrogen is balanced by the evolution of nitrogen from the melt[5]. At all nitrogen partial pressures investigated the nitrogen content of the weld metal exceeds the equilibrium solubility limit calculated at the weld pool temperature. This is consistent with available literature[5,6,7,8] and confirms that

Sievert's law is not obeyed during arc welding. The high nitrogen solubility limit in the presence of an arc plasma is generally attributed to the presence of monatomic nitrogen in the arc[8,9,10].

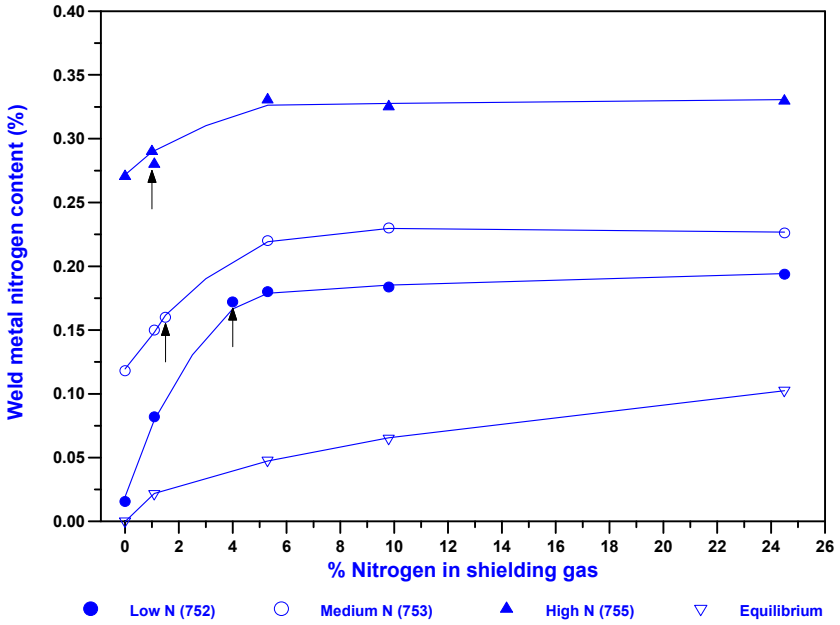

Figure 4.7 Weld metal nitrogen concentration as a function of the shielding gas nitrogen content for the experimental high sulphur alloys. The arrows indicate the onset of bubble formation during welding.

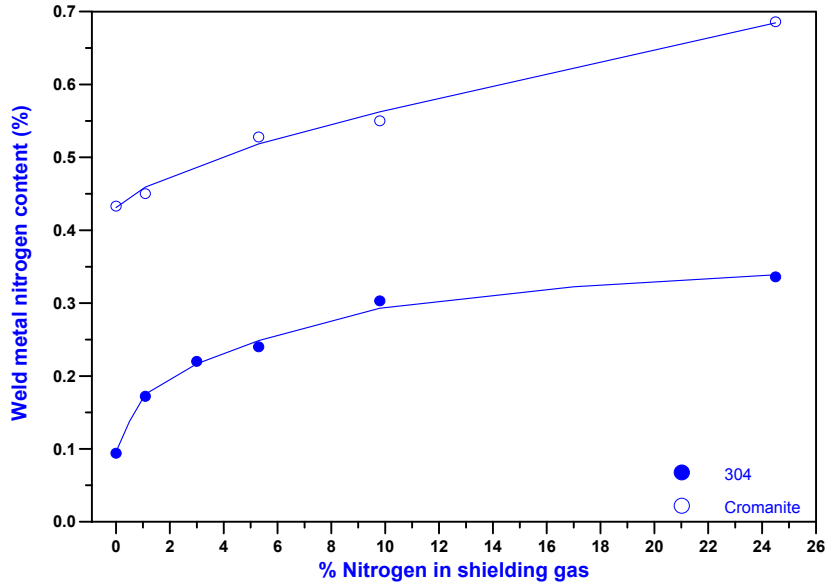

Figure 4.8 Weld metal nitrogen concentration as a function of the shielding gas nitrogen content for the commercial alloys.

It is interesting to note that the influence of the base metal nitrogen content on the absorption and desorption of nitrogen during welding appears to be dependent on the surface active element

concentration in the metal. In the case of the low sulphur alloys (Figure 4.6), an increase in the initial nitrogen level of the base metal causes an increase in the weld metal nitrogen content at low nitrogen partial pressures in the shielding gas. At higher nitrogen partial pressures, the nitrogen content of the welds approaches a steady-state value that is very similar for all three low sulphur alloys and virtually independent of the base metal nitrogen content. In the case of the high sulphur alloys (Figure 4.7), an increase in the base metal nitrogen content results in higher weld metal nitrogen contents over the entire range of nitrogen partial pressures evaluated, including a significant increase in the steady-state nitrogen concentration. This is contrary to the conclusions of Okagawa *et al*[11] and Suutala[12] who reported that the nitrogen content of welds is not influenced by the base metal nitrogen content prior to welding. This inconsistency can probably be attributed to the low base metal nitrogen and sulphur levels in the alloys studied by these authors (0,025% N and 0,009% S in the alloys studied by Okagawa *et al*[11] and between 0,008 and 0,076% N in the alloys investigated by Suutala[12]).

In order to explain the results described above, Figures 4.6 and 4.7 were redrawn in the form of Figures 4.9 and 4.10 to examine the influence of sulphur concentration on the low and high nitrogen alloys, respectively. Figure 4.9 shows that a high weld metal sulphur content reduces the steady-state nitrogen concentration in the case of the low nitrogen alloys (VFA 657 and VFA 752). This suggests that, in the absence of significant amounts of nitrogen in the base metal prior to welding, the surface active element concentration mainly influences the rate of nitrogen absorption from the arc atmosphere. The validity of this conclusion will be examined in Chapter 5. The sulphur content also has a significant influence on the weld metal nitrogen content in alloys containing high levels of base metal nitrogen (VFA 659 and VFA 755), with higher sulphur concentrations leading to considerably higher levels of nitrogen after welding (as shown in Figure 4.10). High base metal nitrogen contents also seem to increase the level of supersaturation in the weld metal over that required to nucleate nitrogen bubbles at atmospheric pressure. Since a higher sulphur concentration in the weld metal implies increased weld pool surface coverage, the higher nitrogen levels measured in the presence of an increased surface active element concentration suggest that, in the presence of high levels of base metal nitrogen, the nitrogen desorption reaction is retarded. This is consistent with the results shown in Figure 1.24 for iron-oxygen alloys, and with the findings of Battle and Pehlke[13] and Katz and King[10], who found the nitrogen desorption rate constant to be proportional to $(1-\theta_\Gamma)^2$, where $(1-\theta_\Gamma)$ is the total fraction of vacant surface sites (as shown in Figure 4.11). The influence of sulphur on the rate of nitrogen desorption during welding is expected to be more significant than its influence on the rate of the absorption reaction, since nitrogen evolution from the weld pool requires two surface sites for the adsorption and recombination of nitrogen atoms to form each N_2 molecule, whereas the absorption of monatomic nitrogen from the arc plasma requires only one surface site per atom dissolved (as shown in equations (1.10) to (1.12) in Chapter 1).

It is therefore postulated that a high nitrogen absorption rate in alloys with low base metal nitrogen contents, in conjunction with a high desorption rate in alloys with high base metal nitrogen levels, allows the weld metal nitrogen content of the low sulphur alloys to approach a steady-state value that is not influenced to any significant extent by the initial nitrogen content of the base metal (as shown in Figure

4.6). In the high sulphur alloys, the higher surface active element concentration retards the rate of nitrogen evolution from the weld pool by occupying a high fraction of the surface sites required for the recombination of nitrogen atoms to form N_2. As a result, more of the nitrogen initially present in the base metal is maintained in solution in the weld pool and the original nitrogen content is therefore expected to have a more significant influence on the subsequent weld nitrogen content (as confirmed by Figure 4.7). This is consistent with the results of Arata *et al*[14], who showed that the total weld metal nitrogen content is the sum of the residual nitrogen content of the base metal and any nitrogen picked up from the interaction between the shielding gas and the molten weld metal. The validity of these conclusions will be considered in Chapter 5 where the nitrogen absorption and desorption reaction rate constants are determined as a function of the surface active element concentration in the experimental alloys.

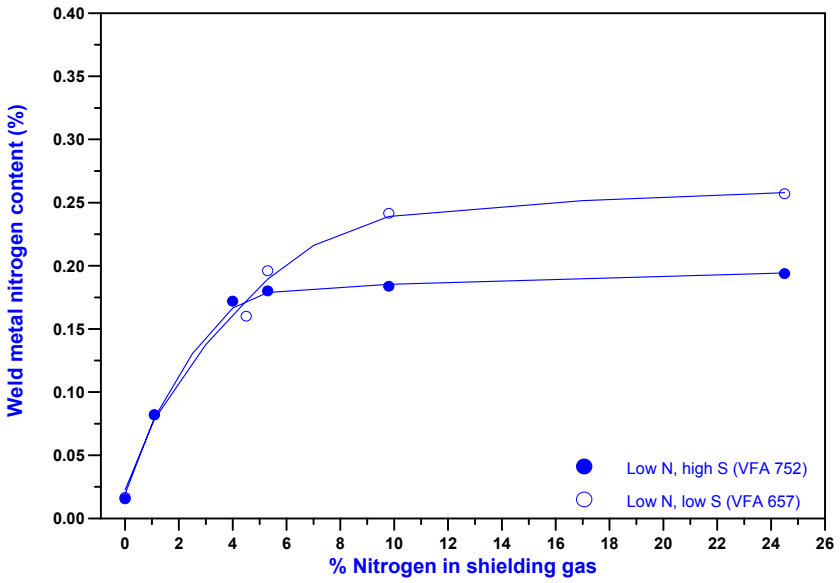

Figure 4.9 The influence of sulphur concentration on the weld metal nitrogen contents of the experimental low nitrogen alloys (VFA 657 and VFA 752).

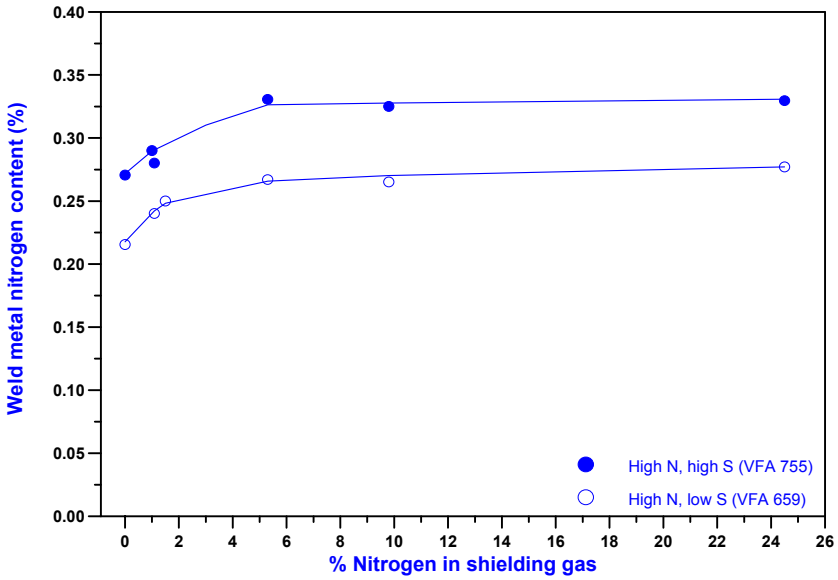

Figure 4.10 The influence of sulphur concentration on the weld metal nitrogen contents of the experimental high nitrogen alloys (VFA 659 and VFA 755).

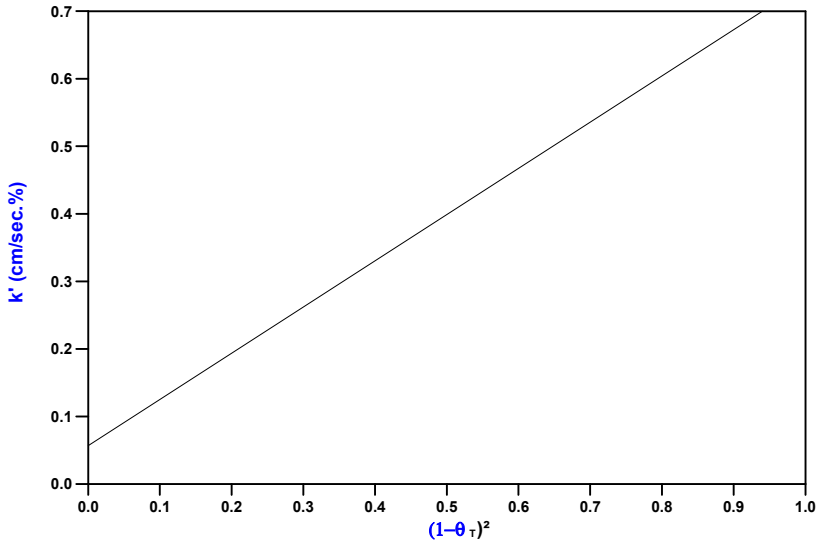

Figure 4.11 The initial apparent rate constant, k', for nitrogen desorption from liquid iron during plasma arc melting as a function of the surface availability, $(1-\theta_T)$[10].

The nitrogen contents of autogenous AISI 304 and Cromanite welds also increase with an increase in the nitrogen content of the shielding gas at low nitrogen partial pressures, followed by steady-state behaviour at higher partial pressures (Figure 4.8). The weld metal nitrogen content of Cromanite is significantly higher than that of AISI 304 over the entire range of partial pressures evaluated. This can be attributed to the higher initial nitrogen concentration in Cromanite, and the high chromium and manganese contents, which increase the nitrogen solubility limit in this steel. The rapid initial increase in the weld metal

nitrogen content with an increase in nitrogen partial pressure is not as evident in the case of Cromanite since steady-state behaviour initiates at a much lower shielding gas nitrogen content in this steel than in any of the other alloys investigated.

4.3 THE MINIMUM SHIELDING GAS NITROGEN CONTENT THAT LEADS TO NITROGEN BUBBLE FORMATION IN THE WELD POOL DURING WELDING

In order to determine the minimum shielding gas nitrogen content necessary to initiate steady-state behaviour, and consequently nitrogen bubble formation, in each of the alloys investigated, the shielding gas nitrogen content was increased from 0,5% to 5% in 0,5% increments during welding. The observed behaviour of the arc and weld pool during welding and the visual appearance of the completed weld as a function of the shielding gas nitrogen content are described in Table 4.2 (following page) for each of the alloys investigated (with the exception of Cromanite). Cromanite was not evaluated since it displays violent degassing and spattering, even in the absence of any nitrogen in the shielding gas during welding. Based on the visual observations described in Table 4.2, the minimum shielding gas nitrogen content that leads to nitrogen desorbtion and degassing from the weld pool and the corresponding weld metal nitrogen contents are shown in Table 4.3 for the experimental alloys and type 304.

Table 4.2 Experimental observations of the welding arc and weld pool during welding and the visual appearance of the completed weld of each of the experimental alloys and type 304 stainless steel as a function of the shielding gas nitrogen content during welding.

A. Alloy	Shielding gas composition									
	Ar - 0,5% N_2	Ar - 1,0% N_2	Ar - 1,5% N_2	Ar - 2,0% N_2	Ar - 2,5% N_2	Ar - 3,0% N_2	Ar - 3,5% N_2	Ar - 4,0% N_2	Ar - 4,5% N_2	Ar - 5,0% N_2
AISI 304	No degassing or visible porosity, smooth profile	No degassing or visible porosity, smooth profile	No degassing or visible porosity, smooth profile	Limited bubble formation, smooth profile, no porosity	Limited bubble formation and instability, smooth profile, no porosity	Spattering and degassing, no visible porosity	Periodic spattering and degassing, no visible porosity	Severe spattering and degassing, some visible porosity	Severe spattering and degassing, visible porosity	Severe spattering and degassing, visible porosity
VFA 657 Low N, low S	No degassing or visible porosity, smooth profile	No degassing or visible porosity, smooth profile	No degassing or visible porosity, smooth profile	No degassing or visible porosity, smooth profile	No degassing or visible porosity, smooth profile	No degassing or visible porosity, smooth profile	No degassing or visible porosity, smooth profile	Slight bubble formation and instability, no visible porosity, smooth profile	Degassing, pool instability and flashing, no spattering or visible porosity	Degassing and flashing, no spattering or visible porosity
VFA 658 Medium N, low S	No degassing or visible porosity, smooth profile	No degassing or visible porosity, smooth profile	No degassing or visible porosity, smooth profile	Limited bubble formation, smooth profile, no visible porosity	Pool slightly unstable, degree of degassing, no visible porosity	Pool slightly unstable, degree of degassing, periodic flashing, no visible porosity	Severe spattering and degassing, some visible porosity	Severe spattering and degassing, visible porosity	Severe spattering and degassing, visible porosity	Severe spattering and degassing, visible porosity
VFA 659 High N, low S	Limited periodic instability, smooth weld profile, no visible porosity	Limited bubble formation and spattering, smooth profile, no porosity	Severe spattering and degassing, no visible porosity	Severe spattering and degassing, no visible porosity	Severe spattering and degassing, no visible porosity	Severe spattering and degassing, no visible porosity	Severe spattering and degassing, some visible porosity	Severe spattering and degassing, visible porosity	Severe spattering and degassing, visible porosity	Severe spattering and degassing, visible porosity
VFA 752 Low N, high S	No degassing or visible porosity, smooth profile	No degassing or visible porosity, smooth profile	Limited bubble formation, smooth profile, no visible porosity	Limited bubble formation, smooth profile, no porosity	Limited bubble formation, smooth profile, no porosity	Limited bubble formation, pool stable, smooth profile, no visible porosity	Periodic spattering and degassing, uneven weld profile, no visible porosity	Slight bubble formation and instability, no visible porosity, smooth profile	Slight bubble formation and instability, no visible porosity, smooth profile	Degassing, spattering and flashing, uneven weld profile, little visible porosity
VFA 753 Medium N, high S	No degassing or visible porosity, smooth profile	No degassing or visible porosity, smooth profile	Periodic degassing, no visible porosity	Periodic degassing, no visible porosity	Severe spattering and degassing, some visible porosity	Severe spattering and degassing, some visible porosity	Severe spattering and degassing, visible porosity	Severe spattering and degassing, visible porosity	Severe spattering and degassing, visible porosity	Severe spattering and degassing, visible porosity
VFA 755 High N, high S	Limited bubble formation, smooth weld profile, no instability or porosity	Severe spattering and degassing, no visible porosity	Severe spattering and degassing, no visible porosity	Severe spattering and degassing, some visible porosity	Severe spattering and degassing, some visible porosity	Severe spattering and degassing, some visible porosity	Severe spattering and degassing, visible porosity	Severe spattering and degassing, visible porosity	Severe spattering and degassing, visible porosity	Severe spattering and degassing, visible porosity

Table 4.3 Minimum shielding gas nitrogen content required to initiate steady-state behaviour and bubble formation (percentage by mass).

Alloy	Comments	Minimum shielding gas nitrogen content required to initiate degassing	Corresponding weld metal nitrogen content
VFA 657	Low N, low S	4,5 %	0,160%
VFA 658	Medium N, low S	2,5 %	0,200%
VFA 659	High N, low S	1,5 %	0,250%
VFA 752	Low N, high S	4,0 %	0,172%
VFA 753	Medium N, high S	1,5 %	0,160%
VFA 755	High N, high S	1,0 %	0,290%
AISI 304	-	3,0 %	0,220%

From the results shown in Table 4.3, it is evident that the minimum shielding gas nitrogen content required to initiate steady-state behaviour in the experimental alloys is a function of both the base metal nitrogen content of the alloy and the surface active element concentration. The results show that the weld metal saturation limit is reached at progressively lower shielding gas nitrogen contents as the base metal nitrogen level increases. This again confirms that the base metal nitrogen participates in the nitrogen absorption and desorption reactions during welding. Less nitrogen is required in the shielding gas to reach the saturation limit and initiate steady-state behaviour in the high sulphur alloys because an appreciable fraction of the nitrogen already present in the base metal is prevented from escaping by the higher level of surface coverage. A significant amount of the nitrogen present in the base metal prior to welding is therefore available to participate in the nitrogen absorption/desorption reactions in addition to any nitrogen absorbed from the shielding gas during welding. This is in agreement with the earlier results of this investigation and the conclusions of Arata *et al*[14] described in §4.2.2 above.

In the case of Cromanite, severe nitrogen degassing was evident even in the absence of nitrogen in the shielding gas during welding. This is consistent with the results shown above, which indicate that degassing initiates at lower shielding gas nitrogen levels as the base metal nitrogen content increases. The initial nitrogen content of Cromanite therefore appears to be sufficient to cause nitrogen degassing and to initiate steady-state behaviour in pure argon shielding gas.

4.4 CONCLUSIONS

- Nitrogen absorption and desorption processes in the presence of nitrogen-containing shielding gas during the autogenous welding of stainless steel do not obey Sievert's law. The weld metal nitrogen content initially increases with an increase in the shielding gas nitrogen content at low nitrogen partial pressures. At higher partial pressures a dynamic equilibrium is created where the amount of nitrogen absorbed by the weld metal is balanced by the amount of nitrogen evolved from the weld pool during welding.

- The nitrogen content of autogenous stainless steel welds is a function of the nitrogen partial pressure in the shielding gas, the base metal nitrogen content and the surface active element concentration in the weld metal. In alloys with low surface active element concentrations, the steady-state nitrogen content of the weld metal is not influenced to any significant extent by the base metal nitrogen content. In the case of alloys with high surface active element concentrations, an increase in the base metal nitrogen content results in higher weld metal nitrogen contents over the entire range of nitrogen partial pressures evaluated, including a significant increase in the steady-state nitrogen concentration. It is postulated that the surface active element concentration in the weld metal influences the nitrogen absorption and desorption rates by occupying surface sites required for the absorption of monatomic nitrogen from the arc plasma and the recombination of nitrogen atoms to form N_2 (desorption).
- The minimum shielding gas nitrogen content required to initiate steady-state behaviour and nitrogen bubble formation in the experimental alloys is also a function of the base metal nitrogen content of the alloy and the surface active element concentration. The weld metal saturation limit is reached at progressively lower shielding gas nitrogen contents as the base metal nitrogen level increases. It is postulated that less nitrogen is required in the shielding gas to reach the saturation limit in the high sulphur alloys because an appreciable fraction of the nitrogen already present in the base metal is prevented from escaping by the higher level of surface coverage.

The next chapter describes a kinetic model developed to examine and test the hypotheses developed in this chapter. The model aims at quantifying the influence of the base metal nitrogen content and the surface active element concentration on the rate of the nitrogen absorption and desorption reactions during welding.

4.5 REFERENCES

1. A.A. Howe, "Estimation of liquidus temperatures for steels". Iron and Steelmaking, vol. 15, no. 3. 1988. pp. 134-142.
2. T. Kuwana, H. Kokawa, and K. Naitoh, "The nitrogen absorption of stainless steel weld metal during gas tungsten arc welding". Transactions of the Japan Welding Society, vol. 17, no. 2. October 1986. pp. 117-123.
3. W.S. Bennett, and G.S. Mills, "GTA weldability studies on high manganese stainless steels". Welding Journal, vol. 53, no. 12. 1974. pp. 548s-553s.
4. H. Wada, and R.D. Pehlke, "Solubility of nitrogen in liquid Fe-Cr-Ni alloys containing manganese and molybdenum". Metallurgical Transactions B, vol. 8B. December 1977. pp. 675-682.
5. P.D. Blake, and M.F. Jordan, "Nitrogen absorption during the arc melting of iron". Journal of the Iron and Steel Institute. March 1971. pp. 197-200.
6. V.I. Lakomskii, and G.F. Torkhov, "Absorption of nitrogen from a plasma by liquid metal". Soviet Physics - Doklady, vol. 13, no. 11. May 1969. pp. 1159-1161.
7. T. Kuwana, and H. Kokawa, "The nitrogen absorption of iron weld metal during gas tungsten arc welding". Transactions of the Japan Welding Society, vol. 17, no. 1. April 1986. pp. 20-26.
8. G. den Ouden, and O. Griebling, "Nitrogen absorption during arc welding". Proceedings of the 2nd International Conference on Trends in Welding Research, Gatlinburg, USA. 14-18 May 1989. ASM International. pp. 431-435.

9. A. Bandopadhyay, A. Banerjee, and T. DebRoy, "Nitrogen activity determination in plasmas". Metallurgical Transactions B, vol. 23B. April 1992. pp. 207-214.

10. J.D Katz, and T.B. King, "The kinetics of nitrogen absorption and desorption from a plasma arc by molten iron". Metallurgical Transactions B, vol. 20B. April 1989. pp. 175-185.

11. R.K. Okagawa, R.D. Dixon, and D.L. Olson, "The influence of nitrogen from welding on stainless steel weld metal microstructures". Welding Journal, vol. 62, no. 8. August 1983. pp. 204s-209s.

12. N. Suutala, "Effect of manganese and nitrogen on the solidification mode in austenitic stainless steel welds". Metallurgical Transactions A, vol. 13A. December 1982. pp. 2121-2130.

13. T.D. Battle, and R.D. Pehlke, "Kinetics of nitrogen absorption and desorption by liquid iron and iron alloys". Ironmaking & Steelmaking, vol. 13, no. 4. 1986. pp. 176-189.

14. Y. Arata, F. Matsuda, and S. Saruwatari, "Varestraint test for solidification crack susceptibility in weld metal of austenitic stainless steels". Transactions of the JWRI, vol. 3. 1974. pp. 79-88.

CHAPTER 5

KINETIC MODEL OF NITROGEN ABSORPTION AND DESORPTION DURING WELDING

As discussed in §1.4.2, the results reported by Kuwana *et al*[1] suggest that a kinetic approach may be more appropriate than a thermodynamic method for describing the dissolution of nitrogen in high chromium alloy and stainless steel welds. In order to combine the results described in the previous chapter in a suitable theoretical framework, a kinetic model was developed to describe the absorption and evolution of nitrogen during the welding of stainless steel. The ultimate aim of the model is to predict the maximum amount of nitrogen that can be accommodated in the shielding gas before the onset of steady-state behaviour associated with degassing and nitrogen bubble formation. This will facilitate the addition of limited amounts of nitrogen to argon shielding gas during the autogenous welding of nitrogen-strengthened stainless steels, thereby preventing the nitrogen losses generally associated with autogenous welding of these alloys. Maintaining the shielding gas nitrogen content below the saturation level will prevent the formation of nitrogen-induced porosity during autogenous welding in practice.

5.1 OUTLINE OF THE KINETIC MODEL

The kinetic model is based on the following assumptions:

(a) Nitrogen enters the molten weld pool from two sources:

- the arc atmosphere, i.e. the dissolution of monatomic and diatomic nitrogen from the arc plasma into the liquid metal, and
- the nitrogen-containing base metal that melts at the leading edge of the weld pool during autogenous welding.

(b) Dissolved nitrogen is removed from the weld pool by:

- recombining to form nitrogen molecules which can escape to the atmosphere, and
- solidification of nitrogen-containing weld metal at the rear of the weld pool.

(c) Under steady-state conditions a state of dynamic equilibrium is created whereby the amount of nitrogen entering the weld pool is equal to the amount of nitrogen leaving the weld pool per unit time.

(d) The molten weld pool is completely covered by plasma using the welding parameters described in §3.2.

(e) The rate of solidification of the weld metal at the rear of the weld pool is proportional to the welding speed.

(f) Due to rapid convection in the molten weld metal, the pool is well mixed with a uniform nitrogen concentration. Rapid mass flow in the weld pool also ensures a fairly homogeneous temperature distribution in the molten metal during welding.

(g) The model is only valid under conditions where the evolution of nitrogen occurs at the weld pool surface and no bubble formation takes place in the weld metal.

The model is illustrated schematically in Figure 5.1 and considered below in more detail.

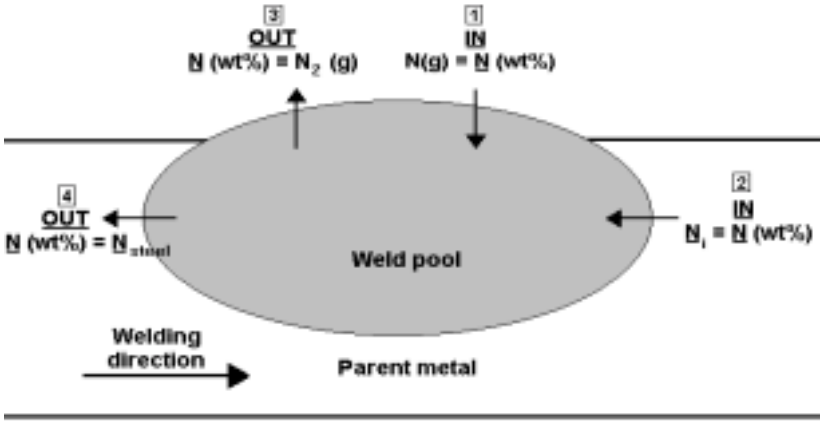

Figure 5.1 Schematic illustration of the proposed kinetic model for the absorption and desorption of nitrogen from autogenous stainless steel weld metal.

The proposed rate equations for the four processes responsible for nitrogen entering and leaving the molten weld pool, as illustrated in Figure 5.1, are given below:

(1) Nitrogen entering the weld pool from the arc atmosphere:

The absorption of monatomic nitrogen from the arc plasma, reaction (5.1), is best described by a first order rate equation, with the rate of mass transfer for this reaction represented by equations (5.2) and (5.3). Rewriting this expression in terms of mass percentages yields equation (5.4).

$$\mathrm{N\,(g)} \rightarrow \underline{\mathrm{N}}\,(\mathrm{wt\%}) \qquad \ldots(5.1)$$

$$\frac{dm_N}{dt} = Ak[N(g) - N_{eq}(g)] \qquad \ldots(5.2)$$

$$\therefore \quad \frac{dm_N}{dt} = Ak\left[N(g) - \frac{N_{steel}}{K}\right] \qquad \ldots(5.3)$$

$$\therefore \quad \frac{d\underline{N}(wt\%)}{dt} = \frac{100Ak}{\rho V}\left[N(g) - \frac{N_{steel}}{K}\right] \qquad \ldots(5.4)$$

where: $\frac{dm_N}{dt}$ is the rate of mass transfer of nitrogen (kg.s^{-1}),

A is the weld pool surface area (m^2),

k is the reaction rate constant for reaction (5.1) (kg.m^{-2}.s^{-1}.atm^{-1}),

N(g) is the monatomic nitrogen content of the welding arc (atm),

N_{eq}(g) is the monatomic nitrogen content of the arc plasma required for equilibrium with the nitrogen in the steel (atm),

N_{steel} is the weld metal nitrogen content (wt%),

K is the apparent equilibrium constant for reaction (5.1),

ρ is the density of the molten weld metal (kg.m^{-3}), and

V is the volume of the molten weld pool (m^3).

(2) Nitrogen entering the weld pool as a result of nitrogen-containing base metal melting at the leading edge of the weld pool:

If the weld pool has a length L, the time required to melt a volume of metal equal to the volume of the weld pool is equal to L/v, where v is the travel speed of the arc during welding. The melting rate of the base metal (in kg.s^{-1}) is therefore represented by equation (5.5).

$$\text{Melting rate} = \rho V\left(\frac{v}{L}\right) \qquad \ldots(5.5)$$

The rate of mass transfer of nitrogen from the base metal into the weld pool is then given by equation (5.6). Rewriting in terms of mass percentages yields equations (5.7) and (5.8):

$$\frac{dm_N}{dt} = \frac{N_i(wt\%)}{100}\rho V\left(\frac{v}{L}\right) \qquad \ldots(5.6)$$

$$\therefore \quad \frac{d(\%\underline{N})}{dt} = \frac{100}{\rho V}\frac{N_i(wt\%)}{100}\rho V\left(\frac{v}{L}\right) \qquad \ldots(5.7)$$

$$\therefore \quad \frac{d(\%\underline{N})}{dt} = N_i(wt\%)\left(\frac{v}{L}\right) \qquad \ldots(5.8)$$

where: N_i is the initial nitrogen content of the base metal (wt%).

(3) Nitrogen leaving the weld pool by recombining to form N_2:

The evolution of nitrogen from the weld metal is represented by equation (5.9), and the rate of mass transfer for this reaction by the second order rate equations (5.10) and (5.11). Rewriting this expression in terms of mass percentages yields equation (5.12).

$$2\underline{N}\ (wt\%) \rightarrow N_2\ (g) \qquad \ldots(5.9)$$

$$\frac{dm_N}{dt} = -k'A({N_{steel}}^2 - {N_{eq}}^2) \qquad \ldots(5.10)$$

$$\therefore \quad \frac{dm_N}{dt} = -k'A({N_{steel}}^2 - K'P_{N_2}) \qquad \ldots(5.11)$$

$$\therefore \quad \frac{d(\%\underline{N})}{dt} = -\frac{100Ak'}{\rho V}[{N_{steel}}^2 - K'P_{N_2}] \qquad \ldots(5.12)$$

where: k' is the reaction rate constant for reaction (5.9) (kg.m^{-2}.s^{-1}.[%N]$^{-2}$),

N_{eq} is the equilibrium nitrogen content of the molten metal at the weld pool temperature (wt%) for equilibrium with the nitrogen in the shielding gas,

K' is the apparent equilibrium constant for the reaction: $N_2\,(g) \rightarrow 2\underline{N}$ (wt%), and

P_{N_2} the nitrogen partial pressure in the shielding gas (atm).

(4) Nitrogen leaving the weld metal by resolidifying at the rear of the molten pool:

Since the solidification rate at the rear of the weld pool is equal to the melting rate (given by equation (5.5)), the rate at which nitrogen leaves the pool by resolidifying is represented by equation (5.13).

$$\frac{d(\%\underline{N})}{dt} = -N_{steel}\left(\frac{v}{L}\right) \qquad \ldots(5.13)$$

Assumption (c) listed above states that the amount of nitrogen entering the weld pool is equal to the amount of nitrogen leaving the weld pool per unit time under steady-state conditions. From the above, it follows that N_{steel} must be equal to the steady-state nitrogen content, N_{ss}, and the total of equations (5.4) and (5.8) must be equal to the total of equations (5.12) and (5.13) under steady-state conditions:

$$\therefore \quad \frac{100Ak}{\rho V}\left[N(g)-\frac{N_{ss}}{K}\right]+N_i(wt\%)\left(\frac{v}{L}\right)=\frac{100Ak'}{\rho V}[N_{ss}{}^2-K'P_{N_2}]+N_{ss}\left(\frac{v}{L}\right) \qquad \ldots(5.14)$$

Rearranging equation (5.14) to collect all the terms containing the steady-state nitrogen content, N_{ss} (wt%), on the left yields equation (5.15):

$$\frac{100Ak'}{\rho V}N_{ss}{}^2+\frac{v}{L}N_{ss}+\frac{100Ak}{\rho V}\frac{N_{ss}}{K}=\frac{100Ak'}{\rho V}K'P_{N_2}+\frac{100Ak}{\rho V}N(g)+\frac{v}{L}N_i(wt\%) \qquad \ldots(5.15)$$

For a specific shielding gas composition and set of welding parameters, the weld pool area, A, length, L, and volume, V, the monatomic nitrogen content of the arc, N(g), the welding speed, v, the density of the molten metal, ρ, the equilibrium constants, K and K', and the nitrogen partial pressure in the shielding gas, P_{N_2}, should remain constant, regardless of the base metal nitrogen content, N_i(wt%), and the surface active element concentration in the weld metal. The following conclusions can now be drawn from equation (5.15):

According to equation (5.15), the steady-state nitrogen content, N_{ss}(wt%), is dependent on the base metal nitrogen content, N_i(wt%), with an increase in the base metal nitrogen concentration leading to an increase in the steady-state nitrogen content. This has been observed experimentally, as shown in Figures 4.6 and 4.7. The extent of this dependence, however, is determined by the magnitude of the two reaction rate constants, k (for the absorption reaction) and k' (for the desorption reaction). Earlier results suggested that these rate constants vary with the surface active element concentration in the weld metal. In the low sulphur steels, desorption of nitrogen from the weld pool is rapid, leading to high values of k', whereas desorption is retarded in the high sulphur alloys, resulting in low k' values. The absorption rate constant, k, is not expected to be a strong function of the surface active element concentration. The values of the reaction rate constants for the experimental alloys will be determined in §5.2.5.

Due to the low desorption rate constant in the high sulphur alloys, equation (5.15) suggests that the steady-state nitrogen content is a strong function of the base metal nitrogen content, with N_{ss}(wt%) increasing as N_i(wt%) increases. This is consistent with the results shown in Figure 4.7. In the case of the low sulphur alloys, k' is expected to be higher and gas-metal (or plasma-metal) reactions should therefore play a more significant role in determining the steady-state nitrogen content. According to equation (5.15), the influence of the base metal nitrogen content on the steady-state weld metal nitrogen level is less pronounced in the presence of high k' values. This is consistent with the results shown in Figure 4.6.

5.2 VALUES OF THE CONSTANTS

In order to use equation (5.15) to predict the nitrogen content of the experimental alloys after welding, a number of constants, including the partial pressure of monatomic nitrogen in the arc, N(g), the weld pool surface area, A, volume, V, and length, L, the density of the molten metal, ρ, the two apparent equilibrium constants for the absorption and desorption reactions, K and K', and the two reaction rate constants, k and k', have to be determined. This section describes how the values of these constants were determined experimentally or calculated using relationships available in published literature.

5.2.1 Partial pressure of monatomic nitrogen in the arc plasma

The partial pressure of monatomic nitrogen in the arc plasma can be estimated using the method developed by Mundra and DebRoy[2] and Palmer and DebRoy[3] as part of the two-temperature model described in §1.4.1. These authors derived equation (5.17) for calculating the partial pressure of monatomic nitrogen formed as a result of the dissociation of molecular nitrogen, reaction (5.16), in the arc plasma:

$$\tfrac{1}{2}N_2\,(g) \rightarrow N\,(g) \qquad \ldots(5.16)$$

$$P_N = \sqrt{P_{N_2}}\exp\left(-\frac{\Delta G^0_{16,T_d}}{RT_d}\right) \qquad \ldots(5.17)$$

where: P_N *is* the partial pressure of monatomic nitrogen in the arc plasma (atm),
P_{N_2} is the partial pressure of diatomic nitrogen in the arc plasma (atm),
$\Delta G^0_{16,Td}$ is the standard free energy for reaction (5.16) at T_d,
T_d is the effective dissociation temperature of diatomic nitrogen, and
R is the universal gas constant (8,314 $J.K^{-1}.mol^{-1}$).

The extent of dissociation of diatomic nitrogen at T_d can be calculated from equation (5.17) if the values of P_{N_2}, T_d and $\Delta G^0_{16,Td}$ are known. Since the extent of dissociation of diatomic nitrogen is low under typical welding conditions, P_{N_2} can be assumed to be equal to the partial pressure of N_2 in the inlet gas. The free energy of formation of monatomic nitrogen from diatomic N_2, $\Delta G^0_{16,Td}$, used by Mundra and DebRoy[2] and Palmer and DebRoy[3] (given by equation (5.18)) was obtained from the compilation by Elliott and Gleiser[4]. However, the data in this reference appears to be in error, specifically with regards to the heat of formation of N from N_2. Elliott and Gleiser quote a value of 358,0 kJ/mol (of N), whereas Kubaschewski *et al*[5] report 472,7 kJ/mol. The latter value agrees exactly with the bond strength of the diatomic molecule of 945,44 kJ/mol (of N_2)[6]. It therefore appears that the value given by Elliott and Gleiser is in error.

$$\Delta G^0_{16,T} = 86596 - 15{,}659T \qquad \text{(cal/mol)} \qquad \ldots(5.18)$$

One implication of this is that the conclusion of Palmer and DebRoy[3] that the effective plasma temperature (as regards the dissociation of N_2) is 100°C higher than the metal surface temperature, is in error, because this conclusion was based on the data of Elliott and Gleiser[4]. In the current work, this inaccuracy was corrected by recalculating the "effective dissociation temperature" as that temperature

which yields - for the conditions of the Palmer and DebRoy[3] experiments – the same partial pressure of monatomic nitrogen when the Kubaschewski *et al*[5] data are used, as does the Elliott and Gleiser data at a temperature of 1400°C, which is 100°C higher than the surface temperature in the Palmer and DebRoy investigation. This yields a reassessed effective plasma temperature of 1933°C, or 633°C higher than the surface temperature – much higher than the value reported by Palmer and DebRoy.

If the surface temperature of the weld pool is assumed to be approximately equal to the measured weld pool temperature of 1722°C, the values of P_{N_2}, $\Delta G^0_{16,Td}$, T_d and R can be substituted into equation (5.17), and the partial pressure of monatomic nitrogen in the arc plasma can be estimated for all the shielding gas atmospheres used in this investigation. The calculated monatomic nitrogen partial pressures are shown in Table 5.1, taking into consideration that total atmospheric pressure in Pretoria, where the experiments were performed, is 0,86 atm.

Table 5.1 The estimated monatomic nitrogen partial pressure in the arc atmosphere as a function of the shielding gas nitrogen content for an effective plasma temperature of 2628 K.

Shielding gas nitrogen content	Nitrogen partial pressure, P_{N_2}	Monatomic nitrogen partial pressure, P_N
1,09 %	0,0094 atm	$8{,}43.10^{-8}$ atm
5,3 %	0,0456 atm	$1{,}86.10^{-7}$ atm
9,8 %	0,0843 atm	$2{,}53.10^{-7}$ atm
24,5 %	0,2107 atm	$4{,}00.10^{-7}$ atm

5.2.2 The weld pool surface area, *A*, length, *L*, and volume, *V*

The area and length of the weld pool were estimated by assuming that the crater at the end of each weld bead, where insufficient liquid metal was present to fill the depression created by the arc jet, has the same dimensions as the weld pool during welding. In order to determine these dimensions, the end craters of seven weld beads were photographed, and the resulting photographs enlarged. An example is shown in Figure 5.2. The maximum length of each crater was measured, taking into consideration the magnification, and the area was determined by superimposing the outline of the depression in each photograph on graph paper. The average values of the weld pool length and area determined using this method are shown in Table 5.2.

Table 5.2 Weld pool dimensions.

Weld pool surface area	$34{,}1 \pm 4{,}8$ mm^2
Weld pool length	$7{,}4 \pm 0{,}5$ mm
Weld pool volume	$63{,}9 \pm 6{,}3$ mm^3

The volume of the weld pool was estimated by sectioning two weld beads and photographing polished and etched cross sections. An example of such a photograph is shown in Figure 5.3. If it is assumed that the weld pool has the shape of a section of a sphere, equation (5.19) can be used to calculate the weld pool volume[7].

Figure 5.2 The end crater of a weld bead. Magnification: 10x.

Figure 5.3 A cross section of a weld bead. Magnification: 10x.

$$V = \frac{1}{3}\pi r^3(2 - 3\cos\theta + \cos^3\theta) \qquad \ldots(5.19)$$

where: r is the radius of the sphere, and

θ is the angle between the fusion line and the plate at the surface of the sample.

The average weld pool volume is shown in Table 5.2.

5.2.3 The apparent equilibrium constants, *K* and *K'*

- The apparent equilibrium constant for the desorption reaction, *K'*

If nitrogen desorption from the weld pool during welding is represented by equation (5.9), the apparent equilibrium constant, *K'*, for this reaction is given by equation (5.20).

$$K' = \frac{[N_{eq}(wt\%)]^2}{P_{N_2}} \qquad \ldots(5.20)$$

As described in §1.2.3, the equilibrium nitrogen content as a function of temperature can be calculated using equation (5.21)[8].

$$\log(\underline{N_{eq}}) = -\frac{247}{T} - 1{,}22 - \left(\frac{4780}{T} - 1{,}51\right)\log f_{N,1873} - \left(\frac{1760}{T} - 0{,}91\right)(\log f_{N,1873})^2 \qquad \ldots(5.21)$$

where: T is the temperature (K), and

$f_{N,1873}$ is the nitrogen activity coefficient f_N at 1873 K.

The activity coefficient, f_N, that is required for substitution in equation (5.21) can be calculated from the chemical composition of the steel using equation (5.22).

$$\begin{aligned}\log f_N = \{&-164[\%Cr] + 8{,}33[\%Ni] - 33{,}2[\%Mo] - 134[\%Mn] + 1{,}68[\%Cr]^2 - 1{,}83[\%Ni]^2 \\ &- 2{,}78[\%Mo]^2 + 8{,}82[\%Mn]^2 + (1{,}6[\%Ni] + 1{,}2[\%Mo] + 2{,}16[\%Mn]).[\%Cr] + \\ &(-0{,}26[\%Mo] + 0{,}09[\%Mn]).[\%Ni]\}/T + \{0{,}0415[\%Cr] + 0{,}0019[\%Ni] + \\ &0{,}0064[\%Mo] + 0{,}035[\%Mn] - 0{,}0006[\%Cr]^2 + 0{,}001[\%Ni]^2 + 0{,}0013[\%Mo]^2 - \\ &0{,}0056[\%Mn]^2 + (-0{,}0009[\%Ni] - 0{,}0005[\%Mo] - 0{,}0005[\%Mn]).[\%Cr] + \\ &(0{,}0003[\%Mo] + 0{,}0007[\%Mn]).[\%Ni]\} + 0{,}13[\%C] + 0{,}06[\%Si] + 0{,}046[\%P] \\ &+ 0{,}007[\%S] + 0{,}01[\%Al] - 0{,}9[\%Ti] - 0{,}1[\%V] - 0{,}003[\%W] - 0{,}12[\%O]\end{aligned} \qquad \ldots(5.22)$$

where: [%M] is the alloying element content in wt%.

Calculation yields the equilibrium nitrogen contents shown in Table 5.3 at a weld pool temperature of 1722°C, taking into consideration that total atmospheric pressure in Pretoria is 0,86 atm. These values were substituted into equation (5.20) to yield an average apparent equilibrium constant of $4{,}28.10^{-2}$ for the nitrogen desorption reaction.

Table 5.3 The equilibrium nitrogen content of the weld metal at the temperature of the centre of the pool (1722°C) as a function of the partial pressure of nitrogen in the shielding gas.

Shielding gas nitrogen content	Nitrogen partial pressure, P_{N_2}	Equilibrium nitrogen content, N_{eq}
1,09 %	0,0094 atm	0,0200 wt%
5,3 %	0,0456 atm	0,0442 wt%
9,8 %	0,0843 atm	0,0601 wt%
24,5 %	0,2107 atm	0,0950 wt%

- The apparent equilibrium constant for the absorption reaction, K

If the dissolution of monatomic nitrogen into the weld pool during welding is represented by equation (5.1), the apparent equilibrium constant, K, for this reaction is given by equation (5.23). In order to calculate the value of K, the relationship between K, K' (the apparent equilibrium constant for the desorption of nitrogen) and K_1 (the equilibrium constant for the dissociation of molecular nitrogen to form

monatomic nitrogen in the arc) must be established. This relationship is shown in equation (5.24) with the equilibrium constant, K_1, for nitrogen dissociation (reaction (5.16)) given by equation (5.25).

$$K = \frac{N_{eq}}{P_N} \qquad \ldots(5.23)$$

where: N_{eq} is the nitrogen concentration in the steel in equilibrium with the monatomic nitrogen content of the arc plasma.

$$K = \frac{\sqrt{K'}}{K_1} \qquad \ldots(5.24)$$

where: $$K_1 = \frac{P_N}{\sqrt{P_{N_2}}} \qquad \ldots(5.25)$$

Since the partial pressure of molecular nitrogen in the arc, P_{N_2}, and the value of the equilibrium constant for the nitrogen desorption reaction, K', are known (refer to §5.2.3), and the partial pressure of monatomic nitrogen in the arc plasma at the weld pool temperature can be determined, the apparent equilibrium constant for the absorption of monatomic nitrogen, K, can be calculated. Calculation yields an average K value of $2{,}55.10^8$ at the weld pool temperature of 1722°C.

5.2.4 Density of the molten weld pool

The densities of liquid iron, nickel, chromium and manganese as linear functions of temperature, T, in °C can be calculated using equations (5.26) to (5.29)[9], where T is the temperature of the centre of the weld pool in°C.

Iron:	$8{,}30 - 8{,}36.10^{-4}T$	…(5.26)
Nickel:	$9{,}60 - 12{,}00.10^{-4}T$	…(5.27)
Chromium:	$7{,}83 - 7{,}23.10^{-4}T$	…(5.28)
Manganese:	$7{,}17 - 9{,}30.10^{-4}T$	…(5.29)

This method yields a density of 6,755 g.cm^{-3} or 6755 kg.m^{-3} for the experimental type 310 alloys used in this investigation.

5.2.5 The nitrogen desorption and absorption rate constants, *k'* and *k*

- The nitrogen desorption rate constant, *k'*

Correlations based on the rate of reaction of molecular nitrogen with pure iron were used to estimate the rate constant for the loss of nitrogen from the weld pool as N_2 (reaction (5.9)). The available data on this rate constant were summarised by Belton[10] and Turkdogan[11]. For the reaction N_2 (g) → 2N (wt%), the rate constant (for temperatures ranging from 1550 to 1700°C) is given by equation (5.30):

$$k_1 = \frac{10^{(-6340/T+1{,}85)}}{1+260 f_O[\%O]+130 f_S[\%S]} \quad \text{g.cm}^{-2}.\text{min}^{-1}.\text{atm}^{-1} \qquad \ldots(5.30)$$

where: T is the temperature in K,

f_O is the activity coefficient of dissolved oxygen,

[%O] is the mass percentage of dissolved oxygen,

f_S is the activity coefficient of dissolved sulphur, and

[%S] is the mass percentage of dissolved sulphur.

The rate expression used with this rate constant is as follows:

$$\frac{d\underline{N}(\text{wt\%})}{dt} = \frac{100A}{\rho V} k_1 \left[P_{N_2} - \frac{[\text{N(wt\%)}]^2}{K'} \right] \qquad \ldots(5.31)$$

This expression can be rewritten as:

$$\frac{d\underline{N}(wt\%)}{dt} = -\frac{100A}{\rho V} \frac{k_1}{K'} \left[[N(wt\%)]^2 - K' P_{N_2} \right] \qquad \ldots(5.32)$$

Equation (5.32) can be seen to be the same expression as equation (5.12), with $k' = k_1/K'$.

For stainless steels, the rate constant for this reaction is generally larger than that for liquid iron by a factor of about 6[10,12]. However, this conclusion is based on experiments conducted at 1600°C, and (as will be shown later) it appears that increasing the rate constant by this factor leads to an overestimate.

For stainless steels, the activity coefficient of sulphur, f_S, can be estimated as follows[13]:

$$\log f_S = [\%\text{Cr}] \left(-\frac{94{,}2}{T} + 0{,}040 \right) \qquad \ldots(5.33)$$

where: T is the absolute temperature, and

[%Cr] is the mass percentage of chromium in the steel.

For a weld pool temperature of 1722°C and an average chromium content of 24,4%, this yields a value of $f_S = 0{,}67$.

In these calculations, the effect of dissolved oxygen on the rate constant was neglected, since no data were available on the oxygen levels. However, the activity of oxygen is expected to be low in chromium-rich steels, and since the sulphur levels are comparatively high, neglecting the effect of dissolved oxygen is not expected to affect the calculations significantly.

Substitution of the constants and unit conversion yield the following expression for the rate constant, for a temperature of 1722°C:

$$k' = \frac{0{,}183}{1 + 87[\%\text{S}]} \quad \text{kg.m}^{-2}.\text{s}^{-1}.(\%)^{-2} \qquad \ldots(5.34)$$

This value of the desorption rate constant is for liquid iron, not for stainless steel. However, it appears that it better predicts the rate of the formation of molecular nitrogen than if the rate constant is increased by a factor of 6, which has been suggested to be appropriate for stainless steels[10]. Part of the reason for choosing not to increase the rate constant over that for pure iron is illustrated in Figure 5.4 below, which

compares the measured and predicted reduction in the weld nitrogen content, for welding under pure argon. When welding in pure argon, no dissociated (monatomic) nitrogen is assumed to form in the plasma, and hence the (unknown) rate constant k (for the reaction $N_{plasma} \rightarrow [\underline{N}]_{steel}$) has no effect on the weld nitrogen content which is calculated with equation (5.15). As the figure shows, both values of the rate constant k' overpredict the decrease in nitrogen content of the weld, but the correspondence is much better for the smaller rate constant.

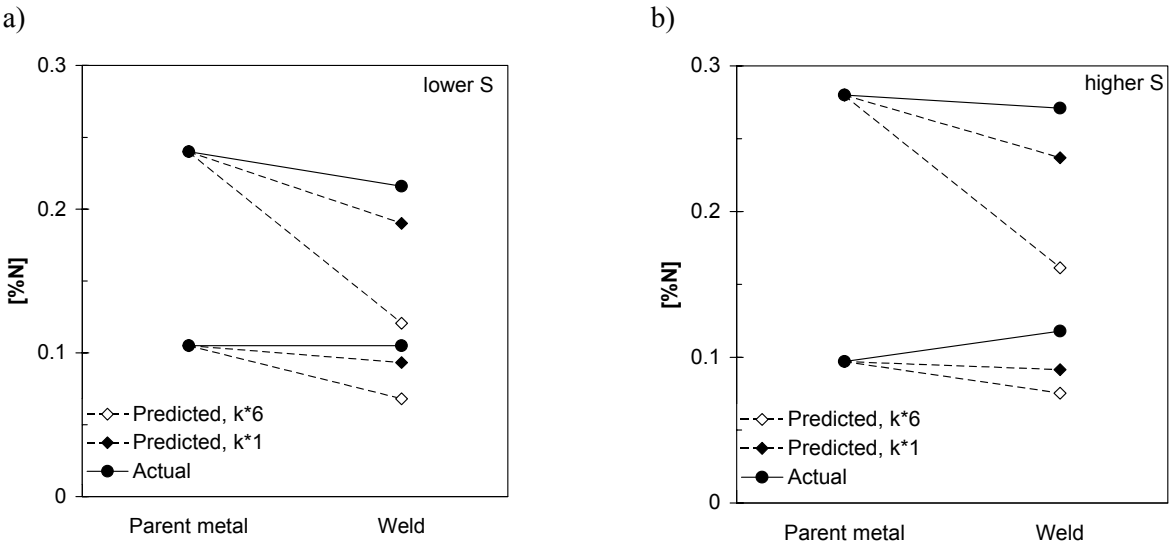

Figure 5.4 Comparison of the actual decrease in nitrogen content from the original parent metal composition (filled circles), with the calculated decrease using the rate constant for liquid iron (filled diamonds), and for the case where this rate constant is increased by a factor of 6 (open diamonds). Results are shown for a) the low sulphur and b) the high sulphur steels, in both cases for welding in pure argon.

Based on these conclusions, equation (5.34) yields values for the desorption rate constant, k', of $6{,}28.10^{-2}$ and $3{,}21.10^{-2}$ $kg.m^{-2}.s^{-1}.(\%)^{-2}$ for the low and high sulphur alloys, respectively. The reduction in the desorption rate constant at higher surface active element concentrations is consistent with a site blockage model, where sulphur atoms are assumed to occupy a fraction of the surface sites required for the adsorption of nitrogen.

- The nitrogen absorption rate constant, k

Literature data on the value of the rate constant k for the reaction of dissociated (monatomic) nitrogen with the stainless steel melt are very limited. For this reason, this constant was estimated from the experimental data, for the case where the shielding gas contained 1,09% nitrogen. These data were used, since nitrogen bubbles formed in the weld pool at higher nitrogen contents. Formation of nitrogen bubbles render one of the assumptions on which the model is based, invalid. Calculated values of the absorption rate constant are summarised in Table 5.4 below.

As the table shows, use of the larger rate constant k' yields values for the constant k which appear to depend on the initial nitrogen content of the steel. There appears to be no fundamental reason why this should be the case. When the rate constant k' for liquid iron is used in its original form, the rate constant

k is approximately the same for all the steels. Interestingly, no strong effect of the sulphur content on the rate constant for dissociated nitrogen is found. This is in contrast with the case for the reaction which involves molecular nitrogen, where an increase in sulphur from 0,022% to 0,054% causes a decrease in the rate constant k' by a factor of approximately 2. Given the weak dependence of k on steel composition, an average value of $3{,}5.10^4$ $kg.m^{-2}.s^{-1}.atm^{-1}$ was used in the subsequent calculations (together with the value of k' as for liquid iron).

Table 5.4 Calculated values of the rate constant k for the absorption of dissociated nitrogen by the weld pool.

a) Rate constant k' for liquid iron.

Alloy	Comments	Base metal nitrogen content	Sulphur content	$10^{-3}k$ ($kg.m^{-2}.s^{-1}.atm^{-1}$)
VFA 657	Low N, low S	0,005	0,023	38
VFA 658	Medium N, low S	0,105	0,023	43
VFA 659	High N, low S	0,240	0,022	35
VFA 752	Low N, high S	0,006	0,052	36
VFA 753	Medium N, high S	0,097	0,061	30
VFA 755	High N, high S	0,280	0,049	27

b) Rate constant k' taken to be 6 times that for liquid iron.

Alloy	Comments	Base metal nitrogen content	Sulphur content	$10^{-3}k$ ($kg.m^{-2}.s^{-1}.atm^{-1}$)
VFA 657	Low N, low S	0,005	0,023	57
VFA 658	Medium N, low S	0,105	0,023	124
VFA 659	High N, low S	0,240	0,022	210
VFA 752	Low N, high S	0,006	0,052	46
VFA 753	Medium N, high S	0,097	0,061	61
VFA 755	High N, high S	0,280	0,049	159

5.2.6 Summary of the constants required in equation (5.15)

A summary of all the constants required for substitution into equation (5.15) is given in Table 5.5.

5.3 PREDICTED CHANGE IN THE WELD METAL NITROGEN CONCENTRATION WITH INCREASING SHIELDING GAS NITROGEN CONTENT

Figure 5.5 below shows the predicted change in weld nitrogen content, for shielding gases with increasing nitrogen content. The calculations were performed for parent metal with the same composition as the experimental alloys. It can be seen that the predicted behaviour is close to that found experimentally (Figures 4.6 and 4.7), with marked increases in the weld nitrogen content at low shielding gas nitrogen

contents. The influence of the base metal nitrogen content and the surface active element concentration on the weld metal nitrogen content is also consistent with that observed experimentally.

Table 5.5 Summary of the constants required in equation (5.15).

Constant	Value
P_N	$8{,}43.10^{-8}$ atm if P_{N_2} = 0,0094 atm $1{,}86.10^{-7}$ atm if P_{N_2} = 0,0456 atm $2{,}53.10^{-7}$ atm if P_{N_2} = 0,0843 atm $4{,}00.10^{-7}$ atm if P_{N_2} = 0,2107 atm
A	34,1 mm^2
L	7,4 mm
V	63,9 mm^3
K	$2{,}55.10^{8}$
K'	$4{,}28.10^{-2}$
ρ	6755 $kg.m^{-3}$
v	2,7 $mm.s^{-1}$
k	$3{,}5.10^{4}$ $kg.m^{-2}.s^{-1}.atm^{-1}$
k'	$6{,}28.10^{-2}$ $kg.m^{-2}.s^{-1}.(\%)^{-2}$ for the low sulphur alloys $3{,}21.10^{-2}$ $kg.m^{-2}.s^{-1}.(\%)^{-2}$ for the high sulphur alloys

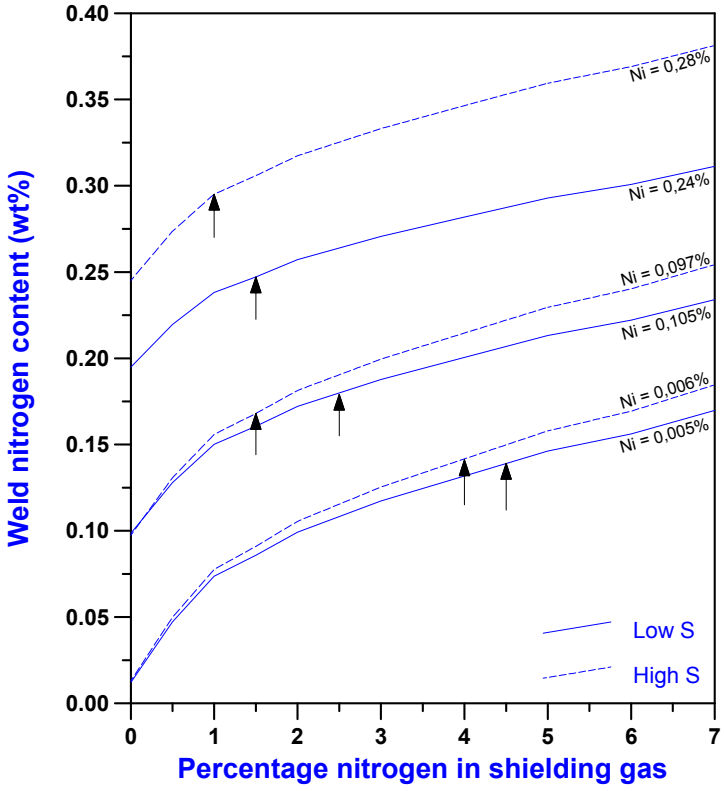

Figure 5.5 Predicted change in weld nitrogen content for shielding gases which are increasingly rich in nitrogen. Calculated for the parent metal compositions of the experimental alloys. The arrows indicate the minimum shielding gas compositions where bubbling was observed experimentally.

The results shown in Figure 5.5 are only valid until the onset of bubble formation. The shielding gas compositions where bubbling was observed visually are indicated on this figure. Beyond this point, nitrogen is removed from the weld pool not only by the gas-metal reaction at the weld pool surface, but also by bubble formation within the weld pool. This condition is not covered by the simple kinetic model presented here. For shielding gas compositions at the onset of bubbling, the predicted rates at which nitrogen enters and leaves the welding pool by the four mechanisms considered in the model are summarised in Table 5.6. This shows that the main mechanism by which nitrogen enters the weld pool is a function of the initial nitrogen content of the alloy, with nitrogen absorption from the arc plasma playing a dominant role at low base metal nitrogen contents, and the melting of nitrogen-containing base metal at high initial nitrogen levels. The main exit mechanism appears to be nitrogen leaving the pool due to the solidification of nitrogen-containing weld metal at the rear of the weld pool, rather than nitrogen desorption to the atmosphere as N_2. It is evident from Figure 5.6 that higher concentrations of sulphur in the weld pool slightly retard the desorption of N_2 to the atmosphere (giving higher nitrogen contents in the weld pool for a similar base metal nitrogen content). This is consistent with a site blockage model, where sulphur atoms occupy a fraction of the surface sites required for the adsorption of nitrogen.

Table 5.6 The relative contributions of the four reactions which add or remove nitrogen to or from the weld pool, at the respective shielding gas compositions where bubble formation was observed experimentally.

		$\frac{dN(wt\%)}{dt}$, mg.s^{-1}			
Alloy	**Comments**	**(1) Absorption of monatomic N from plasma**	**(2) Melting of base metal at leading edge of weld pool**	**(3) Desorption of N_2 from the weld pool**	**(4) Solidification at the rear of the weld pool**
VFA 657	Low N, low S	0,203	0,008	-0,025	-0,185
VFA 658	Medium N, low S	0,151	0,165	-0,055	-0,261
VFA 659	High N, low S	0,116	0,378	-0,120	-0,374
VFA 752	Low N, high S	0,191	0,009	-0,014	-0,187
VFA 753	Medium N, high S	0,117	0,153	-0,024	-0,246
VFA 755	High N, high S	0,095	0,441	-0,093	-0,442

Two factors are of interest in the practical welding situation: the change in nitrogen content upon welding, and the formation of nitrogen bubbles. The former situation appears to be fairly well described by the kinetic model presented here. However, the latter is more difficult to predict. As Figures 4.6 and 4.7 show, bubble formation was observed for weld nitrogen contents ranging from 0,16% to 0,29%. In comparison, the equilibrium nitrogen content for a nitrogen partial pressure of 0,86 atm (atmospheric pressure in Pretoria) is 0,19% at 1722°C. (The saturation concentration depends somewhat on temperature, as shown in Figure 5.6 for the experimental alloys).

For the formation of a nitrogen bubble in the weld pool, the nitrogen partial pressure within the bubble must at least equal atmospheric pressure (in fact, it must be slightly larger than atmospheric pressure to

balance the surface tension of the bubble). Considering that the nitrogen saturation content at 0,86 atm is 0,19%, the high nitrogen alloys display a significant degree of supersaturation prior to the onset of bubble formation (as shown in Figure 5.5). This is consistent with the results of Blake and Jordan[14], who reported that the steady-state nitrogen content of molten iron is in excess of that required to provide an internal pressure of one atmosphere at the assumed temperature of the liquid metal, and concluded that some degree of supersaturation occurs. The increased levels of supersaturation for the higher-nitrogen alloys are presumably related to the higher rate of nitrogen removal as N_2 at the onset of bubble formation; this higher rate of N_2 formation is evident from Table 5.6. Given that nitrogen bubble formation and detachment require bubble nucleation and growth, it appears reasonable to assume that a higher nitrogen removal rate (as bubbles) would require a higher degree of supersaturation (a larger "driving force" for the reaction). Such a link between supersaturation and the rate of nitrogen removal is also evident in the experimental results shown in Figures 4.6 and 4.7, where the weld metal nitrogen concentration increases if the shielding gas nitrogen content is increased beyond the onset of bubble formation.

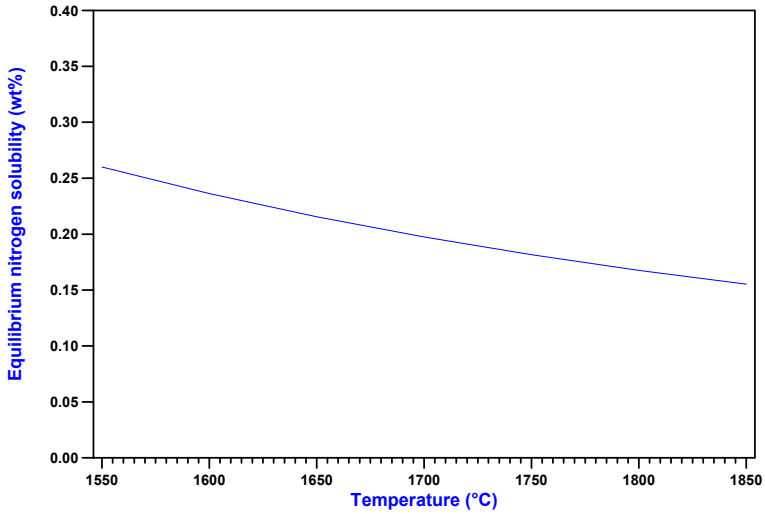

Figure 5.6 The influence of weld pool temperature on the equilibrium nitrogen concentration in the experimental alloys at a nitrogen partial pressure of 0,86 atm. (Calculated using Wada and Pehlke's equations and interaction parameters[8]).

On the other hand, it does not appear possible to form bubbles at weld nitrogen contents below 0,19%, as was found experimentally for most of the lower nitrogen alloys. Possible reasons for this discrepancy include deviation of the (average) weld pool temperature from that measured, deviation of the actual saturation concentration of nitrogen from that predicted by the correlation for f_N, and errors in chemical analysis. Some of these factors are briefly considered below.

As shown in Figure 5.6, a change in temperature has a limited influence on the equilibrium nitrogen concentration of the experimental steels at 0,86 atm. A variation in the weld pool temperature from that measured during the course of this investigation is therefore not expected to have a significant influence

on the equilibrium solubility at 0,86 atm. Experimental error in chemical analysis may, however, be largely responsible for the discrepancy described above. In order for inert gas fusion analysis for nitrogen to be as accurate as possible, weld metal drillings have to be removed very carefully to prevent base metal contamination. Since the weld pools formed during this investigation were relatively shallow, a limited amount of contamination may have occurred. This will influence the nitrogen contents associated with the onset of bubble formation in the experimental alloys. An additional complicating factor is that the minimum shielding gas nitrogen content required to initiate bubbling in each of the experimental alloys (as shown by the arrows in Figure 5.5) was determined by visually observing the weld pool during welding. The transition from nitrogen evolution at the weld pool surface to bubble formation is gradual, making it difficult to accurately ascertain the minimum shielding gas nitrogen level required to initiate bubbling. It is therefore debatable whether any deviation of the measured nitrogen content at the onset of bubble formation from the equilibrium solubility at 0,86 atm is significant.

5.4 THE INFLUENCE OF THE SURFACE ACTIVE ELEMENT CONCENTRATION ON THE PREDICTED WELD NITROGEN CONTENT

Since it has been shown that the rate constant for the nitrogen absorption reaction, k, is only weakly dependent on the steel composition, and the influence of the sulphur concentration on the desorption rate constant, k', can be calculated using equation (5.34), the kinetic model can be used to quantify the influence of the surface active element concentration, and in particular the sulphur content, on the weld nitrogen content. As stated earlier, the effect of dissolved oxygen on the rate constants can be neglected, since the activity of oxygen is expected to be low in chromium-rich steels. The influence of the sulphur concentration in the experimental steels on the predicted steady-state nitrogen content for a shielding gas nitrogen content of 1,09% is shown in Figure 5.7.

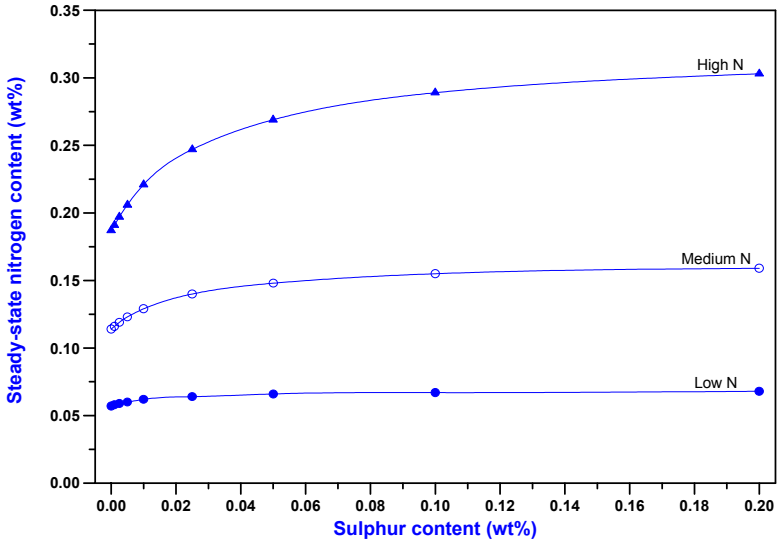

Figure 5.7 The steady-state nitrogen content of the experimental steels as a function of sulphur content at a shielding gas nitrogen content of 1,09%.

Figure 5.7 shows that the steady-state nitrogen content initially increases and then approaches a constant value as the sulphur content increases. The decrease in the steady-state nitrogen content at low sulphur concentrations can be attributed to an increase in the desorption rate constant, k', as demonstrated by equation (5.34). As a result of the lower level of surface coverage at low sulphur concentrations, more nitrogen can escape to the atmosphere during welding, resulting in higher nitrogen desorption rates and lower weld nitrogen contents. As the sulphur content increases, the desorption rate is reduced due to increased site blockage. Since the rate of nitrogen desorption is small in the experimental alloys (refer to Table 5.6), a further increase in sulphur content will have a limited influence on the total reaction rate, and the weld nitrogen content becomes independent of the surface active element concentration. The steady-state nitrogen content in the presence of surface active elements also appears to be a strong function of the base metal nitrogen content, which is consistent with the influence of the surface active element content on the desorption rate constant. In the presence of high levels of sulphur, the nitrogen desorption rate decreases and more of the nitrogen originally present in the base metal remains in solution in the weld metal. Higher base metal nitrogen contents therefore lead to higher weld nitrogen concentrations. This is consistent with the results shown in Figure 4.7 for the high sulphur alloys.

5.5 THE INFLUENCE OF WELDING PARAMETERS ON THE PREDICTED WELD NITROGEN CONCENTRATION

Several researchers have reported that welding parameters, in particular the welding current, arc voltage and torch travel speed, have a significant influence on nitrogen absorption and desorption during welding. The results of some of these investigations were described in §1.6. The potential impact of a change in welding parameters on the weld nitrogen content calculated using the kinetic model, is considered below.

According to Kuwana and Kokawa[15] and Kuwana *et al*[16], an increase in welding current reduces the weld metal nitrogen content. Since it has been shown that the welding current does not have a significant influence on the temperature of the weld pool, its effect on the weld nitrogen content appears to be related to a change in the weld pool dimensions. The weld pool surface area, volume and length are all expected to increase with an increase in welding current. The weld pool dimensions are also influenced by a change in the arc voltage and torch travel speed. The weld cross-sectional area initially increases with an increase in arc length (and therefore arc voltage), but becomes constant at higher arc lengths, whereas the weld pool area decreases markedly with an increase in travel speed.

Since an investigation into the influence of welding parameters on the dimensions of the weld pool falls outside the scope of this study, an attempt will be made to show how an arbitrary increase in the weld pool surface area, either as a result of an increase in welding current or arc voltage, or a decrease in torch travel speed, influences the steady-state nitrogen content predicted by the kinetic model.

If it is assumed that the weld pool has the shape of a section of a sphere (as shown schematically in Figure 5.8), equations (5.19) and (5.35) can be used to determine how an arbitrary change in weld pool surface area impacts on the weld pool volume and length. If, for example, a change in welding parameters causes the weld pool surface area to double in size from 34,1 mm^2 (refer to Table 5.2) to 68,2 mm^2, the weld

pool length, L, is expected to change from 7,4 mm to 9,6 mm, and the volume, V, from 63,9 mm^3 to 151,7 mm^3. These values can now be substituted into equation (5.15) to calculate the steady-state nitrogen content for the new set of welding parameters.

$$A = \pi r^2 \sin \theta \qquad \ldots(5.35)$$

where: A is the area of a section of a sphere, where the sphere has a radius, r.

The weld nitrogen contents of two experimental alloys, VFA 657 and VFA 755 (i.e. the low N, low S and high N, high S steels) were calculated for the adjusted weld pool dimensions and are shown in Figure 5.9 as a function of the shielding gas nitrogen content. It is evident from this figure that a change in the weld pool dimensions as a result of a change in welding parameters does not cause a significant variation in the predicted weld nitrogen content.

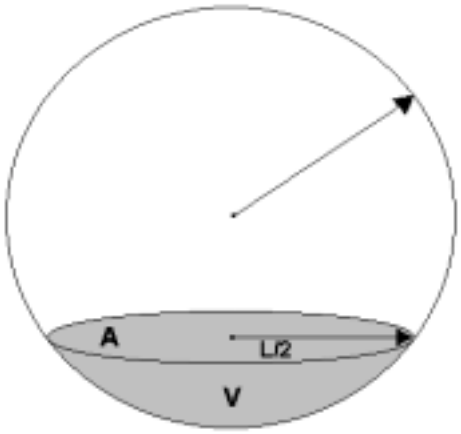

Figure 5.8 The weld pool as a section of a sphere with radius, r. A is the area of the circular section, V is the volume of the section, and L is the diameter of the circular section (as shown above).

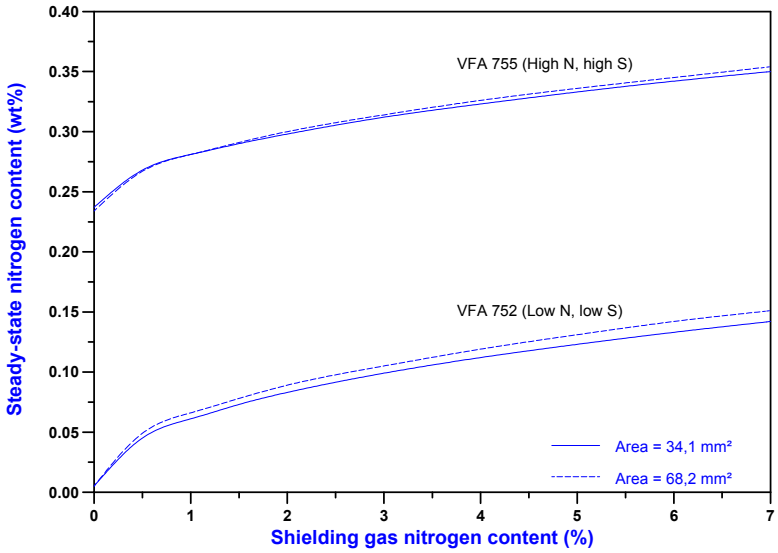

Figure 5.9 The influence of a change in the weld pool dimensions on the steady-state nitrogen content of two experimental alloys.

A number of factors not considered in this approach may influence the calculated steady-state nitrogen content. These factors are listed below.

- As the torch travel speed increases during welding, the weld pool shape changes from circular or oval to teardrop shaped. When this happens, the assumption that the weld pool has the shape of a section of a sphere is no longer acceptable, and the ratio of the weld pool length, L, to the weld pool surface area, A, will increase. Since, according to the kinetic model, the weld pool length affects the rate at which nitrogen enters the weld pool due to melting and the rate at which nitrogen leaves the weld metal due to solidification, and these effects are important in determining the overall reaction rate, this change in weld pool shape is expected to have a significant influence on the predicted steady-state nitrogen content.

- Kuwana *et al*[15] suggested that, in the presence of pure nitrogen shielding gas, the nitrogen content of the weld metal may be controlled mainly by nitrogen evolution during cooling. According to these authors, an increase in the weld cross-sectional area results in a decrease in the cooling rate after welding, thereby prolonging the period of time before solidification and resulting in an increase in the amount of evolved nitrogen. Since a change in cooling rate after welding is not considered by the kinetic model, this may result in slightly lower nitrogen levels than those predicted.

- A change in welding parameters may change the extent of coverage of the weld pool by the arc plasma. Since full coverage of the weld pool by the arc was assumed on deriving the kinetic model, this is likely to impact on its predictions. Complete coverage of the weld pool by the plasma can be assumed if welding is performed at reasonably low currents and the weld pool is fairly narrow. Since nitrogen absorption only occurs under the plasma impingement area, whereas nitrogen desorption takes place over the entire weld pool surface area, incomplete coverage of the weld pool by plasma is expected to increase the desorption rate, resulting in lower steady-state nitrogen contents.

- Excessive arc lengths during welding will increase the likelihood of atmospheric contamination as more nitrogen from the surrounding atmosphere (air) is entrained in the arc plasma. This will change the nitrogen content of the arc and result in variations in the values of P_N and P_{N_2} from those expected based on the shielding gas nitrogen content.

5.6 CONCLUSIONS

- A kinetic model can be used to describe nitrogen absorption and desorption during the welding of the experimental stainless steels. The proposed model considers the absorption of monatomic nitrogen from the arc plasma, the evolution of N_2 from the weld pool, nitrogen entering the weld metal during the melting of nitrogen-containing base metal, and nitrogen leaving the weld pool due to the solidification of weld metal at the rear of the pool. The predictions of the model show good agreement with the experimental results discussed in Chapter 4.

- The calculated nitrogen desorption rate constant is a function of the surface active element concentration in the alloy, with the rate constant decreasing at higher concentrations of sulphur in the steel. This is consistent with a site blockage model, where surface active elements occupy a fraction of the surface sites required for nitrogen adsorption. The rate constant for the absorption of dissociated nitrogen is, however, not a strong function of the surface active element concentration.

- Nitrogen desorption rates are significantly lower in the presence of higher concentrations of surface active elements. The main mechanism by which nitrogen enters the weld pool is dependent on the initial nitrogen content of the alloy, with nitrogen absorption from the arc plasma playing a dominant role at low base metal nitrogen contents, and the melting of nitrogen-containing base metal at high initial nitrogen levels. The main exit mechanism appears to be nitrogen leaving the pool due to the solidification of nitrogen-containing weld metal at the rear of the weld pool, rather than nitrogen desorption to the atmosphere as N_2.

- Although the minimum shielding gas nitrogen content that leads to bubbling cannot be determined from the model, it is evident that some supersaturation above that required to nucleate nitrogen bubbles in the melt occurs in the high nitrogen alloys. This can probably be attributed to the higher rate of nitrogen removal as N_2 at the onset of bubble formation.

- A change in welding parameters does not appear to influence the steady-state nitrogen content in the experimental alloys to any significant extent.

5.7 PRACTICAL IMPLICATIONS

The results of the current investigation show that nitrogen losses from nitrogen-alloyed stainless steels can be expected during autogenous welding in pure argon shielding gas. In the experimental alloys this effect was most pronounced at base metal nitrogen contents in excess of 0,1%. Small amounts of nitrogen can be added to the shielding gas to counteract this effect, but this should be done with care to avoid bubble formation. However, supersaturation before bubble formation does extend the range of shielding gas compositions which can be used.

Higher concentrations of surface active elements have a beneficial influence on the behaviour of high nitrogen stainless steels during welding. Due to the lower desorption rates associated with higher surface active element concentrations, more of the base metal nitrogen originally present in the alloy will be maintained in solution in the weld pool. Higher sulphur contents also increase the steady-state nitrogen content of stainless steels and the amount of nitrogen that can be accommodated in the weld metal prior to nitrogen evolution in the form of bubbles. Although higher sulphur contents may not be viable in practice, small amounts of oxygen added to the shielding gas during welding will have a similar effect.

5.8 REFERENCES

1. T. Kuwana, H. Kokawa, and M. Saotome, "Quantitative prediction of nitrogen absorption by steel during gas tungsten arc welding". 3rd International Seminar on the Numerical Analysis of Weldability. Graz-Seggau, Austria. 25-27 September 1995.
2. K. Mundra, and T. DebRoy, "A general model for partitioning of gases between a metal and its plasma environment", Metallurgical and Materials Transactions B, vol. 26B. February 1995. pp. 149-157.
3. T.A. Palmer, and T. DebRoy, "Physical modeling of nitrogen partition between the weld metal and its plasma environment". Welding Journal, vol. 75, no. 7. July 1996. pp. 197s-207s.
4. J.F. Elliott, and M. Gleiser, "Thermochemistry for Steelmaking I". Addison-Wesley Publishing Company, Reading, USA. 1963. p. 75.
5. O. Kubaschewski, C.B. Alcock, and P.J. Spencer, "Materials Thermochemistry", 6th Edition. Pergamon, Oxford. 1993.
6. R.C. Weast, "CRC Handbook of Chemistry and Physics", 62nd Edition. CRC Press, Boca Raton, Florida. 1981.
7. R.E. Reed-Hill, and R. Abbaschian, “Physical Metallurgy Principles”, 3rd Edition. PWS Kent, Boston, USA. 1992. p. 497.
8. H. Wada, and R.D. Pehlke, "Solubility of nitrogen in liquid Fe-Cr-Ni alloys containing manganese and molybdenum". Metallurgical Transactions B, vol. 8B. December 1977. pp. 675-682.
9. R.J. Fruehan (ed.), "The making, shaping and treating of steel", 11th Edition, Steelmaking and Refining volume. AISE Steel Foundation, Pittsburgh, USA. 1998. p. 75.
10. G.R. Belton, "How fast can we go ? The status of our knowledge of the rates of gas-liquid metal interactions". Metallurgical Transactions B, vol, 24B. April 1993. pp. 241-258.
11. E.T. Turkdogan, "Fundamentals of Steelmaking". The Institute of Materials, London. 1996.
12. R.J. Fruehan, "Nitrogen control in chromium steels". INFACON 6. Proceedings of the 1st International Chromium Steel and Alloy Congress. Cape Town, South Africa. Volume 2. SAIMM, Johannesburg, South Africa. pp. 35-41.
13. The 19th Committee on Steelmaking, The Japan Society for the Promotion of Science, "Steelmaking data sourcebook". Gordon and Breach, New York. 1988.
14. P.D. Blake, and M.F. Jordan, "Nitrogen absorption during the arc melting of iron". Journal of the Iron and Steel Institute. March 1971. pp. 197-200.
15. T. Kuwana, and H. Kokawa, "The nitrogen absorption of iron weld metal during gas tungsten arc welding". Transactions of the Japan Welding Society, vol. 17, no. 1. April 1986. pp. 20-26.
16. T. Kuwana, H. Kokawa, and K. Naitoh, "The nitrogen absorption of stainless steel weld metal during gas tungsten arc welding". Transactions of the Japan Welding Society, vol. 17, no. 2. October 1986. pp. 117-123.